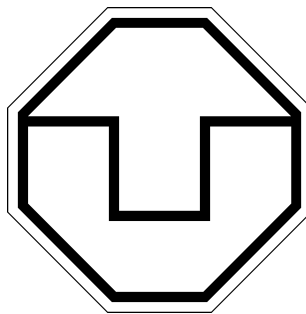


**Institut für Theoretische Physik
TU Dresden**

Quark Mass Dependence of One-Loop Self-Energies in Hot QCD

von

Daniel Seipt



2008

Institut für Theoretische Physik
Fachrichtung Physik
Fakultät Mathematik und Naturwissenschaften
der Technischen Universität Dresden

Quark Mass Dependence of One-Loop Self-Energies in Hot QCD

**Towards the Chiral Extrapolation of the Equation
of State of Strongly Interacting Matter**

Diplomarbeit
zur Erlangung des akademischen Grades
Diplom-Physiker

vorgelegt von
Daniel Seipt
geboren am 5. Oktober 1981 in Marienberg

Dresden 2008



Eingereicht am 29.05.2007

1. Gutachter: Prof. Dr. R. Schmidt
2. Gutachter: Prof. Dr. B. Kämpfer

Kurzfassung:

Es wird die Abhängigkeit der Einschleifen- und "Hard Thermal Loop"-Selbstenergien von endlichen Quarkmassen m_q untersucht, für den Fall heißer, stark wechselwirkender Materie. Basierend auf der fundamentalen Theorie der starken Wechselwirkung, der Quantenchromodynamik (QCD), werden die Selbstenergien sowie die daraus abgeleiteten Dispersionsrelation $\omega_i(p)$, $i \in \{q, g\}$, von Quarks (q) und Gluonen (g), welche durch die Polstellen der resummierten Propagatoren gegeben sind, abgeleitet. Diese sind wesentliche Bestandteile für die Beschreibung des Quark-Gluon-Plasmas durch ein Quasiteilchenmodell. Dieses Quasiteilchenmodell erlaubt die parametrische Beschreibung der Zustandsgleichung für stark wechselwirkende Materie, die mit Hilfe von Gitterrechnungen gewonnen wurde, sowie deren Extrapolation hin zu höheren Temperaturen und Baryonendichten. Dazu benutzt das Modell eine effektive Kopplung $G^2(T)$, welche eine geeignete Parametrisierung der laufenden Kopplung der QCD darstellt. Die laufende Kopplung wird dabei in einem massenabhängigen Renormierungsschema berechnet, was eine sichere Parametrisierung der Quarkmasseneffekte in $G^2(T; m_q)$ erlaubt. Die Abhängigkeit dieser für Quasiteilchenmodelle wichtigen Größen von den Quarkmassen erlaubt eine zuverlässige chirale Extrapolation von QCD Gitterdaten, welche oft nur für endliche Quark-Massenparameter zur Verfügung stehen.

Abstract:

A systematic study of the quark mass (m_q) dependence of one-loop and hard thermal loop (HTL) self-energies in hot quantum chromodynamics (QCD) is presented from first principle calculations. These self-energies enter a quasi-particle description of the quark gluon plasma via the quasi-particle dispersion relations $\omega_i(p)$, $i \in \{q, g\}$, given by the pole positions of resummed propagators of quarks (q) or gluons (g) as a function of momentum p . The quasi-particle model allows to parameterize and extend finite temperature lattice QCD results for the equation of state, utilizing an effective coupling $G^2(T)$, representing a suitable parameterization of the running QCD coupling. The running coupling is calculated in a mass dependent renormalization scheme, allowing a reliable parameterization of bare quark mass effects, providing $G^2(T; m_q)$. The quark mass dependence of these important ingredients for quasi-particle descriptions allows to handle the chiral extrapolation of lattice QCD data, available often only at finite quark mass parameters.

Contents

1	Introduction	7
1.1	The Standard Model	7
1.2	Quantum Chromodynamics: Confinement and Asymptotic Freedom	9
1.3	Quark Gluon Plasma	10
1.3.1	Breakdown of Perturbation Theory and Hard Thermal Loop Resummation	12
1.3.2	Quasi-Particle Description of Strongly Interacting Matter	15
2	Thermal Field Theory and Self-Energies	19
2.1	Imaginary Time Formalism	19
2.2	Paths in the Complex Time Plane	21
2.3	The Gluon Self-Energy	25
2.4	The Quark Self-Energy	27
2.5	Renormalization of UV-Divergencies	30
2.6	Mass Dependent Running Coupling	32
3	The Gluon Self-Energy	37
3.1	The Photon Polarization Tensor	37
3.2	Photon Dispersion Relations	48
3.3	The Gluon Self-Energy	55
3.4	Gluon Dispersion Relation	57
4	The Quark Self-Energy	61
4.1	The One-Loop Quark Self-Energy	61
4.2	mHTL for the Quark Self-Energy	62
4.2.1	HTL Quark Self-Energy in the Chiral Limit	63
4.2.2	Finite Quark Masses	65
4.3	Quark Dispersion Relations	72
4.3.1	Chiral Limit	72
4.3.2	Finite Quark Masses	76
4.3.3	Asymptotic Quark Dispersion Relation	78
5	Applications	83
5.1	Chiral Expansion of the Asymptotic Dispersion Relations	83
5.2	Asymptotic Dispersion Relations for Thermodynamic Calculations	90
6	Summary and Outlook	97

Appendices	99
A Formulary	99
A.1 Units, Notations & Conventions	99
A.2 $\text{SU}(3)$ -Color Algebra	100
A.3 Dirac Matrix Algebra	101
B Feynman Rules	103
B.1 Feynman Rules in Minkowski Space	103
B.2 Feynman Rules in Euclidean Space – ITF	105
B.3 Analytic Continuation	107
B.4 Renormalized Lagrangian	107
C Frequency Sums	109
C.1 Path Integral Technique	109
C.2 Listing of Frequency Sums	111
D Gauge Dependence of the One-Loop Fermion Self-Energy	113
E Elementary Integrals	117
Bibliography	119

1 Introduction

The major goal of theoretical physics has always been to describe a large set of observable phenomena in an unified framework with a preferably small set of equation describing all observable interactions by forces between the fundamental matter constituents. For instance, in the 19th century, Maxwell's equations unified all electric and magnetic phenomena, that had been accounted for two distinct types of forces, in one set of coupled equations, showing that they are just two realizations of the same fundamental force. At the beginning of the 20th century, physicists discovered the structure of the atom, as a small massive nucleus, composed of positively charged protons and electrically neutral neutrons, which are called hadrons¹, and negatively charged electrons forming the quantized orbitals of the shell. Hence, the variety of chemical elements could be described by means of three "fundamental" particles and differences in their number and orbital structure. Nonetheless, the problem arose that the atomic nucleus should not be stable due to the electrostatic repulsion of the positively charged protons. Another force, the strong force, that compensates the electric repulsion and binds the atomic nuclei, had to be introduced as a logical consequence.

Gell-Mann and Zweig formulated the concept of quarks, carrying a different type of charge dubbed color charge (red, green, blue), as constituents of hadrons, which made it possible to describe very well the large amount of many newly found hadrons with only a few different quark flavors. The quarks have never been observed as free particles; they are always confined into hadrons, either as mesons (bound states of a constituent quark and an constituent anti-quark), i.e. π , K , ρ or as (anti-)baryons (3 constituent (anti-)quarks), i.e. the nucleons p , n , which are all color neutral (white) states.

1.1 The Standard Model

Until now, 6 quark flavors (**u**p, **d**own, **s**trange, **c**harm, **b**ottom, **t**op) have been discovered. Within the present standard model of particle physics, these seem to form a complete set accounting for the known phenomena of strongly interacting particles. Their electric charges² are $+\frac{2}{3}e$ or $-\frac{1}{3}e$. There is another set of particles belonging to the sector of electroweak interactions. These leptons uncover electrons, muons and τ -leptons and their accompanying neutrinos, see fig. 1.1 for an illustration. Being fermions with a spin of $s = 1/2$, all these particles are considered fundamental meaning that no internal structure has

¹Hadron comes from the Greek word *hadros*, meaning "thick", "heavy" or "strong".

² e denotes the absolute value of the fundamental electric charge of an electron, $e = 1.602\,176 \cdot 10^{-19}$ As. Thus, the charge of an electron is $-e$.

been observed yet. In the standard model, the electromagnetic, strong and weak interactions among the mentioned fundamental particles are described by the exchange of gauge bosons with spin $s = 1$. These gauge bosons couple to their appropriate charges, e.g. the photon couples to the electric charge. Mathematically, the interactions in the standard model are formulated within gauge field theories, which means that the Lagrangians of the charged particle fields are invariant under certain gauge transformations. The structure of the interactions follows from the corresponding gauge group, which is in the case of quantum electrodynamics (QED) the Abelian $U(1)$ leading to only one gauge boson – the photon – that carries no charge itself. However, the gauge group of quantum chromodynamics (QCD) describing strong interactions is a non-Abelian $SU(3)$, where the 3 in $SU(3)$ is related to the threefold degeneracy of each quark flavor, called color. The non-Abelian group $SU(3)$ has a much richer structure than the Abelian $U(1)$. Quarks appear in the fundamental representation of $SU(3)$. There are 8 gauge bosons (gluons), corresponding to the 8 independent combinations of color and anti-color charges. They appear in the adjoint representation of $SU(3)$. Since the gluons carry color charge themselves, they are able to interact with each other.

Due to quantum fluctuations, the vacuum is not empty, but it is filled with virtual particle-antiparticle pairs. In the case of QED, these virtual electron-positron pairs are virtual dipoles being aligned in the presence of electric charges and screening them. Thus, at long distances, or small momentum transfers, the strength of the interaction decreases. The coupling "constant" actually is no constant but a scale dependent quantity, called running coupling. In QCD, the picture is just opposite of QED. Due to the strong self interactions among the gluons, the screening of color charges by virtual quark-antiquark pairs is over-compensated and the color charge is surrounded by a cloud of color-charged gluons amplifying the charge with increasing distance, so that color charges are anti-screened. The coupling increases with increasing distance, which leads to the confinement. If one tries to remove one quark from another one e.g. in a meson, the energy spent to separate the quark from the anti-quark leads to the creation of another quark-antiquark pair, resulting in 2 mesons. On the other hand, with decreasing distance, or increasing momentum transfer, the coupling decreases, which is known as asymptotic freedom.

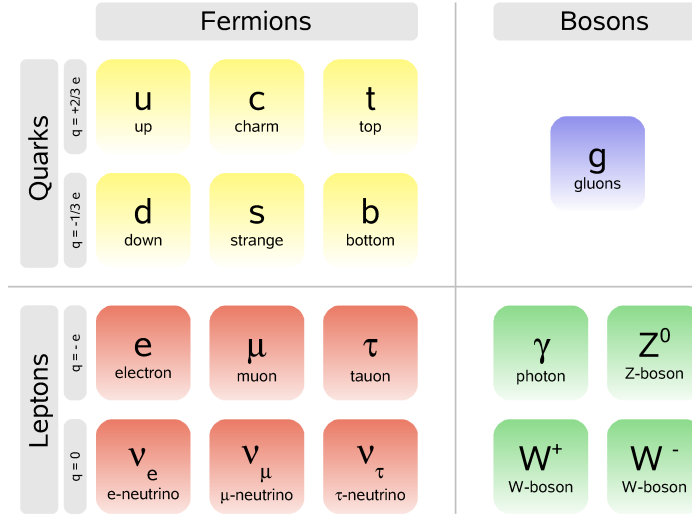


Figure 1.1: Illustration of the known fundamental particles in the Standard Model, not depicting anti-particles and the Higgs-boson. The left column depicts the $\text{spin-}1/2$ particles, while the right column represents the quanta of the spin-1 gauge fields.

1.2 Quantum Chromodynamics: Confinement and Asymptotic Freedom

The classical Lagrangian \mathcal{L}_{cl} , which is the foundation of QCD³, has a local non-Abelian color $SU_c(3)$ gauge symmetry and reads

$$\mathcal{L}_{cl} = -\frac{1}{4}F_{\mu\nu}F^{\mu\nu} + \bar{\psi}(i\mathcal{D} - m)\psi \quad (1.1)$$

with the quark fields ψ , which is a color-triplet and a vector of length N_F in flavor space. m is the $N_F \times N_F$ quark mass matrix⁴ and $\mathcal{D} = \gamma^\mu D_\mu$ denotes the covariant derivative

$$D_\mu = \partial_\mu + igA_\mu \quad (1.2)$$

with coupling constant g , gauge field $A_\mu = A_\mu^a t^a$ and the gauge group matrices t^a in the fundamental representation. $F_{\mu\nu}$ is the field strength tensor of the gluon fields, defined as the commutator of the covariant derivatives via

$$F_{\mu\nu} := -\frac{i}{g}[D_\mu, D_\nu] \quad (1.3)$$

³In order to quantize the classical theory, which leads to quantum chromodynamics, one has to fix the gauge and introduce Faddeev-Popov fields to absorb the unphysical degrees of freedom from the gauge fields. For the complete Lagrangian see Appendix B.1. For details of the quantization of non-Abelian gauge theories see [Muta87].

⁴The dynamical quark fields that appear in the Lagrangian have to be distinguished from the constituent quarks of Gell-Mann and Zweig. Although they carry the same quantum numbers such as isospin or strangeness the masses are different. The masses of the dynamical up and down quark in the Lagrangian (1.1) are of the scale of a few MeV, whereas the constituent quarks have masses of a few hundred MeV.

and reads

$$F_{\mu\nu} = \partial_\mu A_\nu - \partial_\nu A_\mu + ig[A_\mu, A_\nu], \quad (1.4)$$

where the commutator of the gauge fields is nonlinear in the gauge fields and the corresponding expressions in \mathcal{L}_{cl} leads to three- and four-gluon vertices (such self-couplings of gauge quanta do not occur in Abelian theories like QED). Since the strong coupling g is large at low energies, perturbative calculations are not justified and the non-perturbative QCD vacuum has a nontrivial structure. Thus, at low energies, the strong interactions are appropriately described by effective theories with hadrons as degrees of freedom, such as chiral perturbation theory (see [Ber06] and references therein). Furthermore, the chiral symmetry of the classical Lagrangian (1.1) is spontaneously broken⁵, which is reflected in the non-vanishing vacuum expectation value of the chiral quark condensate $\langle \bar{\psi}\psi \rangle \sim -(240 \text{ GeV})^3$. The quark condensate can be related to the constituent quark masses of a few hundred MeV in contrast to the (almost) vanishing current quark masses of up and down quarks. The spontaneously broken chiral symmetry is expected to be restored under certain conditions; the quark condensate serves, therefore, as an order parameter for phase transitions of QCD.

In contrast, at high energy scales, with momentum transfers of a few hundred GeV, which are achieved e.g. in deep-inelastic-scattering experiments, the coupling is small and perturbative calculations are reliable.

1.3 Quark Gluon Plasma

The concept of asymptotic freedom suggests the conclusion that, if the hadron density is so large that individual particles start to overlap – the interaction distance between the individual quarks gets very small as well as the coupling – hadrons will start to "dissolve" and the quarks and gluons will propagate quasi-freely [Col75]. This is the famous deconfinement transition. This notion stands for changing the degrees of freedom in a strongly interacting medium from hadrons to quarks and gluons.

There are two possibilities to achieve such a dense system. Consider the following gedanken-experiments: When the QCD vacuum in a box is heated, the lowest lying hadronic states (such as pions, kaons etc.), are thermally excited with increasing temperature. The density n of the light hadrons can be estimated as $n \propto T^3$, where T denotes the temperature. Since all hadrons have the typical size of $\approx 1 \text{ fm}^3$, the whole volume will be filled with hadrons at a critical temperature of approximately $T_c \sim 200 \text{ MeV}$. When the temperature is increased further, the hadrons "melt" into quasi-freely roaming quarks and gluons. Numerical calculations within more sophisticated models yield values of $T_c \sim 150 - 200 \text{ MeV}$ depending on the number of active quark flavors N_F . The latter state of matter is called quark gluon plasma (QGP). For an orientation one often employs the phase diagram as sketched in fig. 1.2. Another possibility might be the compression of normal hadronic matter over a critical

⁵This has to be seen in contrast to the explicit breaking of chiral symmetry by finite bare quark masses.

density where again the hadrons start to overlap and dissolve into a plasma of degenerate quark matter, which has a high baryon net density. Numerical calculations show that the critical density is several times the density of normal nuclear matter.

The question whether this transition is a proper phase transition of first or second order or a continuous crossover has not been answered yet completely. However, numerical calculations show that the details of the deconfinement transition are very sensitive to the number of involved quark flavors and their masses (see [Ris04] and references therein for an overview). It is assumed, although not proven yet, that the restoration of chiral symmetry and the deconfinement transition coincide [Kar02]. According to the high temperature or density that is needed to form a QGP, it is expected to be relevant under three different circumstances:

1. In the early universe, after the Big Bang between the electroweak phase transition and the confinement transition at about $10^{-5}s$, the state of cosmic matter was dominated by deconfined, strongly interacting matter.
2. In compact stellar objects, such as the cores of neutron stars.
3. At the early stages of relativistic heavy ion collisions, for example at RHIC (Relativistic Heavy Ion Collider, Brookhaven), at the SPS (Super Proton Synchrotron, CERN), LHC (Large Hadron Collider, CERN) or at SIS 300 (FAIR-GSI, Darmstadt).

In item 1. temperature effects are important; in item 2. the density effects are relevant, while in 3. one meets a superposition of both ones.

In all three cases, one assumes that the system under consideration is in thermal equilibrium and a thermodynamic description is justified. Then the equation of state (EoS) of strongly interacting matter plays a crucial role for the relevant physics. In the following we will give some examples for currently ongoing experiments, that need theoretical support on the EoS of the QGP focusing on the high temperature regime:

Ad 1: During the cooling of the universe, after the electroweak phase transition at temperatures of the order of 200 GeV, the EoS was dominated by the strongly interacting matter, i.e. quarks and gluons. The EoS in this particular temperature regime between 200 GeV and the confinement transition at $T_c \sim 160$ MeV is supposed to be relevant for relic densities of weakly interacting massive particles (WIMPs)⁶, which are considered as candidates for dark matter. Non-perturbative calculations showed that the QCD EoS differs significantly from the ideal gas result even at comparatively high temperatures indicating the relevance of strong interactions. Anticipating the new Planck satellite mission to measure the estimated relic densities with less than 1%

⁶The relic densities are usually given as abundances $Y = n/s$ as number density per entropy density. It is approximately given by $Y \propto g_*^{-1/2}(T_f)$, where T_f is the freeze-out temperature of the WIMP. $g_*^{1/2}$ is a parameter depending on the effective number of degrees of freedom and thus depending on the EoS (for more details see [Hin05]).

error, one surely needs an improved EoS that exceeds the ideal gas assumption. 10% uncertainty in the EoS translate into errors of $0.5 - 1\%$ in the relic densities [Hin05]. It is also necessary to include finite quark mass effects into that EoS, since the mass thresholds of charm, bottom and even top quarks are crossed in this temperature region.

Ad 3: Descriptions of the early stages of heavy ion collision experiments using relativistic Boltzmann equations indicate a fast equilibration of the quark gluon plasma at short time scales of about $0.5 \text{ fm}/c$. After this initial stage, the plasma is assumed to be thermally equilibrated with a lifetime of approximately $10 \text{ fm}/c$. Thus, the expansion of the fireball might be described by means of relativistic hydrodynamics, with the conservation of energy-momentum and baryon number

$$\partial_\mu T^{\mu\nu} = 0, \quad (1.5)$$

$$\partial_\mu j_B^\mu = 0. \quad (1.6)$$

Here, j_B^μ denotes the baryon number current and $T^{\mu\nu}$ the energy-momentum tensor given by (e.g. assuming negligible dissipative effects)

$$T^{\mu\nu} = (e - p)u^\mu u^\nu + pg^{\mu\nu} \quad (1.7)$$

for an ideal fluid, where e is the energy density, p the pressure and u^μ the 4-velocity of the plasma. In order to solve this set of coupled differential equations, one needs an interrelation given e.g. by the equation of state of strongly interacting matter, preferably in the form $e(p)$. This EoS may be obtained by methods of statistical quantum field theory. Details of this equation of state might have observable consequences on measurable quantities such as transverse momentum spectra dN/dp_T or its azimuthal anisotropy coefficient v_2 (cf. e.g. [Huo06, Blu07a] for a discussion).

Lattice gauge theory is a powerful numerical method to calculate non-perturbative properties of QCD from first principles using Monte Carlo methods on a discretized space-time grid dubbed lattice. In principle the exact calculation of all thermodynamic quantities, such as the EoS, is possible on the lattice. Nonetheless, this procedure is strongly limited by extraordinary calculational expense. For technical reasons, lattice results for the EoS are only known for small baryon density. Additionally, lattice calculations utilize large and sometimes temperature dependent quark masses $m_q \sim T$ [Kar02]. Hence, it is essential to extrapolate the resulting EoS to physical quark masses. This procedure is called chiral extrapolation, since up and down quarks may be treated as massless in the relevant temperature region.

1.3.1 Breakdown of Perturbation Theory and Hard Thermal Loop Resummation

Perturbative expansions of thermodynamic quantities such as pressure p or entropy density s are reliable only for very high temperature, where the coupling is sufficiently small. They are poorly convergent at lower temperatures

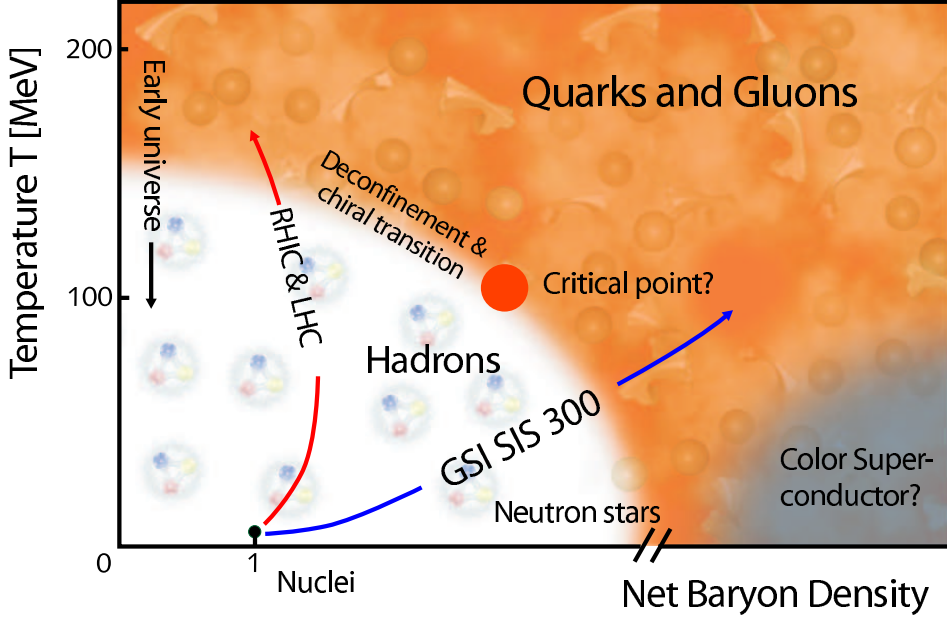


Figure 1.2: Part of the QCD phase diagram in a schematic plot. The temperature and net baryon density serve as coordinates in the thermodynamic state space. At low temperature and density the relevant degrees of freedom of strongly interacting matter are hadrons, while at high temperature and large density, the quarks and gluons are thought to represent the degrees of freedom. These regions are distinguished by deconfinement and chiral restoration. The possibility of a critical point is indicated, too, but not considered in this work, as such phenomena as color superconductivity. Additionally, a few dynamical paths are indicated, such as the evolution of cosmic matter near the temperature axis or highly excited nuclear matter in heavy ion collisions at RHIC & LHC or SIS 300 energies. Neutron star matter occupies the phase diagram at low temperature. (source: GSI).

and higher order contributions alternate in sign. The pressure of hot QCD with N_F massless flavors has been calculated in an perturbative series up to $g^6 \ln(1/g)$ [Kaj03] citing only the first contributions:

$$\begin{aligned}
 p(T) &= \frac{8\pi^2}{45} T^4 [c_0 + c_2 g^2 + c_3 g^3 + \mathcal{O}(g^4)], \\
 c_0 &= 1 + \frac{21}{32} N_F, \\
 c_2 &= -\frac{15}{16\pi^2} \left(1 + \frac{5}{12} N_F\right), \\
 c_3 &= \frac{30}{8\pi^3} \left(1 + \frac{1}{6} N_F\right)^{3/2}.
 \end{aligned} \tag{1.8}$$

In the expansion (1.8) a term $\propto g^3$ enters, which is not an integer power of $\alpha_s = g^2/4\pi$ and appears due to the resummation of infrared divergent one-loop diagrams. There are many other indications that naïve perturbation theory breaks down at finite temperature, even if $g \ll 1$. For example, the thermal

self-energies Π are of order $g^2 T^2$. Thus, for soft momenta $p \sim gT$,⁷ the self-energy is of the same order as the bare inverse propagator

$$\Delta^{-1} = \Delta_0^{-1} + \Pi = p^2 + \Pi \sim (gT)^2 + (gT)^2. \quad (1.9)$$

In one-loop calculations, the loop integrals are dominated by hard momenta, but at higher loop order, internal lines may carry soft loop momenta. For such a situation with a soft internal loop momentum $p \sim gT$ one finds that

$$n_B(p) = \frac{1}{e^{p/T} - 1} \sim \frac{T}{p} \sim \frac{1}{g}, \quad (1.10)$$

where n_B denotes the Bose distribution function. Thus, the often employed relation between loop order and order in the coupling constant does not hold at finite temperature meaning that diagrams with an arbitrary high number of loops all may contribute to one certain order in the coupling. Hence, ordinary perturbation theory breaks down at the soft scale $p \sim gT$. This requires the resummation of these diagrams, which is a reorganization of the perturbative expansion, adapted to the thermal medium. Figuratively speaking, in this reorganized perturbation theory, the basis states for the perturbative expansion are medium-modified states, rather than the bare vacuum states. Braaten and Pisarski [BP90a] showed that this may be achieved by the resummation of the hard thermal loop (HTL) self-energies, which are the dominant parts of one-loop self-energies at soft momenta. This procedure may be formalized by the HTL Lagrangian [BP92]

$$\mathcal{L}_{HTL} = \frac{3}{2} m_g^2 \text{tr} \left(F^{\mu\alpha} \left\langle \frac{v_\alpha v^\beta}{-(v \cdot D)^2} \right\rangle F_{\mu\beta} \right) + m_f^2 \text{tr} \left(\bar{\psi} \left\langle \frac{\not{v}}{v \cdot D} \right\rangle \psi \right), \quad (1.11)$$

with the covariant derivative D_μ introduced above and the light-like 4-vector of the group velocity $v^\mu = (i, \hat{\mathbf{k}})$ with $v^2 = 0$. The thermal gluon and quark masses read $m_g^2 = g^2 T^2 (N_c + N_F/2)/6$ and $m_f^2 = C_R g^2 T^2/8$. The traces tr are taken over the color or flavor indices respectively and the angular average over the loop momenta is denoted by

$$\langle f(K) \rangle = \int \frac{d\Omega_{\mathbf{k}}}{4\pi} f(K).$$

One may introduce the effective theory by the formal decomposition

$$\mathcal{L}_{QCD} = \left(\mathcal{L}_{QCD} + \mathcal{L}_{HTL} \right) - \mathcal{L}_{HTL} = \mathcal{L}_{eff} + \delta\mathcal{L}. \quad (1.12)$$

In Wilson's sense of the renormalization group, \mathcal{L}_{eff} describes an effective theory, where the hard degrees of freedom are integrated out. The counter term $\delta\mathcal{L} = -\mathcal{L}_{HTL}$ avoids double-counting. Expanding the effective Lagrangian perturbatively leads to tree-level propagators and vertices that already include the HTL's.

⁷The typical momentum in a plasma is, according to the equipartition theorem, of order $k \sim T$. These momenta are called hard momenta, in contrast to soft momenta $p \sim gT$ with $g \ll 1$.

HTL self-energies are the leading $g^2 T^2$ parts of one-loop self-energies and can be calculated from one-loop self-energies by several kinematic approximations employing that the soft external momentum is much smaller than the hard loop momentum k , ($p \sim gT$) \ll ($k \sim T$). These expressions appear in all amplitudes between N gluons and between a quark pair and $N - 2$ gluons, for all $N \geq 2$, especially in the proper quark and gluon self-energies. They satisfy tree-level-like Ward identities, connecting the different HTL self-energies [BP90b]. Although these amplitudes, such as the gluon self-energy, are in general gauge dependent, the HTL self-energies are inherently gauge independent, which can be shown by explicit calculation in different gauges. For a general proof of the gauge invariance of Green's functions in the HTL approximation, see [Kob91].

1.3.2 Quasi-Particle Description of Strongly Interacting Matter

The concept of quasi-particles turned out to be a powerful tool for describing strongly correlated systems. It is successfully used in condensed matter physics, where for example quantized lattice oscillations or spin-waves are described in a quasi-particle picture. The partition function reads for vanishing chemical potentials

$$Z(T, V) = \prod_{\alpha} (1 \mp e^{-\omega_{\alpha}/T})^{\pm 1} + Z_{int}, \quad (1.13)$$

where V is the volume and ω_{α} is the quasi-particle dispersion relation depending on a set of quantum numbers α describing the system. It is assumed that the quasi-particle excitations are weakly damped. Z_{int} encodes the weak residual interactions of the quasi-particles. From the partition function follows the thermodynamic potential via

$$\Omega(T, V) = -\frac{T}{V} \ln Z(T, V) \quad (1.14)$$

and other thermodynamic quantities are partial derivatives of the thermodynamic potential. The strong correlation effects of the strongly coupled system are encoded in the quasi-particle dispersion relations ω_{α} , which are the pole positions of resummed propagators. Thus, when the residual interaction is weak, the strongly coupled system may be described in terms of non-interacting quasi-particles with effective dispersion relations.

The Rossendorf quasi-particle model for strongly interacting matter uses quark and gluon quasi-particles as basic ingredients. The corresponding dispersion relations are derived from HTL-resummed propagators, approximated by the relevant asymptotic expressions in the vicinity of the light cone. In this limit, the self-energy contribution reduces to a simple, thermally generated mass term which is $\propto g^2 T^2$. This phenomenologically motivated quasi-particle model can also be derived by starting from the Φ functional representation of the thermodynamic potential and following a chain of certain approximations. Although the full Φ functional ansatz is inherently gauge invariant, by truncation of the

infinite series of skeleton diagrams gauge invariance is lost. Thus, it is necessary to employ gauge invariant dispersion relations, to restore the gauge invariance of the thermodynamic quantities (for details see [Blu07b]). On top of this, the running coupling g^2 is replaced by an effective coupling $G^2(T)$ to accommodate non-perturbative effects. This effective coupling is a suitable parametrization of the running coupling, which recovers the perturbative expressions at high temperature $T \gg T_c$. In the vicinity of T_c , the effective coupling is adjusted to lattice QCD calculations. There, the Rossendorf quasi-particle model successfully describes lattice QCD results for the EoS for various numbers of quark flavors [Blu05b].

However, since lattice calculations use unphysical large quark mass parameters, the resulting quasi-particle EoS has to be extrapolated to the physical quark masses. As the up and down quarks may be treated as (current) massless quarks, this procedure is dubbed chiral extrapolation. The quasi-particle dispersion relations and the effective coupling are the relevant ingredients for the quasi-particle model. Thus, in this work, the quark mass dependence of these quantities will be analyzed from first principle calculations in the framework of (perturbative) thermal QCD to yield a tool for a reliable chiral extrapolation.

Even if the dispersion relations entering the quasi-particle model are calculated perturbatively, the model itself has non-perturbative properties. An expansion of the thermodynamic state variables, say the pressure, contain contributions to all orders in the coupling g . In the vicinity of the transition region, which is relevant for heavy ion collisions, the coupling is not small. Thus, one has to study whether the perturbatively derived self-energies and dispersion relations of quarks and gluons, especially the leading HTL contributions are reliable when extrapolated to values of the coupling $g \sim 1$. This has been done by Peshier [Pes98b] and is recapitulated in this work, including the effects of finite bare quark masses. In this context one should mention, that perturbative expansions, which are extrapolated towards large coupling g give the best results, when the perturbative series is truncated at order $n^* \sim 1/g^2$ [Pes02].

Outline of this work

The motivation of this work is to attempt a systematic consideration of quark mass effects for quantities being of utmost importance for a thermo-field description of hot deconfined strongly interacting matter. The degrees of freedom are quarks and gluons. We are guided by the success of the quasi-particle model [Pes94, Pes96, Pes00a, Pes02, Blu05a, Blu05b] which relies on one-loop quantities, in particular the quark and gluon self-energies. To allow for a suitable chiral extrapolation of available lattice QCD results, one needs such an explicit dependence of the mentioned quantities on quark masses.

This work is organized as follows. In chapter 2 we give a general introduction to the formalism of thermal field theory. We present some facts about quark and gluon propagators and self-energies, focusing on the differences between the vacuum and thermal propagators. Additionally some aspects of the renor-

malization of the divergencies of the vacuum self-energies will be discussed in a mass dependent renormalization scheme. In chapter 3 we will analyze the mass dependence of the gauge boson self-energies and also the effects on the excitation spectra are discussed. We establish an approximation scheme that follows the main ideas of the HTL approximation, and is thus gauge invariant, but includes the effects of finite quark masses. In chapter 4 we study the effects of finite quark masses in the quark self-energies and dispersion relations. In both cases we emphasize on the asymptotic dispersion relations in the vicinity of the light cone. In chapter 5 we analyze some in-depth aspects of the asymptotic dispersion relations. We will expand the asymptotic masses in powers of m_q/T , which serves as a simple tool to perform the chiral extrapolation. In addition, we study the reliability of the gauge invariant asymptotic dispersion relations for a quasi-particle description of thermodynamic properties of the quark gluon plasma. The Appendices contain information on the used conventions and some general formulae such as color algebra, integrals, Feynman rules in Minkowski and Euclidean space etc. Additionally, we give details on the calculation of Matsubara sums and prove the gauge invariance of the asymptotic quark dispersion relation.

2 Thermal Field Theory and Self-Energies

In this chapter we give a short introduction to the formalism of quantum field theory at finite temperature, which is called thermal field theory (TFT), basically following [Bla02, LeB96]. Additionally, we establish some basic relations for the self-energies of the matter fields (quarks) and the gauge bosons (gluons), emphasizing especially the differences between the vacuum and finite temperature self-energies. Finally, we study some aspects of the renormalization of ultraviolet singularities that arise in the calculation of loop integrals, such as the self-energies and derive a formula for a mass dependent running coupling $\alpha_s(\kappa^2; m_q)$.

2.1 Imaginary Time Formalism

For a thermally equilibrated system in contact with a heat bath of fixed temperature $T = \beta^{-1}$ (canonical ensemble), the expectation value of an observable \mathcal{A} is given by

$$\langle \mathcal{A} \rangle_\beta = Z^{-1} \text{tr} \mathcal{A} e^{-\beta H}, \quad (2.1)$$

where Z is the partition function

$$Z(\beta) = \text{tr} e^{-\beta H} = \sum_n \langle \phi_n | e^{-\beta H} | \phi_n \rangle \quad (2.2)$$

with the Hamiltonian H and the trace tr summing over the states $|\phi_n\rangle$ that are accessible in the system. If there are conserved charges N_i in the system, the transition to the grand canonical ensemble is performed by introducing associated chemical potentials μ_i and replacing $H \rightarrow H - \mu_i N_i$ in eqs. (2.1) and (2.2). Then, the partition function does not only depend on the volume V of the system and the temperature T but also on the chemical potentials μ_i . It is straightforward to draw a formal analogy between the partition function (2.2) and the time evolution operator $\mathcal{U}(t, t_0) = \exp \{-i(t - t_0)H\}$. The Boltzmann factor $e^{-\beta H}$ can be understood as an evolution operator in imaginary time, keeping the real part of the time argument, which is now analytically continued to complex values, constant:

$$e^{-\beta H} = \mathcal{U}(t_0 - i\beta, t_0) =: \mathcal{U}(\beta). \quad (2.3)$$

The result of $\mathcal{U}(\beta)$ acting on an observable is

$$\mathcal{U}(-\beta) \mathcal{A}(t) \mathcal{U}(\beta) = \mathcal{A}(t - i\beta), \quad (2.4)$$

and \mathcal{U} operating on state vectors yields

$$\mathcal{U}(\beta) |\phi_n(0)\rangle = |\phi_n(\beta)\rangle. \quad (2.5)$$

In this sense, the right hand side of eq. (2.2) can be understood as transition amplitude from the state $|\phi_n(t=0)\rangle$ to $|\phi_n(t=i\beta)\rangle$. In analogy to ordinary vacuum quantum field theory – the states $|\phi_n\rangle$ are now represented by the field configurations $\phi(x)$ ¹ – the partition function has a path integral representation which is

$$Z(\beta) = \mathcal{N} \int_{\phi(0)=\phi(\beta)} [d\phi] \exp \left(- \int_0^\beta d\tau \int d^3x \mathcal{L}_E \right) \quad (2.6)$$

with the Euclidean Lagrangian \mathcal{L}_E and the functional integration $[d\phi]$ runs over all field configurations ϕ that satisfy the periodicity condition $\phi(0) = \phi(\beta)$.² The normalization constant \mathcal{N} drops out in the calculation of Green's functions, but has to be taken into consideration when calculating bulk thermodynamic properties. The Euclidean Lagrangian for a neutral scalar theory as an illustrative example reads

$$\mathcal{L}_E = \frac{1}{2}(\partial_\tau \phi)^2 + \frac{1}{2}(\nabla \phi)^2 + \frac{m^2}{2}\phi^2 + V(\phi) \quad (2.7)$$

with the interaction potential $V(\phi)$. By adding a source term $-j(x)\phi(x)$ to \mathcal{L}_E , where $j(x)$ is an external current, the partition function Z is turned into the generating functional $Z[j]$ of the imaginary-time Green's functions:

$$\langle T_\tau \phi(x_1) \phi(x_2) \dots \phi(x_n) \rangle_\beta = \frac{1}{Z} \text{tr} \{ e^{-\beta H} \phi(x_1) \phi(x_2) \dots \phi(x_n) \} \quad (2.8)$$

$$= \frac{1}{Z[0]} \frac{\delta^n Z[j]}{\delta j(x_1) \delta j(x_2) \dots \delta j(x_n)} \Big|_{j=0}, \quad (2.9)$$

where the imaginary time ordering operator T_τ arranges the operators on the right of it in a way of decreasing imaginary time argument from left to right and $x = (t_0 - i\tau, \mathbf{x})$ with $0 \leq \tau \leq \beta$, and $\phi(x)$ is a field operator in the Heisenberg representation

$$\phi(\tau, \mathbf{x}) = e^{\tau H} \phi(0, \mathbf{x}) e^{-\tau H}. \quad (2.10)$$

In eq. (2.8), the Green's function is calculated via the operator formalism, while eq. (2.9) refers to the path integral formalism. Although both approaches are equivalent, some properties of the thermal Green's functions can be easier derived in the one or the other approach. The 2-point function or imaginary time propagator is defined by

$$\Delta(\tau, \mathbf{x}) = \langle T_\tau \phi(\tau, \mathbf{x}) \phi(0) \rangle_\beta \quad (2.11)$$

¹ $x = (t, \mathbf{x})$, see Appendix A for notations and conventions.

²For illustratory purposes bosonic degrees of freedom are considered here. For fermionic fields ψ one has to require anti-periodicity, $\psi(0) = -\psi(\beta)$.

and satisfies the periodicity condition³

$$\Delta(\tau - \beta) = \Delta(\tau) \quad (2.12)$$

for τ in the interval $[0, \beta]$ which can be derived using the cyclicity of the trace in the operator formulation. This periodicity allows the representation of $\Delta(\tau)$ by a discrete Fourier series as

$$\Delta(\tau) = \frac{1}{\beta} \sum_n e^{-i\omega_n \tau} \Delta(i\omega_n), \quad (2.13)$$

where the frequencies $\omega_n = \frac{2\pi n}{\beta}$, with integer n , are called Matsubara frequencies. The propagator can be easily calculated for a noninteracting system, when $V(\phi) = 0$. The free propagator Δ_0 is then derived from the generating functional via eq. (2.9) using standard methods, and it satisfies the equation of motion

$$\left(-\partial_\tau^2 - \partial_{\mathbf{x}}^2 + m^2 \right) \Delta_0(\tau, \mathbf{x}) = \delta(\tau) \delta(\mathbf{x}). \quad (2.14)$$

This equation is solved using the Fourier representation (2.13). One obtains in Fourier space

$$\Delta_0(i\omega_n, \mathbf{k}) = \frac{1}{\omega_n^2 + \omega_k^2} \quad (2.15)$$

with $\omega_k = \sqrt{\mathbf{k}^2 + m^2}$. This is the free imaginary time or Matsubara propagator in momentum space, which is only defined over the discrete set of Matsubara frequencies ω_n . When calculating perturbative loop corrections in an interacting theory, it is therefore evident that the integral over the time component of the 4-momentum K has to be replaced by a sum over these discrete Matsubara frequencies:

$$\int \frac{d^4 K}{(2\pi)^4} \rightarrow T \sum_{n=-\infty}^{\infty} \int \frac{d^3 k}{(2\pi)^3}. \quad (2.16)$$

One method to evaluate these frequency sums using contour integration techniques is described in Appendix C.

2.2 Paths in the Complex Time Plane

Until now, the real part of the complex time argument was always kept constant, thus only static properties of the medium are described. Since we are finally interested in the dynamics of the system, we have to relax this constraint. In doing so, one always has to specify the path followed in the complex time plane. The path ordered propagator is then defined by

$$\Delta_C(x) = \langle T_C \phi(x) \phi(0) \rangle_\beta \quad (2.17)$$

$$= \theta_C(x_0) \Delta^>(x) + \theta_C(-x_0) \Delta^<(x), \quad (2.18)$$

³Focusing on the temporal properties of the propagators, the spatial coordinates are not noted explicitly for the sake of simplicity.

with $x_0 = t + i\tau$, and the path ordering operator $T_{\mathcal{C}}$ is the generalization of the time ordering operator T_{τ} . It orders operators along the path \mathcal{C} chosen in the complex x_0 plane. One may specify a monotonically increasing parameterization of the time path by $x_0 = x_0(v)$. With $x_{0,1} = x_0(v_1)$, $x_{0,2} = x_0(v_2)$ one has

$$\theta_{\mathcal{C}}(x_{0,2} - x_{0,1}) = \theta(v_2 - v_1). \quad (2.19)$$

The 2-point correlation functions $\Delta^{\lessgtr}(x)$ are given by

$$\Delta(x)^{>} = \langle \phi(x)\phi(0) \rangle_{\beta}, \quad (2.20)$$

$$\Delta(x)^{<} = \langle \phi(0)\phi(x) \rangle_{\beta}. \quad (2.21)$$

To have the propagator in eq. (2.18) well defined, the imaginary part of x_0 must not increase along the path \mathcal{C} [LeB96]. Using the cyclicity of the trace, one can derive the Kubo-Martin-Schwinger (KMS) relation, connecting the 2-point correlators $\Delta^{>}$ and $\Delta^{<}$:

$$\Delta^{>}(x_0, \mathbf{x}) = \Delta^{<}(x_0 + i\beta, \mathbf{x}). \quad (2.22)$$

This implies for the Fourier transforms

$$\Delta^{\lessgtr}(K) = \int d^4x e^{iKx} \Delta^{\lessgtr}(x) \quad (2.23)$$

the KMS relation in momentum space

$$\Delta^{>}(K) = e^{\beta k_0} \Delta^{<}(K). \quad (2.24)$$

The spectral density is defined by

$$\varrho(K) := \Delta^{>}(K) - \Delta^{<}(K) \quad (2.25)$$

and can also be written as the expectation value of the commutator of field operators. Therefore, ϱ is real and has some additional properties:

$$\varrho(-k_0) = -\varrho(k_0), \quad (2.26)$$

$$\text{sgn}(k_0)\varrho(k_0) \leq 0, \quad (2.27)$$

$$\int_{-\infty}^{\infty} \frac{dk_0}{2\pi} k_0 \varrho(k_0) = 1. \quad (2.28)$$

The sum rule (2.28) is a direct implication of the equal time commutation relations of the field operators. The spectral density contains the full information on the interactions in the system, and all propagators can be retrieved from it. In this sense, it comprises only information about the defining differential equation for Green's functions. In contrast to ϱ , the propagators contain additional information on the specific boundary conditions [Pes98b]. In this sense, the boundary conditions are incorporated in the spectral representations of the propagators, but not in the spectral density itself. Combining eqs. (2.24) and

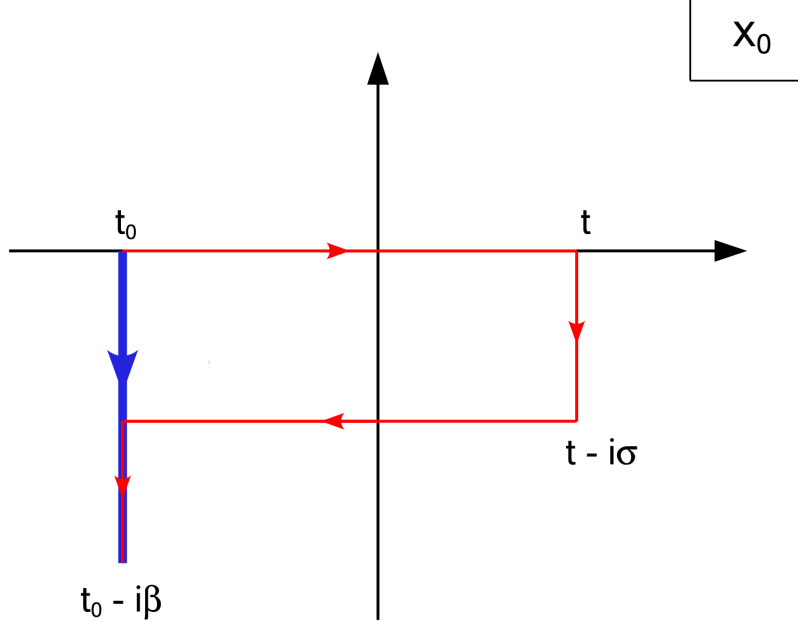


Figure 2.1: Different choices of the path in the complex time plane. The blue straight path from t_0 to $t_0 - i\beta$ is called Matsubara contour. The corresponding Feynman rules are the rules in the imaginary time formalism. The red contour from t_0 to t along the real axis, then to $t - i\sigma$, $t_0 - i\sigma$ and finally to $t_0 - i\beta$, with $0 < \sigma < \beta$, is called the Keldysh contour and leads to Feynman rules in the real time formalism. Since this contour goes along the real time axis, it is possible to determine dynamical quantities immediately. The choice of σ determines the structure of the real time propagators; a commonly used value is $\sigma = \beta/2$. For details about the RTF cf. [Alt93, LeB96].

(2.25) one recovers the 2-point correlation functions $\Delta^{\lessgtr}(K)$ from the spectral density

$$\Delta^>(K) = (1 + f(K))\varrho(K), \quad (2.29)$$

$$\Delta^<(K) = f(K)\varrho(K) \quad (2.30)$$

with $f(K) = (e^{\beta k_0} - 1)^{-1}$ (cf. Appendix A). The spectral representation of the path ordered propagator reads

$$\Delta_C(x) = \int \frac{d^4 K}{(2\pi)^4} e^{-iKx} \varrho(K) \{ \theta_C(x_0) + f(K) \}. \quad (2.31)$$

In addition, one has to specify the path in the complex time plane, with the constraint that along the path the imaginary part of the complex time argument must not increase. The easiest choice one could make is the so called Matsubara contour, which starts at t_0 and goes straight down to $t_0 - i\beta$, cf. fig. 2.1. Using this path in eq. (2.31), one obtains the spectral representation of the imaginary time or Matsubara propagator as

$$\Delta(i\omega_n, \mathbf{k}) = \int_{-\infty}^{\infty} \frac{d\omega}{2\pi} \frac{\varrho(\omega, \mathbf{k})}{\omega - i\omega_n} \quad \text{with } \omega_n = 2\pi nT. \quad (2.32)$$

According to eq. (2.32), the Fourier coefficient $\Delta(i\omega_n, \mathbf{k})$ can be regarded as the value of the function

$$\Delta^{\text{ana}}(k_0, \mathbf{k}) = \int_{-\infty}^{\infty} \frac{d\omega}{2\pi} \frac{\varrho(\omega, \mathbf{k})}{\omega - k_0}, \quad (2.33)$$

for $k_0 = i\omega_n$ and $\Im k_0 \neq 0$. This function is referred to as the analytic propagator. It is the unique continuation of the Matsubara propagator $\Delta(i\omega_n, \mathbf{k})$ towards arbitrary values of the energy k_0 and is analytic off the real energy axis. Using the analytic propagator, one can define the retarded and advanced propagators

$$\Delta^{\text{ret}}(k_0, \mathbf{k}) := \Delta^{\text{ana}}(k_0 + i0^+, \mathbf{k}), \quad (2.34)$$

$$\Delta^{\text{av}}(k_0, \mathbf{k}) := \Delta^{\text{ana}}(k_0 - i0^+, \mathbf{k}). \quad (2.35)$$

They describe the dynamical behavior of the system in real time, respecting causality. In the spectral representations, the causal behavior of the propagators is fixed by the infinitesimal imaginary part, i.e.

$$\Delta^{\text{ret}}(k_0, \mathbf{k}) = \int_{-\infty}^{\infty} \frac{d\omega}{2\pi} \frac{\varrho(\omega, \mathbf{k})}{\omega - (k_0 + i0^+)}. \quad (2.36)$$

By means of the previous equations, the retarded propagator can be obtained from the Matsubara propagator by analytical continuation via

$$\Delta(i\omega_n, \mathbf{k}) \xrightarrow{i\omega_n \rightarrow k_0 + i0^+} \Delta(k_0 + i0^+, \mathbf{k}) = \Delta^{\text{ret}}(k_0, \mathbf{k}). \quad (2.37)$$

Similar relations also hold for the finite temperature self-energies. Using this prescription, it is possible to extend results which have been calculated with the imaginary time formalism (ITF), and do not describe dynamical properties, to real times or energies, respectively. This continuation must not be performed, before all Matsubara sums have been evaluated.

In summary the Feynman rules in the ITF are the same ones as in the 4-dimensional Euclidean vacuum quantum field theory, apart from the fact that the free imaginary time propagator

$$\Delta_0(i\omega_n, \mathbf{k}) = \frac{1}{\omega_n^2 + \omega_k^2} \quad (2.38)$$

with $\omega_k = \sqrt{\mathbf{k}^2 + m^2}$ is only defined at discrete Matsubara frequencies $\omega_n = 2n\pi T$. Consequently, the loop integration over intermediate particle states has to be replaced according to

$$\int \frac{d^4 K}{(2\pi)^4} \longrightarrow T \sum_n \int \frac{d^3 k}{(2\pi)^3}. \quad (2.39)$$

The ITF Feynman rules for realistic quantum field theories, such as QCD or QED, containing spinor and vector fields as fundamental degrees of freedom can be obtained by plugging the corresponding Lagrangian in Euclidean

spacetime into the path integral representation of the partition function (2.6), adding source terms for every field and functional variation with respect to the sources according to eq. (2.9). For bosonic degrees of freedom, one has to require periodicity in imaginary time with period β , but for fermions one has to demand anti-periodicity,

$$\psi(0) = -\psi(\beta), \quad (2.40)$$

due to the anti-commutation relation of the fermionic fields ψ , in contrast to the commutation relations for bosons. Despite of additional spinor or tensor structures, all free propagators for realistic quantum field theories can be linked to the scalar thermal propagator given in eq. (2.38). However, for fermions, the thermal propagator is not defined at the even bosonic Matsubara frequencies but rather for the odd fermionic energies

$$\omega_n = (2n + 1)\pi T, \quad (2.41)$$

which is the direct implication of the antiperiodic boundary conditions in imaginary time. In order to clarify the difference between bosonic and fermionic particles, the bosonic scalar propagators will be denoted by Δ_B and the fermionic scalar propagators by Δ_F in the following.

2.3 The Gluon Self-Energy

The self-energy tensor⁴ $\Pi_{\mu\nu}$ of a gauge boson is related to the inverse full $(i\mathcal{D})_{\mu\nu}^{-1}$ and bare $(i\mathcal{D}_0)_{\mu\nu}^{-1}$ propagators by the Dyson equation

$$\Pi_{\mu\nu} = i\mathcal{D}_{\mu\nu}^{-1} - i\mathcal{D}_{0\mu\nu}^{-1}. \quad (2.42)$$

The propagator and the self-energy satisfy certain fundamental constraints. This is necessary since the propagators are expectation values of field operators that may contain unphysical degrees of freedom, in the case of gauge bosons. Thus, propagators and self-energies may contain redundant information, too. Current conservation in momentum space requires that $\Pi_{\mu\nu}(K)$ is transverse to the gauge boson 4-momentum K^μ ,

$$K^\mu \Pi_{\mu\nu}(K) = 0, \quad (2.43)$$

which holds both in Abelian and non-Abelian gauge theories,⁵ and the propagator obeys

$$K^\mu K^\nu \mathcal{D}_{\mu\nu} = \rho \quad (2.44)$$

with the gauge fixing parameter ρ for covariant gauges⁶. In the vacuum, the gauge boson polarization tensor is a linear combination of the tensors $g_{\mu\nu}$ and

⁴Gauge group indices are omitted often for notational simplicity and are noted explicitly only if necessary.

⁵In fact, at finite temperature, eq. (2.43) is generally not satisfied beyond one-loop order, except in ghost-free gauges such as axial gauges [Fle95, Kaj85].

⁶For Feynman gauge $\rho = 1$.

$K_\mu K_\nu$. Therefore, it only depends on one scalar function $\Pi(K^2)$, which itself depends on the Lorentz invariant quantity $K^2 \equiv K_\mu K^\mu$. The Ward identity eq. (2.43) implies that $\Pi_{\mu\nu}$ has the structure

$$\Pi_{\mu\nu} = \left(g_{\mu\nu} - \frac{K_\mu K_\nu}{K^2} \right) \Pi(K^2) = \mathcal{P}_{\mu\nu} \Pi(K^2) \quad (2.45)$$

with the 4-dimensional transversal projector $\mathcal{P}_{\mu\nu}$, obeying $\mathcal{P}_{\mu\nu} \mathcal{P}^{\nu\lambda} = \mathcal{P}_\mu^\lambda$. At finite temperature or density, the thermal medium defines a local rest frame with 4-velocity u_μ which breaks the Lorentz symmetry $O(1,3)$ of the vacuum to an $O(3)$ rotational symmetry. The general representation of an $O(3)$ symmetric tensor, however, requires a larger tensor basis, which might be extended by including tensor structures such as $u_\mu u_\nu$ and $P_\mu u_\nu + P_\nu u_\mu$. However, it is more convenient to use another tensor basis being more adapted to the physical degrees of freedom, namely the two orthogonal tensors

$$\begin{aligned} \mathcal{P}_{\mu\nu}^T &= g_{\mu\nu} - \frac{K_\mu K_\nu}{K^2} - \frac{\mathcal{P}_{\mu\nu}^L}{-N^2}, \\ \mathcal{P}_{\mu\nu}^L &= -N_\mu N_\nu \quad \text{with} \quad N_\mu = \frac{K_\mu(Ku) - u_\mu K^2}{(Ku)^2 - K^2} \end{aligned} \quad (2.46)$$

with $K^\mu N_\mu = 0$ and $K^\mu \mathcal{P}_{\mu\nu}^{T/L} = 0$, so that they are 4-dimensionally transversal. The superscripts T and L introduced in eq. (2.46) indicate that these tensors project on the subspace transverse respectively longitudinal to the 3-momentum \mathbf{k} . Additionally they satisfy

$$\begin{aligned} \mathcal{P}_{\mu\nu} &= \mathcal{P}_{\mu\nu}^T - \frac{\mathcal{P}_{\mu\nu}^L}{-N^2}, \\ \mathcal{P}_{\mu\alpha} \mathcal{P}^{\alpha\nu} &= \mathcal{P}_\mu^\nu, \\ \mathcal{P}_{\mu\alpha}^T \mathcal{P}^{T\alpha\nu} &= \mathcal{P}_\mu^{T\nu}, \\ \mathcal{P}_{\mu\alpha}^L \mathcal{P}^{L\alpha\nu} &= -N^2 \mathcal{P}_\mu^{L\nu}, \\ \mathcal{P}_{\mu\alpha}^T \mathcal{P}^{\alpha\nu} &= \mathcal{P}_\mu^{T\nu}, \\ \mathcal{P}_{\mu\alpha}^L \mathcal{P}^{\alpha\nu} &= \mathcal{P}_\mu^{L\nu}, \\ \mathcal{P}_{\mu\alpha}^T \mathcal{P}^{L\alpha\nu} &= 0 \\ \text{tr} \mathcal{P}^T &= \mathcal{P}_\mu^{T\mu} = 2, \\ \text{tr} \mathcal{P}^L &= \mathcal{P}_\mu^{L\mu} = \frac{P^2}{p^2}. \end{aligned} \quad (2.47)$$

In the rest frame of the medium $u_\mu = (1, 0, 0, 0)$ and we find $-N^2 = K^2/k^2$. To complete the set of projectors, we define the 4-dimensional longitudinal projector

$$\mathcal{E}_{\mu\nu} = \frac{K_\mu K_\nu}{K^2} \quad (2.48)$$

which satisfies

$$\begin{aligned} \mathcal{E}_{\mu\alpha} \mathcal{E}^{\alpha\nu} &= \mathcal{E}_\mu^\nu \\ \mathcal{E}_{\mu\alpha} \mathcal{P}^{\alpha\nu} &= \mathcal{E}_{\mu\alpha} \mathcal{P}^{T\alpha\nu} = \mathcal{E}_{\mu\alpha} \mathcal{P}^{L\alpha\nu} = 0. \end{aligned} \quad (2.49)$$

With the projectors defined in eq. (2.46), we can write for the thermal self-energies

$$\Pi_{\mu\nu}(k_0, k) = \mathcal{P}_{\mu\nu}^T \Pi_T(k_0, k) + \mathcal{P}_{\mu\nu}^L \Pi_L(k_0, k). \quad (2.50)$$

The functions Π_T and Π_L are called transverse and longitudinal self energy, respectively, which depend in the rest frame of the medium on both, $k_0 = Ku$ and $|\mathbf{k}| = ((Ku)^2 - K^2)^{1/2}$ separately due to the lack of Lorentz invariance. From (2.50) we obtain

$$\Pi_L = -\Pi_{00}, \quad (2.51)$$

$$\Pi_T = \frac{1}{2} \left(\Pi_\mu^\mu - \frac{K^2}{k^2} \Pi_L \right) \quad (2.52)$$

by utilizing the properties of the projectors $\mathcal{P}_{\mu\nu}^{T/L}$, where Π_{00} denotes the time-time component and Π_μ^μ the trace of $\Pi_{\mu\nu}$.

In the given notation, the bare propagator reads

$$i\mathcal{D}_{0\mu\nu}(K) = \frac{1}{K^2} (\mathcal{P}_{\mu\nu} + \rho \mathcal{E}_{\mu\nu}) \quad (2.53)$$

with the gauge fixing parameter ρ . Utilizing the Dyson equation (2.42), one derives the full thermal gauge boson propagator

$$i\mathcal{D}_{\mu\nu}(K) = \mathcal{P}_{\mu\nu}^T \Delta_T + \mathcal{P}_{\mu\nu}^L \frac{k^4}{K^4} \Delta_L + \rho \mathcal{E}_{\mu\nu}, \quad (2.54)$$

$$\text{with} \quad \Delta_T = \frac{1}{K^2 - \Pi_T}, \quad \Delta_L = \frac{1}{\mathbf{k}^2 - \Pi_L}. \quad (2.55)$$

The first term Δ_T describes the propagation of the $\text{tr } \mathcal{P}^T = 2$ transverse vacuum modes in the thermal medium. The longitudinal mode, denoted by Δ_L , does not exist in the vacuum and represents a collective or correlation effect.

2.4 The Quark Self-Energy

For quarks, the self-energy is defined as the difference between the full $i\mathcal{S}^{-1}$ and bare $i\mathcal{S}_0^{-1}$ inverse propagators via the fermionic Dyson equation

$$\Sigma = i\mathcal{S}^{-1} - i\mathcal{S}_0^{-1}. \quad (2.56)$$

At finite temperature, the 4-velocity u_μ of the plasma breaks again the Lorentz symmetry of the vacuum, and the fermion self-energy is in general a linear combination of the matrices $\mathbf{1}$, \not{K} , \not{u} and the commutator $[\not{K}, \not{u}]$. At the one-loop level, terms proportional to $[\not{K}, \not{u}]$ are not generated [Wel82]. In the rest frame of the medium, where $u_\mu = (1, 0, 0, 0)$, the self-energy can be decomposed into

$$\Sigma(p_0, \mathbf{p}) = \gamma_0 K_0(p_0, \mathbf{p}) - \vec{\gamma} \mathbf{p} K(p_0, \mathbf{p}) - m Z(p_0, \mathbf{p}), \quad (2.57)$$

where we separated the temporal and spatial γ -matrices. The three scalar self-energy functions depend separately on the temporal component and on

the absolute value of the spatial components of the 4-momentum. Thus, we obtain the inverse dressed propagator by utilizing the Dyson equation (2.56) and the free propagator (B.2):

$$i\mathcal{S}^{-1}(P) = \gamma_0(p_0 + K_0) - \vec{\gamma}\mathbf{p}(1 + K) - m(1 + Z). \quad (2.58)$$

Inversion gives the result

$$\mathcal{S} = i \frac{\gamma_0(p_0 + K_0) - \vec{\gamma}\mathbf{p}(1 + K) + m(1 + Z)}{(p_0 + K_0)^2 - p^2(1 + K)^2 - m^2(1 + Z)^2}. \quad (2.59)$$

Chiral Limit

In the chiral limit, where all quarks are massless, the projectors onto positive and negative energy states are defined by

$$\Lambda^\pm = \frac{1}{2}(1 \pm \gamma_0 \vec{\gamma} \hat{\mathbf{p}}). \quad (2.60)$$

In addition, the Λ^\pm project on states of positive/negative helicity over chirality and satisfy

$$\Lambda^+ \Lambda^+ = \Lambda^+, \quad (2.61)$$

$$\Lambda^- \Lambda^- = \Lambda^-, \quad (2.62)$$

$$\Lambda^+ \Lambda^- = 0, \quad (2.63)$$

$$\gamma_0 \Lambda^\pm \gamma_0 = \Lambda^\mp. \quad (2.64)$$

Employing these projectors, the free propagator \mathcal{S}_0^{-1} can be decomposed according to

$$\mathcal{S}_0(\omega, p) = \frac{i\Lambda^+ \gamma_0}{\omega - p} + \frac{i\Lambda^- \gamma_0}{\omega + p}, \quad (2.65)$$

as well as the self energy

$$\Sigma(\omega, p) = \Sigma_+(\omega, p) \gamma_0 \Lambda^+ + \Sigma_-(\omega, p) \gamma_0 \Lambda^- \quad (2.66)$$

with

$$\Sigma_\pm(\omega, p) = K_0(\omega, p) \mp p K(\omega, p) \quad (2.67)$$

and the dressed propagator

$$\mathcal{S}(\omega, p) = \frac{i\Lambda^+ \gamma_0}{\omega - p + \Sigma_+} + \frac{i\Lambda^- \gamma_0}{\omega + p + \Sigma_-}. \quad (2.68)$$

Explicitly Broken Chiral Symmetry

When the quark masses are nonzero, the projectors on positive and negative energy states read

$$\Lambda_{\mathbf{p}}^\pm = \frac{1}{2} \left(1 \pm \gamma_0 \frac{\vec{\gamma} \mathbf{p} + m}{\epsilon_{\mathbf{p}}} \right), \quad (2.69)$$

which satisfy

$$\Lambda_{\mathbf{p}}^+ \Lambda_{\mathbf{p}}^+ = \Lambda_{\mathbf{p}}^+, \quad (2.70)$$

$$\Lambda_{\mathbf{p}}^- \Lambda_{\mathbf{p}}^- = \Lambda_{\mathbf{p}}^-, \quad (2.71)$$

$$\Lambda_{\mathbf{p}}^+ \Lambda_{\mathbf{p}}^- = 0. \quad (2.72)$$

Utilizing these projectors, one can once again decompose the bare propagator into states with positive and negative energy solutions.

$$\mathcal{S}_0(\omega, p) = \frac{i\Lambda_{\mathbf{p}}^+ \gamma_0}{\omega - \epsilon_{\mathbf{p}}} + \frac{i\Lambda_{\mathbf{p}}^- \gamma_0}{\omega + \epsilon_{\mathbf{p}}}, \quad (2.73)$$

but the analog decomposition of the dressed propagator $\mathcal{S}(\omega, p)$ fails due to broken chiral symmetry. However, one might introduce new projectors, that already contain the medium modifications by analogy of the free and dressed inverse propagators

$$i\mathcal{S}_0^{-1}(\omega, p) = \omega\gamma_0 - \vec{\gamma}_i \hat{\mathbf{p}}_i p - m, \quad (2.74)$$

$$i\mathcal{S}^{-1}(\omega, p) = \Omega\gamma_0 - \vec{\gamma}_i \hat{\mathbf{p}}_i \mathcal{P} - \mathcal{M} \quad (2.75)$$

with

$$\Omega = \omega + K_0(\omega, p), \quad (2.76)$$

$$\mathcal{P} = p \left(1 + K(\omega, p) \right), \quad (2.77)$$

$$\mathcal{M} = m \left(1 + Z(\omega, p) \right), \quad (2.78)$$

$$\mathcal{E}_{\mathbf{p}} = \sqrt{\mathcal{P}^2 + \mathcal{M}^2}. \quad (2.79)$$

One obtains projectors

$$\Xi^{\pm} := \frac{1}{2} \left(1 \pm \gamma_0 \frac{\vec{\gamma}_i \hat{\mathbf{p}}_i \mathcal{P} + \mathcal{M}}{\mathcal{E}_{\mathbf{p}}} \right). \quad (2.80)$$

that decompose the dressed quark propagator:

$$\mathcal{S}(\omega, p) = \frac{i\Xi^+ \gamma_0}{\Omega - \mathcal{E}_p} + \frac{i\Xi^- \gamma_0}{\Omega + \mathcal{E}_p}. \quad (2.81)$$

In terms of the scalar self energy functions (2.57) one may write

$$\mathcal{S}(\omega, p) = \frac{i\Xi^+ \gamma_0}{\omega - p + \Sigma_+} + \frac{i\Xi^- \gamma_0}{\omega + p + \Sigma_-} \quad (2.82)$$

with

$$\begin{aligned} \Sigma_+(\omega, p) &= K_0 + p - \sqrt{p^2(1+K)^2 + m^2(1+Z)^2}, \\ \Sigma_-(\omega, p) &= K_0 - p + \sqrt{p^2(1+K)^2 + m^2(1+Z)^2}. \end{aligned} \quad (2.83)$$

2.5 Renormalization of UV-Divergencies

When computing thermal self-energies in perturbation theory, which means calculating loop diagrams at finite temperature, one encounters ultraviolet (UV) divergencies which must be taken care of. Self-energies can be decomposed into a temperature independent vacuum part stemming from vacuum fluctuations and an additional temperature part due to statistical fluctuations in the medium:

$$\Pi = \Pi^{T=0} + \Pi^T. \quad (2.84)$$

Fortunately, the medium part Π^T is not divergent [LeB96], so that renormalization of the vacuum part of the self-energy suffices to render the theory finite at non-zero temperature. The reason for this behavior is that the thermal distribution functions do not modify the theory at distances $\ll 1/T$, and thus the ultraviolet (short-distance) singularities are the same as at $T = 0$.

Chapters about renormalization of can be found in almost any textbook about quantum field theory, cf. [PS95, Ryd94, ItZ80]. For a very detailed analysis, with special focus on QCD, see [Muta87]. To handle the singularities of the vacuum self-energies, one has to regularize the loop integrals first. After that, the free parameters of the theory and the field amplitudes are redefined to absorb the singularities, which is called renormalization. QCD is a renormalizable quantum field theory: All divergencies in any order of perturbation theory can be absorbed into counter-terms that have the same structures which are also present in the bare Lagrangian.

The modern approach to regularization is the dimensional regularization. The loop integrals, which are divergent in four space-time dimensions, are finite in $D \neq 4$ dimension. Thus, one moves off from 4-dimensional space-time and replaces the integral d^4k by the D -dimensional one d^Dk . The D -dimensional integral is conveniently handled by performing a Wick rotation and solving the integral in D -dimensional Euclidean space. The loop integrals are finite in D dimensions, and the singularities show themselves in poles of the form

$$\Gamma(\epsilon - n) \simeq \frac{1}{\epsilon} + \text{finite terms} \quad (2.85)$$

with $\epsilon = (4 - D)/2$ and the Γ -function, with integer n .

To subtract the divergencies one defines the renormalization constants for the parameters g , m and ρ by

$$g = Z_g g_R, \quad \rho = Z_3 \rho_R, \quad m = Z_m m_R, \quad (2.86)$$

as well as for the gluon (A_κ^a), quark (ψ) and ghost (η^a) field strengths

$$A_\kappa^a = Z_3^{1/2} A_{\kappa,R}^a, \quad \psi = Z_2^{1/2} \psi_R, \quad \eta^a = \tilde{Z}_3^{1/2} \eta_R^a, \quad (2.87)$$

where renormalized quantities are denoted by a subscript R and are free of divergencies. The divergencies are subtracted at an arbitrary energy scale κ called the renormalization point. Any observable must not depend on κ , whereas the renormalized parameters, like g_R and m_R depend on κ . From the requirement that renormalized n -point Green's functions $F_n(p, g_R, m_R, \kappa)$ have

to be independent of the renormalization point, one obtains the renormalization group equation (RGE)

$$\kappa \frac{d}{d\kappa} F_n(p, g_R, m_R, \kappa) = 0, \quad (2.88)$$

which leads to RG equations – also called flow equations – for the renormalized coupling and masses:

$$\kappa \frac{d}{d\kappa} g_R = -g_R \frac{d \ln Z_g}{d\kappa} =: -g_R \gamma_g = \beta(g_R, m_R, \kappa), \quad (2.89)$$

$$\kappa \frac{d}{d\kappa} m_R = -m_R \frac{d \ln Z_m}{d\kappa} =: -m_R \gamma_m \quad (2.90)$$

with the anomalous dimensions γ_g (γ_m) of the coupling constant (masses), where we also introduced the β -function, which controls the response of the renormalized coupling to a change of the renormalization scale κ .

In order to fix the renormalization constants, one needs an additional prescription how to subtract the singularities which sets up a renormalization scheme [Cel79]. This is necessary, since the divergent loop integrals also contain finite contributions that may or may not be included in the definition of the renormalization constants.

A renormalization prescription that is commonly used nowadays is the Minimal Subtraction scheme (MS). In this scheme only the ϵ -pole contribution is subtracted and used to define the renormalization constants. In the modified minimal subtraction scheme (\overline{MS}), additional factors γ_E^7 and $\ln 4\pi$, that arise in the expansion of the Γ -function and the analytical continuation from D to 4 dimensions, are also absorbed into the renormalization constants. In these schemes, the counter terms and the β -function have very simple structure, since none of the finite parts of the self-energies are included in the renormalization constants. This feature forces these renormalization schemes to be mass independent, since the ϵ -pole and the constants are mass independent by definition. Thus, each fermion field contributes in the same way to the renormalization constants. This violates the Appelquist-Carazzone-theorem, which guarantees the decoupling of very massive fermions fields from Green's functions renormalized at scales much smaller than the heavy mass [App75, Edw82].

The advantage of the MS and \overline{MS} subtraction schemes is that the Slavnov-Taylor identities (see Appendix B.4) are satisfied automatically and the counter terms have simple structures, which simplifies the solution of the RGE (2.88) and the flow equations (2.89) and (2.90).

Another possibility of subtraction is the momentum-space subtraction scheme (MOM). In this scheme, the complete self-energy is subtracted at an arbitrary Euclidean momentum $p^2 = -\kappa^2 < 0$.⁸ This way, the renormalization constants obtain a mass dependence and the Appelquist-Carazzone-theorem is satisfied. It is a drawback of mass dependent renormalization schemes that the β -function depends on the 3-point vertex that is used to define the renormalization constants, even the lowest order coefficient β_0 [Nac78], which breaks the

⁷ $\gamma_E \approx 0.577\,215\,664 \dots$ is the Euler Constant.

⁸This corresponds to processes where t-channel contributions dominate, since the according Mandelstam variable is negative.

Slavnov-Taylor identities. However, the deviations among the couplings defined through different vertices are vanishingly small [Smi01]. Politzer [Pol78] showed that the scheme dependence of the β -function, even in the lowest order perturbation theory, on the specified vertex, is a generic feature, when quantities of the same dimension as the renormalization scale enter the β -function. However, renormalizability ensures that any consistent prescription will lead to the same physical prescription, whether the β -functions are the same or not. The question whether one particular prescription is better than others can only be answered by calculation of higher order terms [Moo77].⁹

2.6 Mass Dependent Running Coupling

We choose a mass dependent renormalization scheme, defining the renormalization constants for the field strengths and the coupling constant at an arbitrary Euclidean off-shell momentum κ^2 (MOM). The renormalized masses are defined via an on-shell renormalization, where the divergencies are subtracted at the pole position of the quark propagator. Thus, the renormalized masses are fixed constants, i.e. there is no flow equation for the renormalized masses in this scheme. De Rújula and Georgi [DeR76] argued that this makes sense to any finite order in perturbation theory, even if free quarks do not exist.

Using these renormalization prescriptions, the renormalization group equation for the truncated connected n -point Green's function $F_n(p, g_R, m_R, \kappa)$ reads

$$\left[\kappa \frac{\partial}{\partial \kappa} + \beta \left(g_R, \frac{m_R}{\kappa} \right) \frac{\partial}{\partial g_R} - n \gamma \left(g_R, \frac{m_R}{\kappa} \right) \right] F_n = 0. \quad (2.91)$$

The renormalized coupling constant satisfies the renormalization group equation

$$\kappa \frac{dg_R}{d\kappa} = \beta \left(g_R, \frac{m_R}{\kappa} \right). \quad (2.92)$$

For dimensional reasons, the β -function depends on the masses via the dimensionless ratio m_R/κ .

We choose to define the renormalization constant of the coupling constant Z_g by subtraction of the gluon-ghost-vertex. Thus, we utilize¹⁰

$$Z_g = \frac{\tilde{Z}_1}{\tilde{Z}_3 \sqrt{Z_3}}, \quad (2.93)$$

and obtain for the β -function the relation

$$\beta = g\kappa \frac{\partial}{\partial \kappa} \left(-\tilde{\delta}_1 + \tilde{\delta}_3 + \frac{1}{2} \delta_3 \right). \quad (2.94)$$

⁹Physical quantities calculated to all orders in perturbation theory are renormalization scheme independent. Truncated perturbative expansions exhibit renormalization scheme dependence. In the \overline{MS} scheme, the β -function depends on the subtracted vertices at three-loop and order.

¹⁰For definitions and relations among renormalization constants Z and counter terms δ , see Appendix B.4.

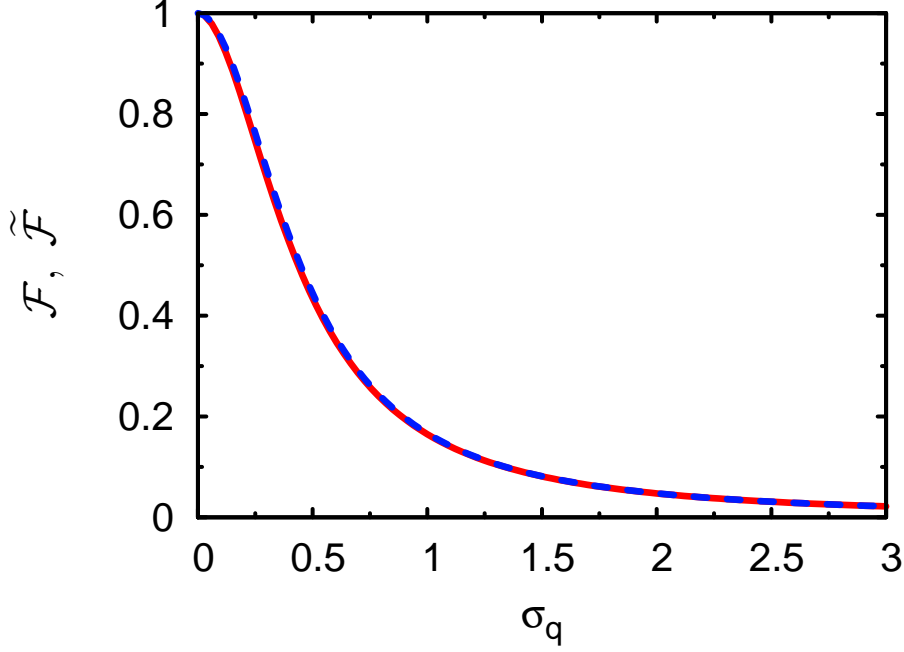


Figure 2.2: The function $\mathcal{F}(\sigma_q)$ (red, solid) and its approximation $\tilde{\mathcal{F}}(\sigma_q)$ (blue, dashed).

In lowest order perturbation theory the β -function reads in this particular scheme

$$\beta\left(g_R, \frac{m_R^q}{\kappa}\right) = \frac{g^3}{4\pi}\beta_0 + \mathcal{O}(g^5), \quad (2.95)$$

$$\beta_0 = -\frac{1}{12\pi} \left(11N_c - 2 \sum_q \mathcal{F}(\sigma_q) \right), \quad (2.96)$$

$$\mathcal{F}(\sigma_q) = 1 - 6\sigma_q^2 + \frac{12\sigma_q^4}{\sqrt{1+4\sigma_q^2}} \ln \left(\frac{\sqrt{1+4\sigma_q^2} + 1}{\sqrt{1+4\sigma_q^2} - 1} \right) \quad (2.97)$$

with $\sigma_q = m_R^q/\kappa$, and m_R^q is the renormalized quark mass, where the sum has to be taken over all quark flavors. Georgi and Politzer [Geo76] gave an approximation to the function \mathcal{F} that has the same limiting values for $\sigma_q \rightarrow 0$ and $\sigma_q \rightarrow \infty$; is accurate to a few percent in between. The approximation reads

$$\mathcal{F}(\sigma_q) \approx \frac{1}{1+5\sigma_q^2} =: \tilde{\mathcal{F}}(\sigma_q). \quad (2.98)$$

In fig. 2.2 the function \mathcal{F} and its approximation $\tilde{\mathcal{F}}$ are compared. One observes an almost perfect agreement within the displayed range of σ_q .

With the approximation (2.98), the flow equation for the running coupling (2.92) may be integrated by separation of variables. We use the definition $\alpha_s = g^2/4\pi$ and the initial value $\alpha(\kappa_0^2) = \alpha_0$. The result is

$$\alpha_s(\kappa^2) = \frac{\alpha_0}{1 + \frac{\alpha_0}{12\pi} \left[11N_c \ln \frac{\kappa^2}{\kappa_0^2} - 2 \sum_q \ln \frac{\kappa^2 + 5m_q^2}{\kappa_0^2 + 5m_q^2} \right]}. \quad (2.99)$$

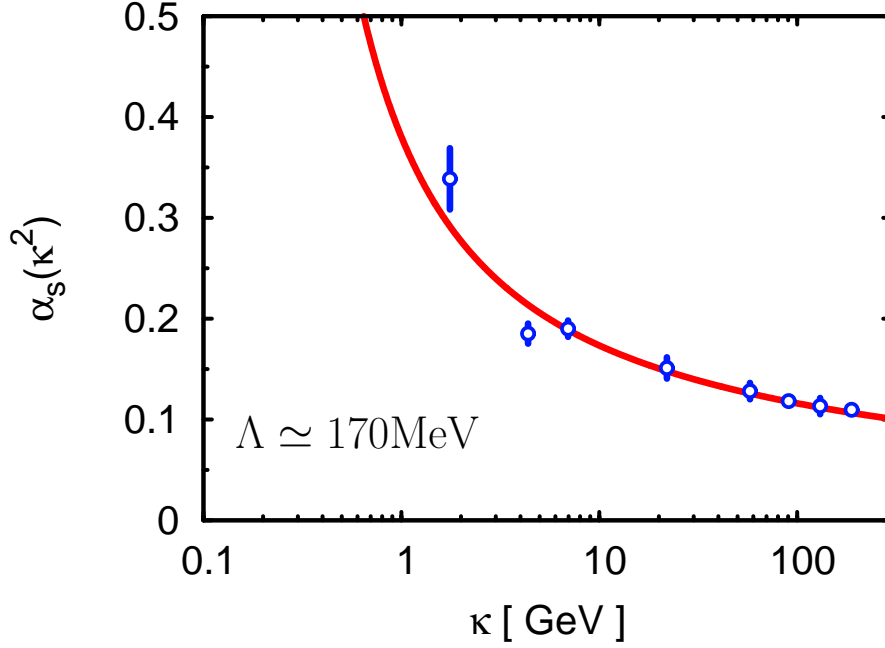


Figure 2.3: The running coupling (2.99) with the initial value $\alpha_s(M_Z = 91.1876 \text{ GeV}) = 0.1176$, utilizing the quark masses $m_{u,d} = 3 \text{ MeV}$, $m_s = 150 \text{ MeV}$, $m_c = 1.25 \text{ GeV}$, $m_b = 4.70 \text{ GeV}$ and $m_t = 174.0 \text{ GeV}$. The blue points show measured data of α_s including error-bars. For details concerning the data, see fig. 9.2 [RPP06].

The initial value α_0 has to be determined by experiment. Nowadays the best measurements are done at the mass of the weak Z -boson [RPP06]

$$\alpha_s(M_Z = 91.1876(21) \text{ GeV}) = 0.1176(20). \quad (2.100)$$

Fig. 2.3 shows the asymptotic freedom of QCD, that $\alpha_s \rightarrow 0$ as $\kappa^2 \rightarrow \infty$. For decreasing κ^2 the value of α_s increases and diverges at some point we call Λ . Using the quark masses and initial value α_0 as given in the caption of the figure, Λ may be estimated as $\Lambda \simeq 170 \text{ MeV}$. One might also use this pole as initial value, which then defines the scale parameter Λ via $\alpha_s^{-1}(\Lambda^2) = 0$. In this form, the running coupling reads

$$\alpha_s(\kappa^2) = 12\pi \left(11N_c \ln \frac{\kappa^2}{\Lambda^2} - 2 \sum_q \ln \frac{\kappa^2 + 5m_q^2}{\Lambda^2 + 5m_q^2} \right)^{-1}. \quad (2.101)$$

It remains to fix the physical scale to the arbitrary renormalization scale κ^2 . In deep-inelastic scattering experiments, the scale is usually fixed by the momentum transfer squared $\kappa^2 = Q^2$. It remains unclear at this point, which is the relevant scale for calculations at finite temperature. Some authors use the first positive, nonzero Matsubara frequency $\kappa = \pi T$ ($\kappa = 2\pi T$) for fermions (bosons) as the relevant temperature scale. Peshier [Pes06] pointed out, that there might be no universal coupling in a thermal medium, the correct scale

has to be related the specific quantity that is calculated, which is especially important for larger coupling.

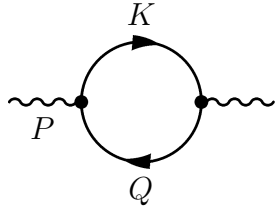
In the form given in (2.101), the running coupling of QCD explicitly depends on the bare quark masses. This dependence is needed to perform a reliable chiral extrapolation of the equation of state of strongly interacting matter within a quasi-particle model.

3 The Gluon Self-Energy

The only contribution to the gluon self-energy that includes mass effects at the one-loop order is the quark loop. In fact, we discover the same structure, apart from a global color factor that appears in the calculation of the photon self-energy at one-loop order. To study the effects of finite quark masses on the excitation spectra, we therefore first examine the photon self-energy and dispersion relations. We establish an approximation scheme which is a generalization of HTL, so that massive particles are allowed to appear in the loops (m HTL). Afterwards, we combine the derived results with the contributions from the gluonic self interactions of the Yang-Mills sector of the theory and calculate the complete gluon self-energy as well as the gluon dispersion relations.

3.1 The Photon Polarization Tensor

The starting point for the calculation of the one-loop photon self-energy tensor $\Pi_{\mu\nu}^\gamma$ is the following Feynman diagram

$$\Pi_{\mu\nu}^\gamma(P) = - \text{Diagram} \quad . \quad (3.1)$$


Using the Feynman rules for the ITF from Appendix B.2, one obtains

$$\Pi_{\mu\nu}^\gamma(P) = -e^2 T \sum_{\omega_n} \int \frac{d^3 k}{(2\pi)^3} \text{tr}[\gamma_\mu S(Q) \gamma_\nu S(K)] \quad (3.2)$$

with the fermion propagator $S(K) = (m - \not{K}) \Delta_F(K)$ and $Q = K - P$. The scalar fermionic propagator $\Delta_F(K) = [K^2 + m^2]^{-1}$ is only defined for the odd fermionic Matsubara frequencies $\omega_n = (2n + 1)\pi T$. Therefore, eq. (3.2) becomes

$$\Pi_{\mu\nu}^\gamma(P) = -e^2 T \sum_{\omega_n} \int \frac{d^3 k}{(2\pi)^3} \text{tr}[\gamma_\mu (m - \not{Q}) \gamma_\nu (m - \not{K})] \Delta_F(Q) \Delta_F(K). \quad (3.3)$$

The evaluation of the trace yields

$$\begin{aligned} \text{tr}[\gamma_\mu (m - \not{Q}) \gamma_\nu (m - \not{K})] &= m^2 \text{tr}[\gamma_\mu \gamma_\nu] + \text{tr}[\gamma_\mu \not{Q} \gamma_\nu \not{K}] \\ &= -4\delta_{\mu\nu} m^2 \\ &\quad + 4[K_\nu Q_\mu + K_\mu Q_\nu - (KQ)\delta_{\mu\nu}]. \end{aligned} \quad (3.4)$$

Within the hard thermal loop (HTL) approximation, i.e. when the external momentum $P \sim gT$ is small compared to the hard loop momentum $K \sim T$, we can safely neglect all terms $\propto P$ in eq. (3.4) and receive with $Q \simeq K$ approximately

$$\text{tr}[\gamma_\mu(m - \not{Q})\gamma_\nu(m - \not{K})] \simeq 8K_\mu K_\nu - 4\delta_{\mu\nu}(K^2 + m^2). \quad (3.5)$$

Using $k_4 = -\omega_n$ and $\epsilon_{\mathbf{k}}^2 = \mathbf{k}^2 + m^2$, we get for Π_{44}^γ

$$\begin{aligned} \Pi_{44}^\gamma(P) &= -4e^2 \int \frac{d^3k}{(2\pi)^3} T \sum_n (\omega_n^2 - \epsilon_{\mathbf{k}}^2) \Delta_F(K) \Delta_F(Q) \\ &= -4e^2 \int \frac{d^3k}{(2\pi)^3} T \sum_n (1 - 2\epsilon_{\mathbf{k}}^2 \Delta_F(K)) \Delta_F(Q), \end{aligned} \quad (3.6)$$

since $\omega_n^2 + \epsilon_{\mathbf{k}}^2 = \Delta_F^{-1}(K)$. For the trace we obtain

$$\begin{aligned} \Pi_\mu^{\gamma\mu} &= 8e^2 \int \frac{d^3k}{(2\pi)^3} T \sum_n (\omega_n^2 + \epsilon_{\mathbf{k}}^2 + m^2) \Delta_F(K) \Delta_F(Q) \\ &= 8e^2 \int \frac{d^3k}{(2\pi)^3} T \sum_n (1 + m^2 \Delta_F(K)) \Delta_F(Q). \end{aligned} \quad (3.7)$$

Utilizing the frequency sums from eqs. (C.11) and (C.13), the result is

$$\begin{aligned} \Pi_{44}^\gamma(\omega, p) &= -4e^2 \int \frac{d^3k}{(2\pi)^3} \left\{ \frac{1}{2\epsilon_{\mathbf{k}}} (1 - 2n_F(\epsilon_{\mathbf{k}})) \right. \\ &\quad + \frac{\epsilon_{\mathbf{k}}^2}{2\epsilon_{\mathbf{k}}\epsilon_{\mathbf{q}}} \left[(1 - n_F(\epsilon_{\mathbf{k}}) - n_F(\epsilon_{\mathbf{q}})) \left(\frac{1}{i\omega - \epsilon_{\mathbf{k}} - \epsilon_{\mathbf{q}}} - \frac{1}{i\omega + \epsilon_{\mathbf{k}} + \epsilon_{\mathbf{q}}} \right) \right. \\ &\quad \left. \left. + (n_F(\epsilon_{\mathbf{q}}) - n_F(\epsilon_{\mathbf{k}})) \left(\frac{1}{i\omega + \epsilon_{\mathbf{k}} - \epsilon_{\mathbf{q}}} - \frac{1}{i\omega - \epsilon_{\mathbf{k}} + \epsilon_{\mathbf{q}}} \right) \right] \right\}, \end{aligned} \quad (3.8)$$

$$\begin{aligned} \Pi_\mu^{\gamma\mu}(\omega, p) &= 8e^2 \int \frac{d^3k}{(2\pi)^3} \left\{ \frac{1}{2\epsilon_{\mathbf{k}}} (1 - 2n_F(\epsilon_{\mathbf{k}})) \right. \\ &\quad - \frac{m^2}{4\epsilon_{\mathbf{k}}\epsilon_{\mathbf{q}}} \left[(1 - n_F(\epsilon_{\mathbf{k}}) - n_F(\epsilon_{\mathbf{q}})) \left(\frac{1}{i\omega - \epsilon_{\mathbf{k}} - \epsilon_{\mathbf{q}}} - \frac{1}{i\omega + \epsilon_{\mathbf{k}} + \epsilon_{\mathbf{q}}} \right) \right. \\ &\quad \left. \left. + (n_F(\epsilon_{\mathbf{q}}) - n_F(\epsilon_{\mathbf{k}})) \left(\frac{1}{i\omega + \epsilon_{\mathbf{k}} - \epsilon_{\mathbf{q}}} - \frac{1}{i\omega - \epsilon_{\mathbf{k}} + \epsilon_{\mathbf{q}}} \right) \right] \right\} \end{aligned} \quad (3.9)$$

with $\epsilon_{\mathbf{q}}^2 = q^2 + m^2 = |\mathbf{k} - \mathbf{p}|^2 + m^2$. These formulae contain a thermal self-energy contribution, denoted by terms $\propto n_F$, and also the vacuum self-energy terms which do not depend on the thermal distributions for fermions and that do not vanish as $T \rightarrow 0$. The latter term is divergent and must be regularized according to section 2.5. However, as we are interested in the medium effects at finite temperature, we will now focus on the finite thermal contributions.

The Chiral Limit of the Photon Self-Energy

Before establishing an approximation scheme similar to HTL for massive loop fermions, we will first consider the chiral limit, where the usual HTL approx-

imation can be performed. In the chiral limit, the medium parts of the self-energy functions read

$$\begin{aligned} \Pi_{44}^\gamma(\omega, p) = & 4e^2 \int \frac{d^3k}{(2\pi)^3} \left\{ \frac{n_F(k)}{k} \right. \\ & + \frac{k^2}{2kq} \left[(n_F(k) + n_F(q)) \left(\frac{1}{i\omega - k - q} - \frac{1}{\omega + k + q} \right) \right. \\ & \left. \left. + (n_F(k) - n_F(q)) \left(\frac{1}{i\omega + k - q} - \frac{1}{i\omega - k + q} \right) \right] \right\}, \end{aligned} \quad (3.10)$$

$$\Pi_\mu^{\gamma\mu}(\omega, p) = -8e^2 \int \frac{d^3k}{(2\pi)^3} \frac{n_F(k)}{k} \quad (3.11)$$

with $q = |\mathbf{k} - \mathbf{p}|$. The HTL approximations can be found in textbooks such as [LeB96] and read

$$|\mathbf{k} - \mathbf{p}| \simeq k - px, \quad (3.12)$$

$$n_F(|\mathbf{k} - \mathbf{p}|) \simeq n_F(k - px) \simeq n_F(k) - \frac{dn_F}{dk} px. \quad (3.13)$$

Utilizing these with (3.10), the angular and k -integrations decouple and after the analytical continuation by replacing $i\omega \rightarrow p_0 + i0^{+1}$, one obtains

$$\begin{aligned} \Pi_{00}^\gamma(p_0, p) &= \frac{e^2}{\pi^2} \int_0^\infty dk k^2 \frac{dn_F}{dk} \int_{-1}^1 dx \frac{x^2}{x^2 - \xi^2} \\ &= \frac{1}{3} e^2 T^2 \left(1 - \frac{\xi}{2} \ln \frac{\xi + 1}{\xi - 1} \right), \end{aligned} \quad (3.14)$$

$$\Pi_\mu^{\gamma\mu} = \frac{1}{3} e^2 T^2 \quad (3.15)$$

with $\xi = p_0/p$. Utilizing (2.52) yields the transverse and longitudinal photon self-energies

$$\Pi_L^\gamma(\xi) = -\frac{1}{3} e^2 T^2 (1 - \xi Q_0(\xi)) = \frac{1}{3} e^2 T^2 Q_1(\xi), \quad (3.16)$$

$$\Pi_T^\gamma(\xi) = \frac{1}{3} e^2 T^2 (\xi^2 + \xi(\xi^2 - 1) Q_0(\xi)) \quad (3.17)$$

with the Legendre functions of the second kind

$$Q_0(\xi) = \frac{1}{2} \ln \frac{\xi + 1}{\xi - 1}, \quad Q_1(\xi) = \xi Q_0(\xi) - 1. \quad (3.18)$$

The real and imaginary parts of Π_L and Π_T , scaled by $m_\gamma^2 = \frac{1}{9} e^2 T^2$, are depicted in figs. 3.1 and 3.2, where they are compared to the full one-loop self-energies (cf. eqs. (3.40 - 3.43)). For a detailed discussion of the comparison of HTL and one-loop self-energies in the chiral limit, see [Pes98a]. The

¹The infinitesimal imaginary part $+i0^+$ is not noted explicitly in the following, but has to be kept in mind.

pronounced structures of the self-energies at the light cone ($p_0 \approx p \Rightarrow \xi \approx 1$), such as the pole of the real part or the discontinuity of the imaginary part of Π_L , originate from the Legendre function $Q_0(\xi)$. Expanding $Q_0(\xi)$ in the vicinity of the light cone, with $\xi = 1 + \delta$, yields

$$\frac{1}{2} \ln \frac{\xi + 1}{\xi - 1} \simeq \frac{1}{2} \left(\ln 2 - \ln \delta \right) + \frac{1}{4} \delta + \mathcal{O}(\delta^2), \quad (3.19)$$

where the term $\ln \delta$ produces the logarithmic singularity of the real part, as well as the imaginary part below the light cone and its discontinuity at $\xi = 1$:

$$\ln \delta = \ln |\delta| - i\pi\theta(-\delta). \quad (3.20)$$

In Π_L^γ , the relevant structure, apart from a constant, is

$$\begin{aligned} \xi Q_0(\xi) &\simeq \frac{\ln 2}{2} - \frac{1}{2} \ln |\delta| + \delta \left(\ln 2 + \frac{1}{2} \right) - \frac{\delta}{2} \ln |\delta| \\ &\quad - \frac{i\pi}{2} (1 + \delta) \theta(-\delta) + \mathcal{O}(\delta^2). \end{aligned} \quad (3.21)$$

The transverse self-energy Π_T^γ has a factor $\xi^2 - 1$ multiplied with the Legendre function, thus, the real part has no pole at $\xi = 1$, and the imaginary part is continuous:

$$\begin{aligned} \xi(\xi^2 - 1)Q_0(\xi) &\simeq (2 - \ln 2)\delta + \delta \ln \delta + \mathcal{O}(\delta^2) \\ &\simeq (2 - \ln 2)\delta + \delta \ln |\delta| - i\pi\delta\theta(-\delta) + \mathcal{O}(\delta^2). \end{aligned} \quad (3.22)$$

According to [Reb96], the origin of the logarithmic singularity at the light-cone is a collinear singularity, appearing when the hard loop momentum \mathbf{k} becomes parallel to the external momentum \mathbf{p} . Any mass for the hard modes in the loop would cut off this singularity.

The m HTL Approximation Scheme

Now we will establish an approximation scheme that will follow the main ideas of the HTL approximation, but includes an arbitrary fermion mass in the loop. This approximation scheme will be called m HTL approximation scheme. Following the ideas in [Alt92] the typical (hard) loop momentum is of order T , because of the thermal measure $\propto n_F$. Therefore, we can safely neglect the term $\sim p^2$ in $\epsilon_{\mathbf{q}} = \epsilon_{\mathbf{k}-\mathbf{p}}$ and expand the remaining part in a Taylor series in powers of p :

$$\begin{aligned} \epsilon_{\mathbf{q}} &= \sqrt{|\mathbf{k} - \mathbf{p}|^2 + m^2} = \sqrt{k^2 + m^2 - 2kp \cos \theta + p^2} \\ &\simeq \sqrt{k^2 + m^2 - 2kp \cos \theta} \\ &= \sqrt{k^2 + m^2} \sqrt{1 - 2 \frac{kp \cos \theta}{\epsilon_{\mathbf{k}}^2}} \\ &\simeq \epsilon_{\mathbf{k}} \left(1 - \frac{pk \cos \theta}{\epsilon_{\mathbf{k}}^2} \right) \\ &= \epsilon_{\mathbf{k}} - \frac{k}{\epsilon_{\mathbf{k}}} p \cos \theta = \epsilon_{\mathbf{k}} - v p x. \end{aligned} \quad (3.23)$$

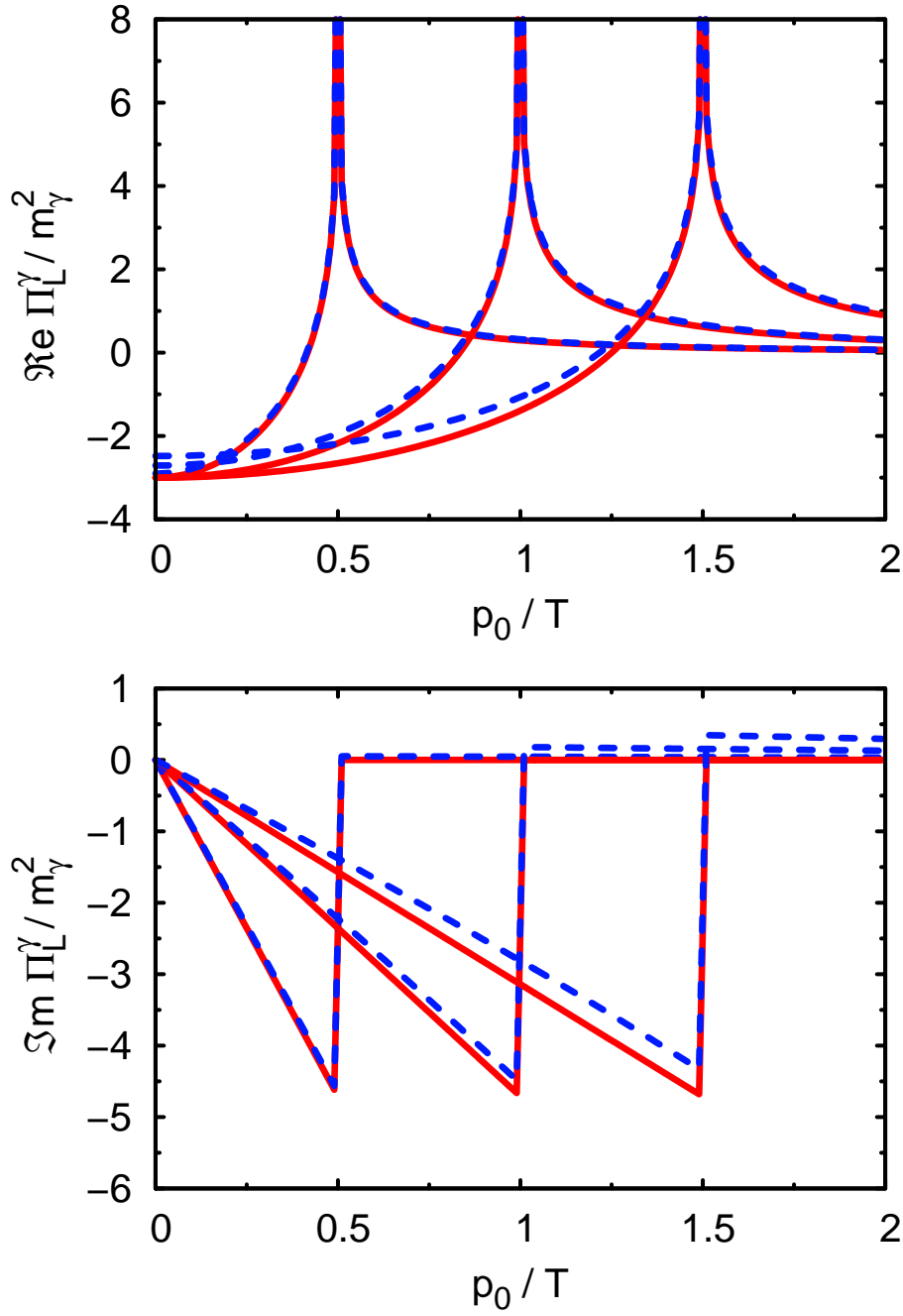


Figure 3.1: Real (upper panel) and imaginary parts (lower panel) of the longitudinal photon self-energy Π_L^γ in the chiral limit. The HTL approximation (red, solid) is compared to the full one-loop result (blue, dashed) for fixed values of $p/T = 0.5, 1.0, 1.5$ (from left to right). The ordinate is scaled by $m_\gamma^2 = \frac{1}{9}e^2T^2$, which is a typical scale for the photon self-energy.

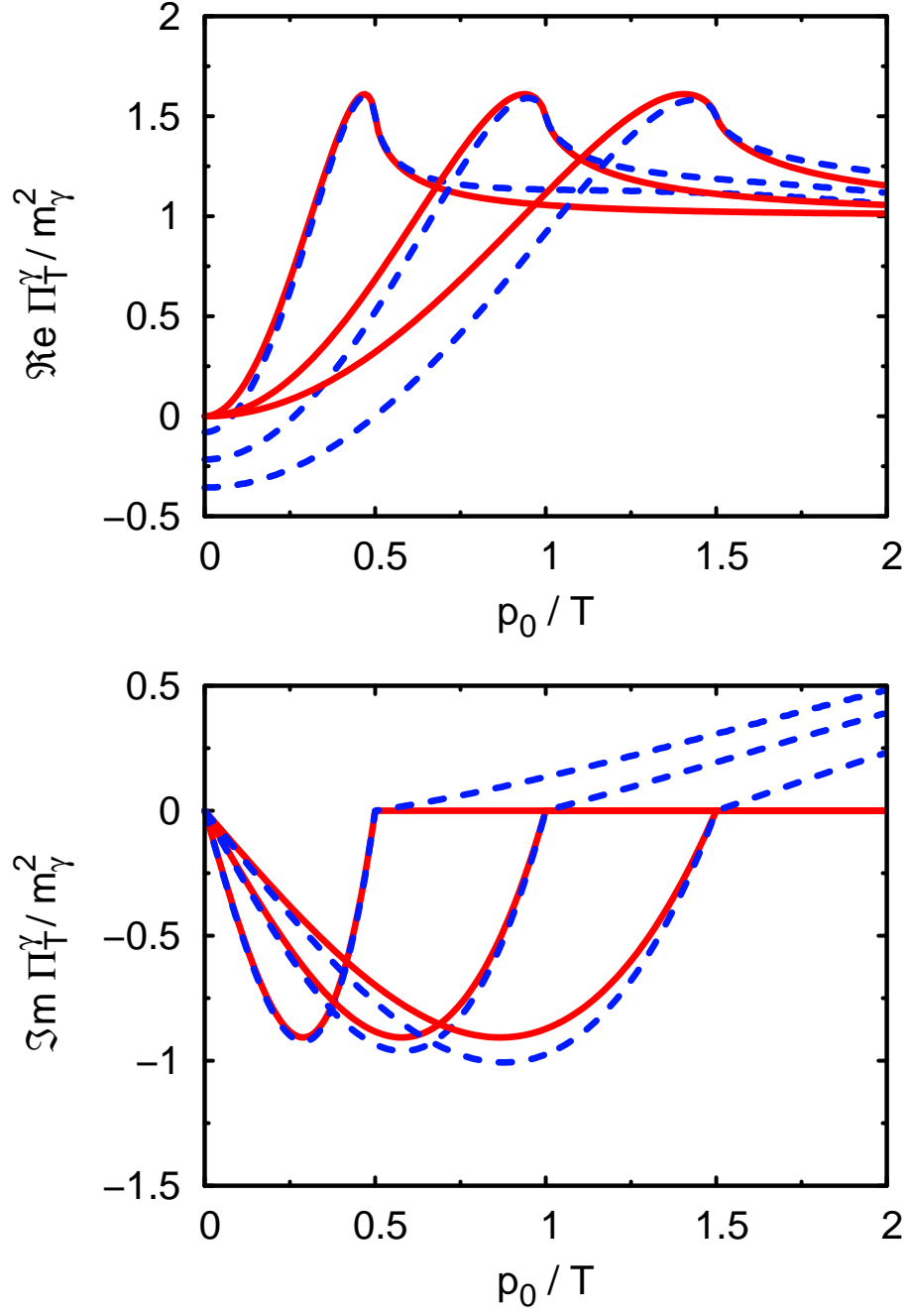


Figure 3.2: The same as fig. 3.1, but for the transverse photon self energy Π_T^γ .

Here we introduced the abbreviations $x = \cos \theta$ for the angle between \mathbf{p} and \mathbf{k} as well as $v = k/\epsilon_{\mathbf{k}}$.² Similarly, we approximate the Fermi distribution whenever the argument is $\epsilon_{\mathbf{k}-\mathbf{p}}$:

$$\begin{aligned} n_F(\epsilon_{\mathbf{q}}) &\simeq n_F(\epsilon_{\mathbf{k}} - vpx) \\ &\simeq n_F(\epsilon_{\mathbf{k}}) - \frac{dn_F}{d\epsilon_{\mathbf{k}}} vpx. \end{aligned} \quad (3.24)$$

Summarizing the m HTL approximations, we will use

$$\epsilon_{\mathbf{k}-\mathbf{p}} \simeq \epsilon_{\mathbf{k}} - vpx, \quad (3.25)$$

$$n_F(\epsilon_{\mathbf{k}-\mathbf{p}}) \simeq n_F(\epsilon_{\mathbf{k}}) - \frac{dn_F}{d\epsilon_{\mathbf{k}}} vpx. \quad (3.26)$$

In the chiral limit, this approximation scheme results in the usual HTL rules which are

$$|\mathbf{k} - \mathbf{p}| \simeq k - px, \quad (3.27)$$

$$n_F(|\mathbf{k} - \mathbf{p}|) \simeq n_F(k) - \frac{dn_F}{dk} px. \quad (3.28)$$

When applying these approximations to Π_{44} , only sums like $\epsilon_{\mathbf{q}} + \epsilon_{\mathbf{k}}$ contribute to the second line in eq. (3.8), which can be approximated as $2\epsilon_{\mathbf{k}} + \mathcal{O}(p) \simeq 2\epsilon_{\mathbf{k}}$. Doing the same for the Fermi distribution, the second line exactly cancels the first one. The remaining contribution from the third line in (3.8) reads

$$\hat{\Pi}_{44}^\gamma = \frac{e^2}{\pi^2} \int_0^{2\pi} \frac{d\varphi}{2\pi} \int_0^\infty dk k^2 \left(\frac{dn_F}{d\epsilon_{\mathbf{k}}} \right) \int_{-1}^1 dx x^2 \left(x^2 + \frac{\omega^2}{v^2 p^2} \right)^{-1}. \quad (3.29)$$

The φ and x integrations can be evaluated analytically, but the k integration has to be performed numerically, in contrast to the chiral limit, where all integrations can be evaluated analytically, due to $v = 1$. After analytical continuation from Euclidean to Minkowski space via the replacement $i\omega \rightarrow p_0 + i0^+$, we get

$$\hat{\Pi}_{00}^\gamma(p_0, p) = -\frac{2e^2}{\pi^2} \int_0^\infty dk k^2 \left(\frac{dn_F}{d\epsilon_{\mathbf{k}}} \right) \left[1 - \frac{p_0}{2pv} \ln \frac{p_0 + vp}{p_0 - vp} \right], \quad (3.30)$$

where the hat denotes the HTL approximation. This is the final result for the time-like component of the photon polarization tensor. It only depends on the variables p_0 and p through the dimensionless ratio $\xi = p_0/p$. We can yet perform an integration by parts to get rid of the derivative of the Fermi distribution function yielding

$$\hat{\Pi}_{00}^\gamma(\xi) = \frac{2e^2}{\pi^2} \int_0^\infty dk \frac{k^2}{\epsilon_{\mathbf{k}}} n_F(\epsilon_{\mathbf{k}}) \left(1 + \frac{\xi^2 - 1}{\xi^2 - v^2} - \frac{\xi}{v} \ln \frac{\xi + v}{\xi - v} \right). \quad (3.31)$$

² $v = \frac{k}{\epsilon_{\mathbf{k}}} = \frac{d\epsilon_{\mathbf{k}}}{dk}$ is the group velocity of the free particles.

In this form, the massless limit is easily obtained since $v = k/\epsilon_{\mathbf{k}} \rightarrow 1$ as $m \rightarrow 0$, and hence

$$\hat{\Pi}_{00}(\xi) \rightarrow \frac{2e^2}{\pi^2} \underbrace{\int_0^\infty dk k n_F(k)}_{=\frac{1}{12}\pi^2 T^2} \left(2 - \xi \ln \frac{\xi+1}{\xi-1} \right) = \frac{1}{3}e^2 T^2 \left(1 - \frac{\xi}{2} \ln \frac{\xi+1}{\xi-1} \right). \quad (3.32)$$

Turning now to the trace Π_μ^μ , we use in eq. (3.9) the same approximations as in the calculation of $\hat{\Pi}_{00}$. Doing so, we get

$$\hat{\Pi}_\mu^{\gamma\mu}(\omega, p) \simeq 8e^2 \int \frac{d^3k}{(2\pi)^3} \left\{ \frac{n_F(\epsilon_{\mathbf{k}})}{\epsilon_{\mathbf{k}}} + \frac{m^2}{2\epsilon_{\mathbf{k}}^2} \left[\frac{n_F(\epsilon_{\mathbf{k}})}{\epsilon_{\mathbf{k}}} - \frac{dn_F}{d\epsilon_{\mathbf{k}}} \frac{x^2}{x^2 + \omega^2/p^2 v^2} \right] \right\}. \quad (3.33)$$

After performing the φ and x integrations as well as the analytical continuation, we end up with

$$\hat{\Pi}_\mu^{\gamma\mu} = \frac{2e^2}{\pi^2} \int_0^\infty dk k^2 \left\{ 2 \frac{n_F}{\epsilon_{\mathbf{k}}} + \frac{m^2}{\epsilon_{\mathbf{k}}^2} \left[\frac{n_F}{\epsilon_{\mathbf{k}}} - \frac{dn_F}{d\epsilon_{\mathbf{k}}} \left(1 - \frac{p_0 E}{2kp} \ln \frac{p_0 E + kp}{p_0 E - kp} \right) \right] \right\}. \quad (3.34)$$

Performing again an integration by parts, the final result is

$$\hat{\Pi}_\mu^{\gamma\mu}(\xi) = \frac{2e^2}{\pi^2} \int_0^\infty dk \frac{k^2}{\epsilon_{\mathbf{k}}} n_F \left(2 + \frac{m^2}{\epsilon_{\mathbf{k}}^2} \frac{\xi^2 - 1}{\xi^2 - v^2} \right). \quad (3.35)$$

Here also the chiral limit is obvious: $\hat{\Pi}_\mu^{\gamma\mu} \rightarrow \frac{1}{3}e^2 T^2$ as $m \rightarrow 0$. The expressions for the longitudinal and transversal self-energy functions follow by utilizing

$$\Pi_L = -\Pi_{00}, \quad (3.36)$$

$$\Pi_T = \frac{1}{2} \left(\Pi_\mu^\mu - \frac{P^2}{p^2} \Pi_L \right) \quad (3.37)$$

from chapter 2.3. We obtain in the HTL approximation the following final results for the photon self-energy

$$\hat{\Pi}_L^\gamma(\xi) = -\frac{2e^2}{\pi^2} \int_0^\infty dk \frac{k^2}{\epsilon_{\mathbf{k}}} n_F(\epsilon_{\mathbf{k}}) \left(1 + \frac{\xi^2 - 1}{\xi^2 - v^2} - \frac{\xi}{v} \ln \frac{\xi + v}{\xi - v} \right), \quad (3.38)$$

$$\hat{\Pi}_T^\gamma(\xi) = \frac{e^2}{\pi^2} \int_0^\infty dk \frac{k^2}{\epsilon_{\mathbf{k}}} n_F(\epsilon_{\mathbf{k}}) \left(2\xi^2 - (\xi^2 - 1) \frac{\xi}{v} \ln \frac{\xi + v}{\xi - v} \right). \quad (3.39)$$

The medium contribution of the full one-loop photon self-energies have been calculated in the literature (cf. [Kal84]) and read

$$\begin{aligned} \Pi_T^\gamma(p_0, p) = & \frac{e^2}{\pi^2} \int_0^\infty dk \frac{k^2}{\epsilon_{\mathbf{k}}} n_F(\epsilon_{\mathbf{k}}) \left\{ 1 + \frac{p_0^2}{p^2} - \frac{p^4 - p_0^4 - 4\epsilon_{\mathbf{k}}^2 p_0^2 + 4k^2 p^2}{8kp^3} \ln \mathcal{A}^f \right. \\ & \left. + \frac{p_0 \epsilon_{\mathbf{k}}}{2kp^3} (p^2 - p_0^2) \ln \mathcal{B}^f \right\}, \end{aligned} \quad (3.40)$$

$$\begin{aligned} \Pi_L^\gamma(p_0, p) = & -\frac{2e^2}{\pi^2} \int_0^\infty dk \frac{k^2}{\epsilon_{\mathbf{k}}} n_F(\epsilon_{\mathbf{k}}) \left\{ 1 - \frac{p^2 - p_0^2 - 4\epsilon_{\mathbf{k}}^2}{8kp} \ln \mathcal{A}^f \right. \\ & \left. - \frac{p_0 \epsilon_{\mathbf{k}}}{2kp} \ln \mathcal{B}^f \right\} \end{aligned} \quad (3.41)$$

with the abbreviations

$$\mathcal{A}^f = \frac{(p^2 - p_0^2 + 2pk)^2 - 4p_0^2 \epsilon_{\mathbf{k}}^2}{(p^2 - p_0^2 - 2pk)^2 - 4p_0^2 \epsilon_{\mathbf{k}}^2}, \quad (3.42)$$

$$\mathcal{B}^f = \frac{(p^2 - p_0^2)^2 - 4(pk + p_0 \epsilon_{\mathbf{k}})^2}{(p^2 - p_0^2)^2 - 4(pk - p_0 \epsilon_{\mathbf{k}})^2}. \quad (3.43)$$

The calculation of these full one-loop self-energies, that include arbitrary masses for the loop fermions, is straightforward but tedious. After the frequency sums, three integrations remain and are conveniently done in angular coordinates. The φ integration is trivial and gives just a factor of 2π . To do the θ integration one has to shift the integration variables $\mathbf{k} \rightarrow \mathbf{k} + \mathbf{p}$ in all terms containing the distribution function $n_F(\epsilon_{\mathbf{q}})$, which is then shifted to $n_F(\epsilon_{\mathbf{k}})$ and does not contain the angle θ anymore. In this form the θ integration can be performed analytically, resulting in the expressions given in eqs. (3.40) to (3.43).

In fig. 3.3, the real part of the longitudinal photon self-energy is represented for different values of the fermion mass m in the loop. For $m = 0$ one observes a logarithmic divergence at $p_0 = p$, which, however, is cut off by finite fermion masses as stated by [Reb96]. For $m = 0$, the relevant structure in the self-energies, that leads to the pronounced structures at the light-cone (see section 3.1), was $Q_0(\xi)$, which evolves into $Q_0(\xi/v)$, with $v = k/\epsilon_{\mathbf{k}}$, when $m \neq 0$. One has to integrate over k from 0 to ∞ , thus v takes any value in $(0, \infty)$. But the integration is weighted by the thermal measure n_F so that contributions from the integration interval where $k > T$ are exponentially suppressed. Therefore, the parameter v is effectively not smaller than

$$v(k \sim T) \approx \frac{T}{\sqrt{T^2 + m^2}} \approx 1 - \frac{m^2}{2T^2}. \quad (3.44)$$

The expansion of $Q_0(\xi/v)$ in the vicinity of the light cone, with $\xi = 1 + \delta$, $\delta \ll \frac{m^2}{2T^2}$, yields

$$\frac{1}{2} \ln \frac{\xi + v}{\xi - v} \approx \frac{1}{2} \ln \frac{1 + v}{1 - v} + \frac{v}{v^2 - 1} \delta + \frac{v}{(v^2 - 1)(v^2 + 1)} \delta^2 + \mathcal{O}(\delta^3). \quad (3.45)$$

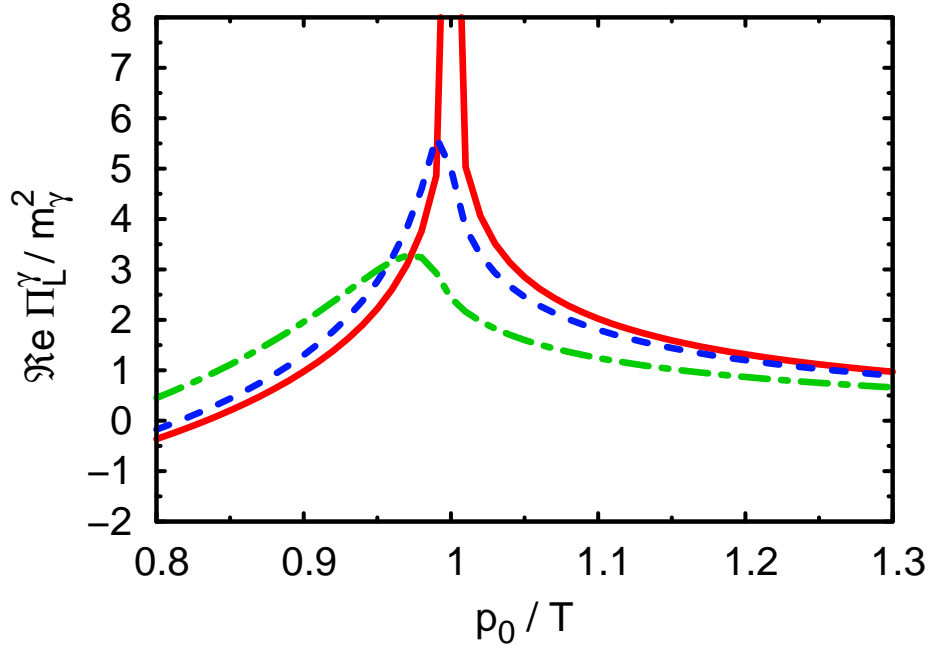


Figure 3.3: The real part of the longitudinal photon self-energy in the HTL approximation for $p/T = 1$. The red solid line corresponds to $m = 0$, the blue dashed line to $m = 0.4T$ and the green dash-dotted line to $m = T$.

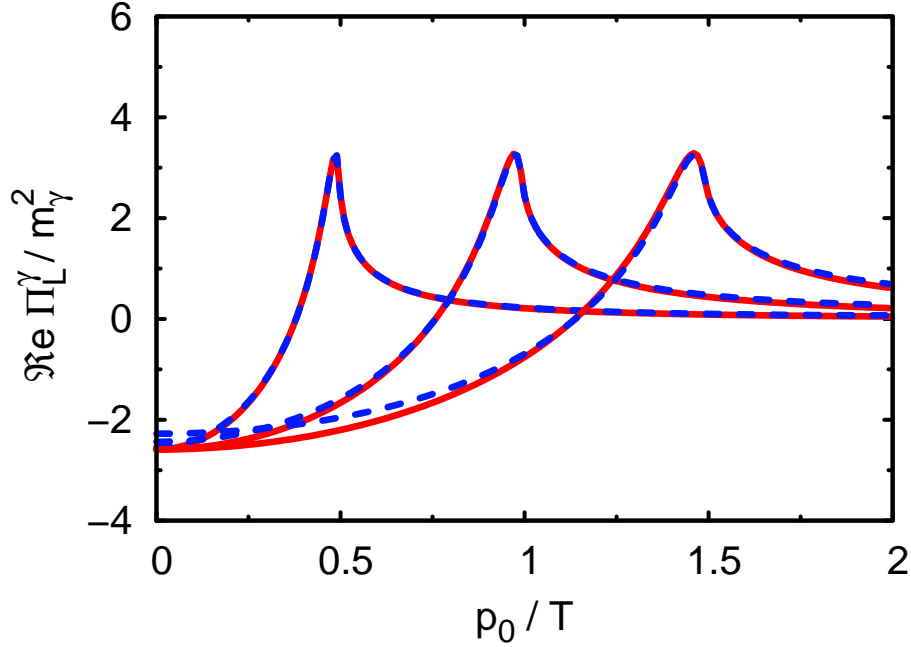


Figure 3.4: The real part of the scaled longitudinal photon self-energy in the HTL approximation (red, solid lines) and in one-loop approximation (blue, dashed lines) for $p/T = 0.5, 1.0, 1.5$ (from left to right). The mass of the fermion in the loop is $m = T$.

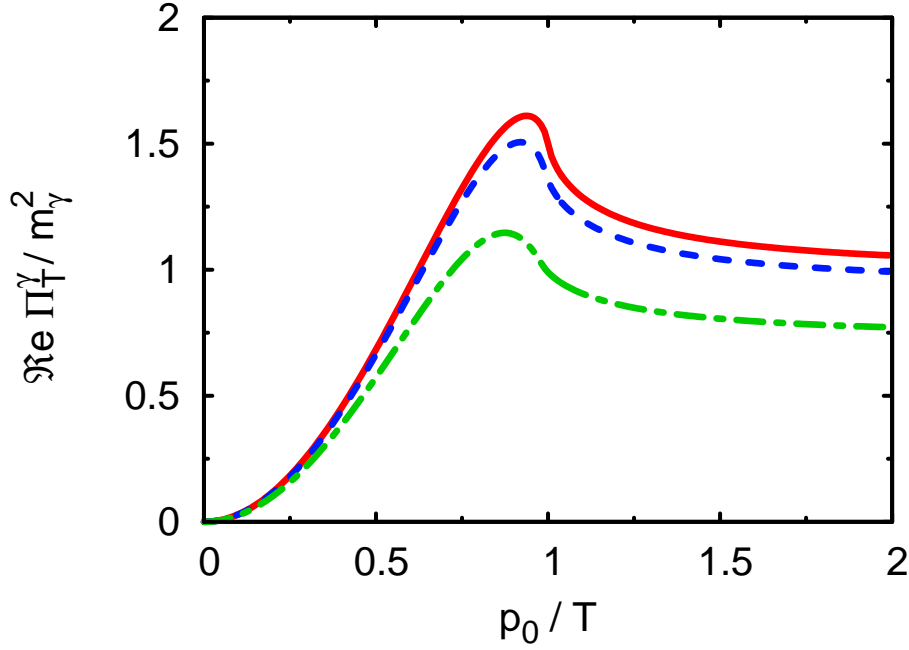


Figure 3.5: The real part of the scaled transversal photon self-energy in the HTL approximation for $p/T = 1$. The line code is the same as in fig. 3.3.

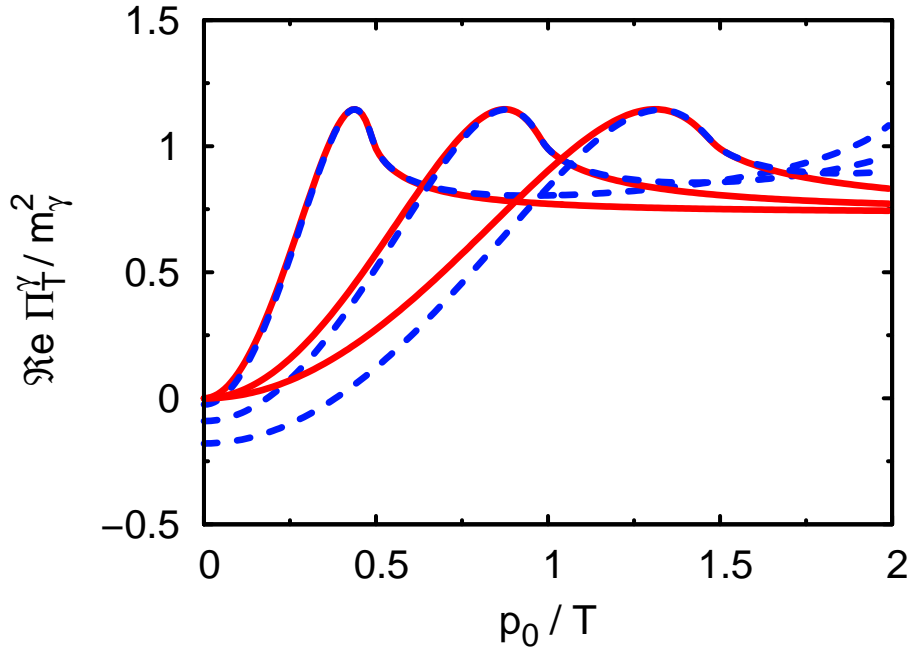


Figure 3.6: The real part of the scaled transverse photon self-energy in the HTL approximation (red, solid lines) and in one-loop approximation (blue, dashed lines) for $p/T = 0.5, 1.0, 1.5$ from left to right. The mass of the fermion in the loop is $m = T$.

In contrast to $m = 0$, eq. (3.19), the term $\propto \ln \delta$ producing the logarithmic singularity of the real part and the discontinuity of the imaginary part is absent for $m \neq 0$. Thus, the real part of Π_L^γ is finite for light-like momenta and the imaginary part is continuous. However, in the above expansion, in eq. (3.45), it is not possible to take the limit $m \rightarrow 0$, since then $v \rightarrow 1$ and the expansion coefficients diverge. At $\xi = v$, the function $Q_0(\xi/v)$ has the same singularities and discontinuities as $Q_0(\xi)$ at $\xi = 1$. However, these are smeared by the integration over k , so that the function is finite and continuous.

Additionally to this behavior, the absolute value of $\Re \hat{\Pi}_L^\gamma$ decreases with increasing masses. Since the k integration is effectively cut at $k \sim T$ by the Fermi distribution function, for large masses ($m \gg T$) the fermion loop contributions can be estimated by $\propto e^{-m/T}$, which indicates that contributions of very massive particles to the gauge boson self-energy are exponentially suppressed, thus they are negligible for many purposes.

In fig. 3.4, the m HTL approximation of Π_L^γ is compared to the full one-loop result. The mass parameter m is chosen to be temperature dependent, $m = 0.4T$ and $m = T$ respectively, as in the set-up of lattice QCD calculations [Kar01]. Like in the massless case, both approaches agree very well, even for momenta for which the HTL assumption $p \ll T$ is not fulfilled a priori.

For the transverse self-energy, depicted in fig. 3.5, the mass dependence is qualitatively the same as for the longitudinal polarization: the absolute value is decreasing with increasing masses. Comparing the transverse m HTL and one-loop results for $\Re \Pi_T^\gamma$ in fig. 3.6, one finds that the general agreement of the m HTL and one-loop self-energies is not as good as for the longitudinal self-energy. But again, both approaches agree very well in the vicinity of the light cone even for large momenta p . For $p_0 = p$, both curves touch each other, which holds for arbitrary values of the mass m and the momentum p .

The imaginary parts of the photon self energies are depicted in fig. 3.7, where the m HTL approximations are compared for $m = 0$ and $m = T$. Although finite masses alter the imaginary parts below the light-cone, there is still no imaginary part produced above the light-cone.

3.2 Photon Dispersion Relations

The dressed gauge boson propagator reads in a general covariant gauge with gauge fixing parameter ρ

$$i\mathcal{D}_{\mu\nu}(P) = \mathcal{P}_{\mu\nu}^T \Delta_T + \mathcal{P}_{\mu\nu}^L \frac{p^4}{P^4} \Delta_L + \rho \frac{P_\mu P_\nu}{P^4} \quad (3.46)$$

with

$$\Delta_T = \frac{1}{P^2 - \Pi_T}, \quad (3.47)$$

$$\Delta_L = \frac{1}{p^2 - \Pi_L}. \quad (3.48)$$

The dispersion relations for transverse (longitudinal) photon modes are given by the poles of the transverse (longitudinal) parts of the photon propagator

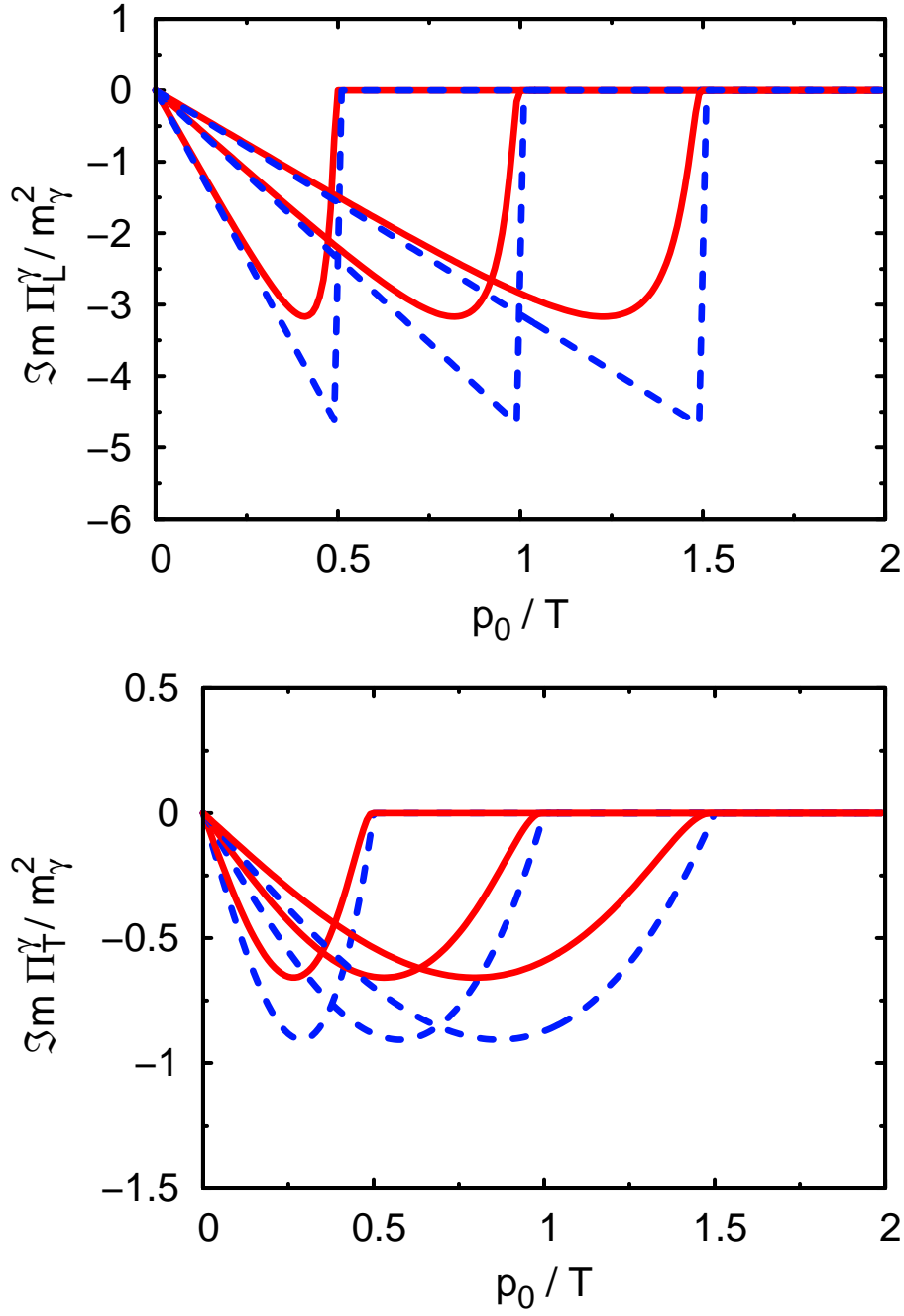


Figure 3.7: The imaginary parts of the scaled longitudinal (upper panel) and the transverse (lower panel) photon self-energy as a function of the photon energy scaled by the temperature. HTL ($m = 0$, blue dashed lines) and mHTL ($m = T$, red solid lines) approximations are compared for $p/T = 0.5, 1.0, 1.5$ (from left to right).

and hence are obtained by solving $\Delta_T^{-1} = 0$ ($\Delta_L^{-1} = 0$) respectively. When neglecting the imaginary parts of the self-energies, corresponding to the assumption of a weak damping of the propagating modes, we can write³

$$\omega_T^2(p) = p^2 + \Re \Pi_T(\omega_T(p), p), \quad (3.49)$$

$$0 = p^2 - \Re \Pi_L(\omega_L(p), p) \quad (3.50)$$

for transverse and longitudinal modes, respectively. In the m HTL approximation we may write, using the photon self-energy functions (3.38) and (3.39),

$$\omega_T^2(p) = p^2 + \frac{e^2}{\pi^2} \int_0^\infty dk \frac{k^2}{\epsilon_{\mathbf{k}}} n_F(\epsilon_{\mathbf{k}}) \left(2\xi^2 - \frac{\xi(\xi^2 - 1)}{v} \ln \left| \frac{\xi + v}{\xi - v} \right| \right), \quad (3.51)$$

$$0 = p^2 + \frac{2e^2}{\pi^2} \int_0^\infty dk \frac{k^2}{\epsilon_{\mathbf{k}}} n_F(\epsilon_{\mathbf{k}}) \left(1 + \frac{\xi^2 - 1}{\xi^2 - v^2} - \frac{\xi}{v} \ln \left| \frac{\xi + v}{\xi - v} \right| \right). \quad (3.52)$$

These equations implicitly contain the desired photon dispersion relations $\omega_{L/T}(p)$ in an involved way and must be solved numerically. However, noting that the self-energy functions Π_L and Π_T solely depend on the external momentum p and energy ω through the dimensionless parameter $\xi = \omega/p$, we can make some analytical predictions. Recalling $\Pi_{T/L} \propto e^2 T^2$, eq. (3.49) can be written as

$$\omega^2 - p^2 = \Re \hat{\Pi}_T(\xi) = e^2 T^2 \tilde{\pi}_T, \quad (3.53)$$

$$\alpha(\xi^2 - 1) = \frac{p^2}{e^2 T^2} (\xi^2 - 1) = \tilde{\pi}_T \quad (3.54)$$

with

$$\tilde{\pi}_T = \frac{1}{\pi^2} \int_0^\infty d\tilde{k} \tilde{k} v \tilde{n}_F \left(2\xi^2 - (\xi^2 - 1) \frac{\xi}{v} \ln \left| \frac{\xi + v}{\xi - v} \right| \right), \quad (3.55)$$

with the definitions $\tilde{k} = k/T$ and $\tilde{n}_F = n_F(\epsilon_{\mathbf{k}}/T)$. From (3.50) we obtain

$$p^2 = \Re \hat{\Pi}_L(\xi) = e^2 T^2 \tilde{\pi}_L, \quad (3.56)$$

$$\alpha = \frac{p^2}{e^2 T^2} = \tilde{\pi}_L \quad (3.57)$$

with

$$\tilde{\pi}_L = -\frac{2}{\pi^2} \int_0^\infty d\tilde{k} \tilde{k} \tilde{n}_F \left(1 + \frac{\xi^2 - 1}{\xi^2 - v^2} - \ln \left| \frac{\xi + v}{\xi - v} \right| \right). \quad (3.58)$$

In both (3.54) and (3.57) the dimensionless parameter $\alpha := p^2/(e^2 T^2)$ plays a crucial role for the dispersion relations. For the transverse photons, this parameter determines whether the dispersion relation develops in the vicinity of the light cone, where the HTL and one-loop self-energies are on top of each

³These arguments also hold for the gluon self-energy and thus the superscript γ will be omitted in the following.

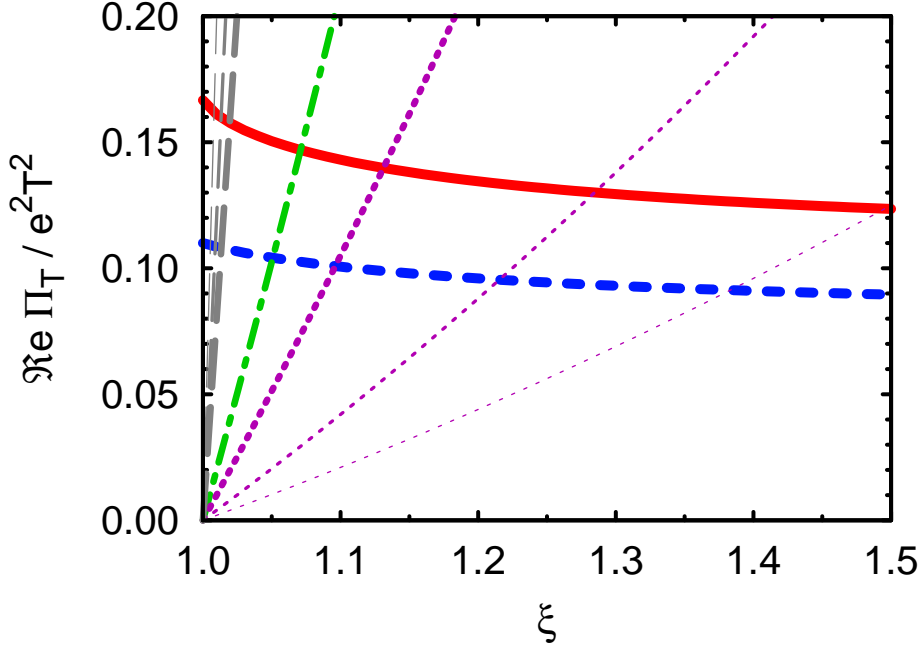


Figure 3.8: These curves serve for a visualization of the transverse photon dispersion relation (3.54). The real part of the scaled transverse self-energy as a function of the scaling variable $\xi = \omega/p$ for $m = 0$ (red, solid) and for $m = T$ (blue, dashed). Additionally, the function $\alpha(\xi^2 - 1)$ is shown for various values of the parameter α . The green dash-dotted line corresponds to $\alpha = 1$ with increasing $\alpha > 1$ for curves on the left and decreasing $\alpha < 1$ for curves on the right. α has to be larger than 1 for the dispersion relation to emerge in the vicinity of the light cone, as the crossing of $\Re \Pi_T / e^2 T^2$ with $\alpha(\xi^2 - 1)$ is a solution. The argumentation is independent of the value of the fermion mass.

other. The situation is depicted in fig. 3.8. If α is much larger than 1, the function $\alpha(\xi^2 - 1)$ has a very steep slope, and the intersection with the real part of the self-energy is close to the light cone. Thus, if

$$\frac{p^2}{T^2} \gg e^2, \quad (3.59)$$

the transverse HTL dispersion relation is a valuable approximation to the full one-loop dispersion relation independent of the fermion mass in the loop. This argumentation only requires the tangency of the transverse HTL and one-loop self-energies at the light cone. Certainly, the HTL dispersion relation is also a good approximation to the full one-loop dispersion relation, if the HTL assumption $p \sim eT$ is fulfilled, since in that case the real parts of the self-energies coincide very well. Although the HTL assumption $p \sim eT$ might be violated, the HTL dispersion relation may nonetheless be a useful approximation to the full one-loop dispersion relation, if eq. (3.59) is satisfied.

For the longitudinal photons, the situation is quite different as depicted in fig. 3.9. For finite fermion masses, the logarithmic singularity at the light cone develops into a finite peak structure below the light cone. Therefore, for finite

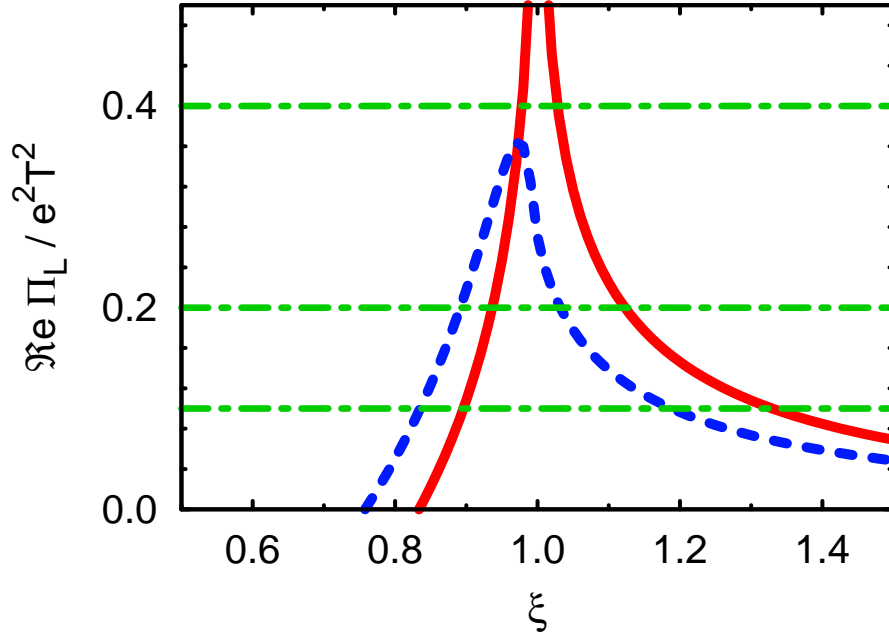


Figure 3.9: The real part of the longitudinal self-energy as a function of ξ is shown for $m = 0$ (red, solid) and $m = T$ (blue, dashed). The left side of eq. (3.57) is depicted for various values of the parameter α (green, dash-dotted). For every mass, there exists a critical α_c , so that for $\alpha > \alpha_c$ the intersection with the self-energy is below the light cone ($\xi < 1$), or there is no intersection at all and thus the solution of eq. (3.57) is in the space-like region, or the equation has no solution at all.

quark masses, we always find a value α_c so that the intersection with the self-energy is in the space-like region or there is no intersection at all. Thus, the longitudinal photon disappears from the spectrum when it descends into the light cone for a finite value of the momentum p_c . According to eq. (3.57), the critical parameter α_c , which depends on the fermion mass, or more precisely on the scale m/T , is calculated by

$$\begin{aligned} \alpha_c(m) &= \tilde{\pi}_L(\xi = 1; m) \\ &= \frac{2}{\pi^2 T^2} \int_0^\infty k n_F \left(\ln \left| \frac{1+v}{1-v} \right| - v \right). \end{aligned} \quad (3.60)$$

The result is shown in fig. 3.10. For $m/T \rightarrow 0$, the critical value α_c diverges, reproducing the usual result of the massless HTL approximation, where Π_L has a pole at the light cone. On the other hand, for $m/T \gtrsim 1$ the function rapidly tends to zero. Thus, for large fermion masses in the loop, the plasmino is strongly suppressed, since it exists only for very soft momenta.

The full numerical results for different masses are plotted in fig. 3.11. The overall appearance of the transverse branch remains generally the same, but the branch gets closer to the light cone for increasing masses. One finds an

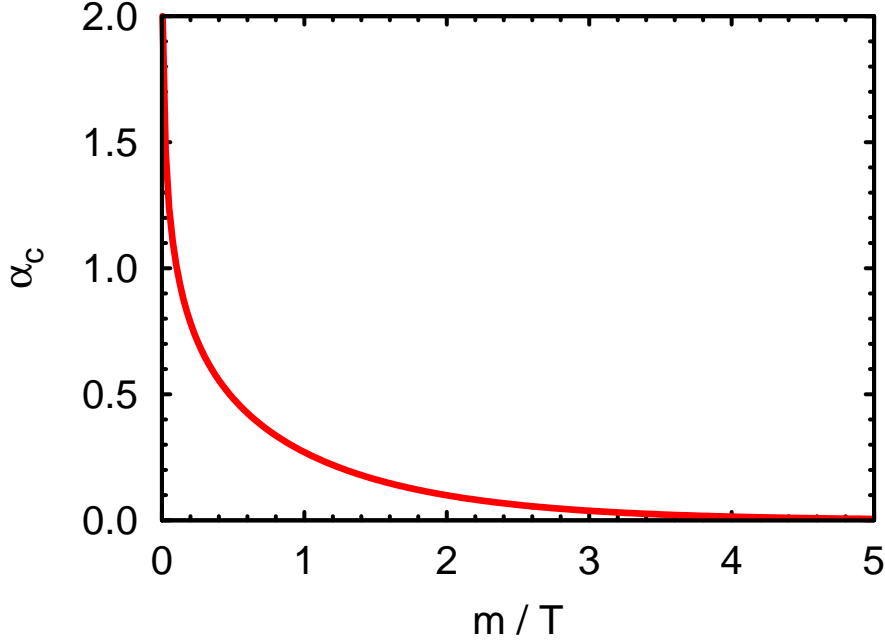


Figure 3.10: Depicted is the value of the critical α_c for which the longitudinal photon decouples from the spectrum according to eq. (3.60), depending on the loop fermion mass.

finite medium contribution for the transverse photons also for large momenta. This contribution can be conveniently parameterized by the asymptotic mass m_∞^2 (cf. eq. (3.67)). For the longitudinal branch one finds the decoupling for large masses at a finite value of p which depends on the mass. The two branches have the same limiting value for $p \rightarrow 0$, the plasma frequency ω_0^2 which is given in eq. (3.62).

For excitations with long wavelengths, i.e. $p \rightarrow 0$, and for the asymptotic region with large momenta in the vicinity of the light cone, analytic solutions can be found. Starting with the long wavelength limit for the longitudinal branch, we have to expand the integrand in eq. (3.50) into a Taylor series, with p/ω as the small quantity. We obtain

$$\omega_L^2(p) = \omega_0^2 + \frac{b_L}{\omega_0^2} p^2 \quad (3.61)$$

with the plasma frequency ω_0 acting as a long-wavelength effective mass and the parameter b_L determining the slope of the dispersion relation at $p \rightarrow 0$ via

$$\omega_0^2 = \frac{2e^2}{\pi^2} \int_0^\infty dk kn_F v \left(1 - \frac{1}{3}v^2\right), \quad (3.62)$$

$$b_L = \frac{2e^2}{\pi^2} \int_0^\infty dk kn_F v^3 \left(1 - \frac{3}{5}v^2\right). \quad (3.63)$$

For the transverse photon branch, using the same expansion technique as for

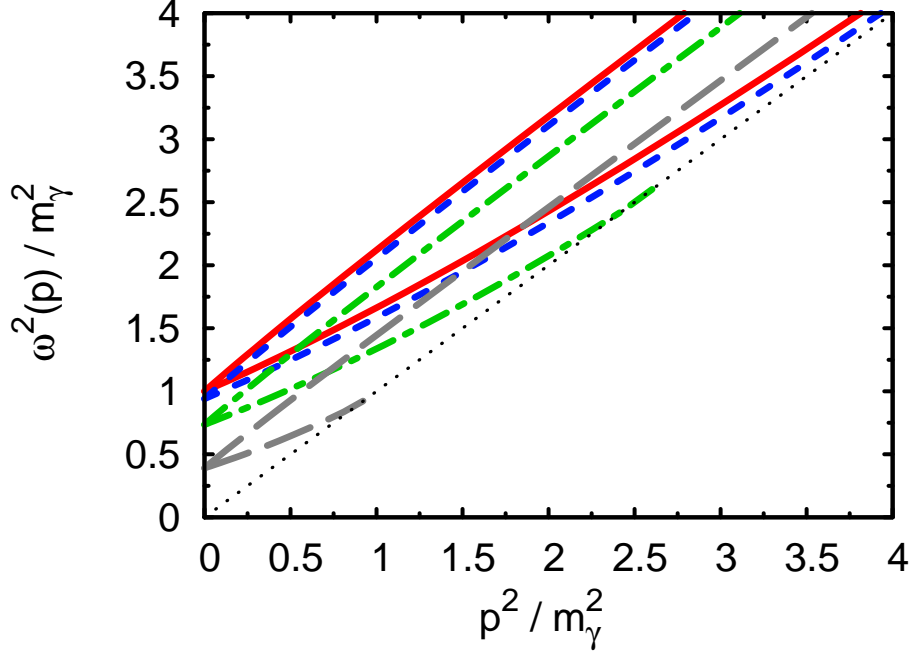


Figure 3.11: Transverse and longitudinal photon dispersion relations (upper and lower branches, respectively) as a function of p^2/m_γ^2 in the HTL approximation for $m = 0$ (red, solid), $m = 0.4T$ (blue, dashed), $m = T$ (green, dash-dotted) and $m = 2T$ (grey, long dashed). The line $\omega = p$ (dotted) marks the light cone depicting the dispersion relation for free photons. At $p = 0$, one notes the decrease of the plasma frequency ω_0 with increasing fermion mass m . Also the decoupling of the longitudinal photon for large masses at finite p can be observed.

ω_L , we find the long-wavelength (soft) dispersion relation

$$\omega_T^2(p) = \omega_0^2 + p^2 \left(1 + \frac{b_T}{\omega_0^2}\right). \quad (3.64)$$

Here the same plasma frequency ω_0 enters necessarily, because for a particle at rest one can not define separately longitudinal and transverse polarizations. We introduced the abbreviation

$$b_T = \frac{2e^2}{3\pi^2} \int_0^\infty dk k n_F v^3 \left(1 - \frac{3}{5}v^2\right) = \frac{1}{3}b_L. \quad (3.65)$$

For large momenta, we obtain the asymptotic transverse dispersion relation near the light cone as

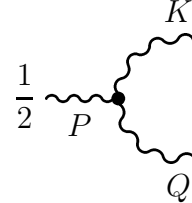
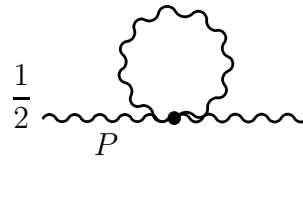
$$\begin{aligned} \omega_T^2(p) &= p^2 + \Re \Pi_T(\omega \rightarrow p, p) \\ &= p^2 + m_\infty^2 \end{aligned} \quad (3.66)$$

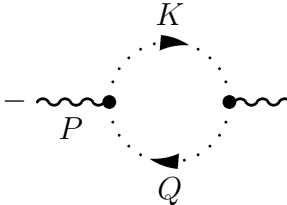
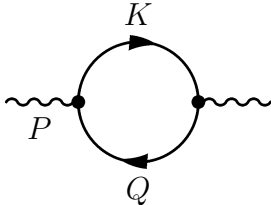
with

$$m_\infty^2 = \frac{2e^2}{\pi^2} \int_0^\infty dk \frac{k^2}{\epsilon_{\mathbf{k}}} n_F(\epsilon_{\mathbf{k}}). \quad (3.67)$$

3.3 The Gluon Self-Energy

In order to calculate the gluon self-energy, one has to sum up the contributions from the non-Abelian gluonic self-interactions and the contributions from the various massive quark loops. Diagrammatically, one has

$$\Pi_{\mu\nu,ab}^g(P) = \frac{1}{2} \text{ (diagram 1) } + \frac{1}{2} \text{ (diagram 2) } \quad (3.68)$$



$$- \text{ (diagram 3) } - \sum_q \text{ (diagram 4) } \quad (3.69)$$



which may be decomposed as

$$\Pi_{\mu\nu,ab}^g(P) = \Pi_{\mu\nu,ab}^{YM}(P) + \sum_q \Pi_{\mu\nu,ab}^q(P), \quad (3.70)$$

where $\Pi_{\mu\nu,ab}^{YM}(P)$ denotes the contributions from the Yang-Mills sector and $\Pi_{\mu\nu,ab}^q(P)$ represents the contribution from the quark loop considered above. For completeness, here color indices a and b are explicitly displayed. Concerning notation, Feynman rules etc., the reader is referred to Appendix B.2. The contribution from each individual quark loop reads

$$\Pi_{\mu\nu,ab}^q(P) = g^2 T \sum_{\omega_n} \int \frac{d^3k}{(2\pi)^3} \text{tr}[(\gamma_\mu t_a) \mathcal{S}(Q)(\gamma_\nu t_b) \mathcal{S}(K)], \quad (3.71)$$

where the trace has to be taken over the Dirac and color indices. The trace over the color matrices gives just a global color factor $\text{tr}(t_a t_b) = C_F \delta_{ab}$. So we can write $\Pi_{\mu\nu,ab}^q(P) = C_F \delta_{ab} \Pi_{\mu\nu}^q(P)$ with the photon polarization tensor $\Pi_{\mu\nu}^q$ from the preceding section, in the HTL approximation, see eqs. (3.38,3.39)

$$\hat{\Pi}_L^q(\xi) = -\frac{2C_F g^2}{\pi^2} \int_0^\infty dk \frac{k^2}{\epsilon_{\mathbf{k}}} n_F(\epsilon_{\mathbf{k}}) \left(1 + \frac{\xi^2 - 1}{\xi^2 - v^2} - \frac{\xi}{v} \ln \frac{\xi + v}{\xi - v} \right), \quad (3.72)$$

$$\hat{\Pi}_T^q(\xi) = \frac{C_F g^2}{\pi^2} \int_0^\infty dk \frac{k^2}{\epsilon_{\mathbf{k}}} n_F(\epsilon_{\mathbf{k}}) \left(2\xi^2 - (\xi^2 - 1) \frac{\xi}{v} \ln \frac{\xi + v}{\xi - v} \right), \quad (3.73)$$

and the contributions from the Yang-Mills sector read [Pis89a]

$$\hat{\Pi}_L^{YM}(p_0, p) = -\frac{C_A g^2 T^2}{3} \left(1 - \frac{\xi}{2} \ln \frac{\xi + 1}{\xi - 1} \right), \quad (3.74)$$

$$\hat{\Pi}_T^{YM}(p_0, p) = \frac{C_A g^2 T^2}{6} \left(\xi^2 + (\xi^2 - 1) \frac{\xi}{2} \ln \frac{\xi + 1}{\xi - 1} \right) \quad (3.75)$$

with the color factors $C_A = N_c = 3$ and $C_F = \frac{1}{2}$, respectively, as given in the Appendix A.2. The self-energy parts of the pure Yang-Mills theory have, apart from a different color factors, exactly the same structure as the quark contributions in the chiral limit. For the quark contributions to the one-loop self-energy, we may use eqs. (3.40 – 3.43), with the replacement $e^2 \rightarrow C_F g^2$, and the gluonic contributions read [Kal84]

$$\begin{aligned} \Pi_L^{YM}(p_0, p) &= -\frac{C_A g^2 T^2}{6} + \frac{C_A g^2}{8\pi^2 p} \int_0^\infty dk n_B(k) \\ &\quad \times \left\{ (2p^2 - p_0^2 - 4k^2) \ln \mathcal{A}^g - 4p_0 k \ln \mathcal{B}^g \right\}, \end{aligned} \quad (3.76)$$

$$\begin{aligned} \Pi_T^{YM}(p_0, p) &= \frac{C_A g^2 T^2}{12} \left(1 + \frac{p_0^2}{p^2} \right) - \frac{C_A g^2 (p^2 - p_0^2)}{16\pi^2 p^3} \int_0^\infty dk n_B(k) \\ &\quad \times \left\{ (3p^2 + p_0^2 + 4k^2) \ln \mathcal{A}^g + 4p_0 k \ln \mathcal{B}^g \right\} \end{aligned} \quad (3.77)$$

with

$$\mathcal{A}^g = \frac{(p^2 - p_0^2 + 2pk)^2 - 4k^2 p_0^2}{(p^2 - p_0^2 - 2pk)^2 - 4k^2 p_0^2}, \quad (3.78)$$

$$\mathcal{B}^g = \frac{(p^2 - p_0^2)^2 - 4k^2 (p + p_0)^2}{(p^2 - p_0^2)^2 - 4k^2 (p - p_0)^2}. \quad (3.79)$$

In fig. 3.12 and 3.13, the real parts of the transverse and longitudinal gluon self-energy for $N_F = 2 + 1$ quark flavors are plotted, normalized to the typical scale $m_g^2 = \frac{1}{9} g^2 T^2 (C_A + C_F N_F)$. As one can see, the deviations between the one-loop and the HTL self energies are much larger than for the photon self-energy, apart from the vicinity of the light cone, where the deviations between the two approximations vanish. Of course, when $p, p_0 \sim gT \ll T$, i.e. if the HTL assumption is satisfied, both self energies are almost identical as is indicated by the leftmost curves in the figures, corresponding to $p = 0.1T$. The origin of this worse correspondence of the HTL and one-loop self-energies is the gluon self-interaction, given by Π^{YM} . However, the modifications of the self energies due to finite quark masses are very small in the case of the gluon self-energy. The gluon self-energy is dominated by the strong non-Abelian self-interactions of the gluons among themselves. The individual quark contributions have much smaller magnitude than Π^{YM} . Thus, the modifications due to finite masses are relatively small in the gluon polarization.

This can be understood by inspecting eq. (3.70), together with the color factors in $\Pi_{L/T}^q$ and $\Pi_{L/T}^{YM}$. There, the contribution from the gauge sector is

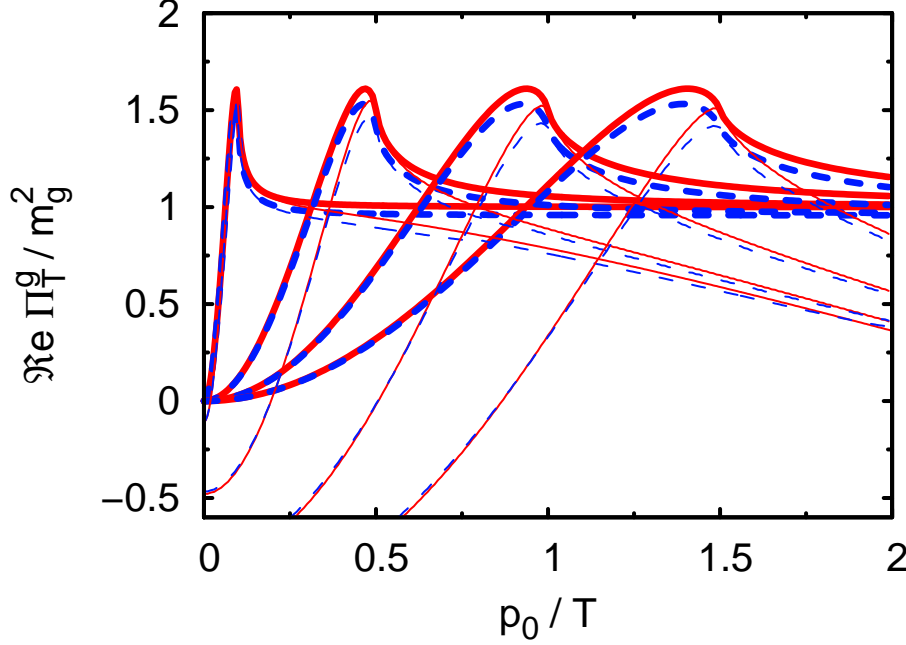


Figure 3.12: The real part of the scaled transverse gluon self-energy as a function of p_0/T in the HTL approximation and the full one-loop result for $N_F = 2+1$ massive (massless) quark flavors represented by dashed (solid) lines for $p/T = 0.1, 0.5, 1.0, 1.5$ (from left to right). The thicker lines represent the HTL approximation and the thinner ones depict the one-loop results. In the massive case, the quark masses are $m_{u,d} = 0.4T$ and $m_s = T$.

proportional to the color factor $C_A = 3$ and the quark loop contribution is proportional to $C_F = \frac{1}{2}$, thus each individual quark loop has only $\frac{1}{6}$ of the magnitude of the Yang-Mills contribution. Thus the mass effects from the quark loops give only minor modifications of the total gluon polarization.

In the longitudinal part of the gluon self-energy we also find the logarithmic singularity stemming from the pure gluonic part Π^{YM} .

3.4 Gluon Dispersion Relation

Utilizing eqs. (3.49) and (3.50), but now employing the gluon self-energy Π^g , we obtain the dispersion relations for the gluons. They are depicted in fig. 3.14 for $N_F = 2+1$ massive ($m_{u,d} = 0.4T, m_s = T$) and massless quarks. The corrections due to the finite quark masses, compared to the chiral limit, are very small, indeed. There are two reasons for this behavior. First, the mass dependence of the self-energies is only sub-leading because of the strong non-Abelian gluon self-interaction and second, the quark masses do not appear explicitly in the propagators for the longitudinal and transverse gluon modes.

In the asymptotic region for large momenta in the vicinity of the light cone,

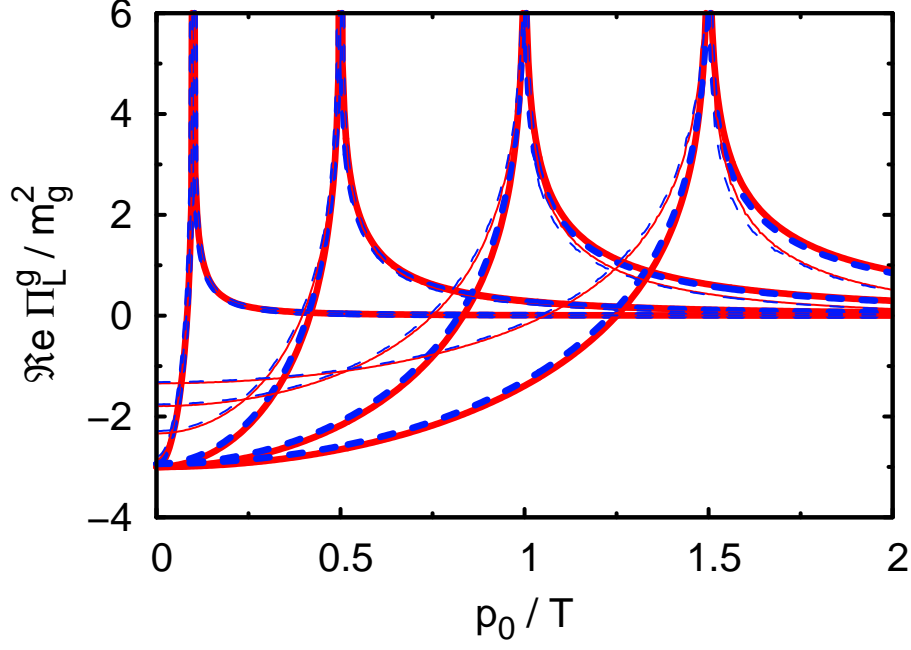


Figure 3.13: The same as fig. 3.12, but for the longitudinal part of the gluon self-energy $\Re \Pi_L^g(p_0, p)$.

the asymptotic gluon mass can be obtained by utilizing

$$\begin{aligned} m_\infty^2 &= \Re \Pi_T^g(\omega \rightarrow p, p) \\ &= \frac{1}{6} g^2 T^2 \left(N_c + C_F \sum_q \mathcal{I}_g \left(\frac{m_q}{T} \right) \right) \end{aligned} \quad (3.80)$$

with

$$\mathcal{I}_g = \frac{12}{\pi^2 T^2} \int_0^\infty dk \frac{k^2}{\epsilon_{\mathbf{k}}} n_F(\epsilon_{\mathbf{k}}). \quad (3.81)$$

The asymptotic dispersion relation then reads

$$\omega^2(p) = p^2 + m_\infty^2. \quad (3.82)$$

It is depicted in fig. 3.15. For larger momenta $p/m_g \geq 2$ the agreement of the full and the asymptotic gluon dispersion relations is very good.

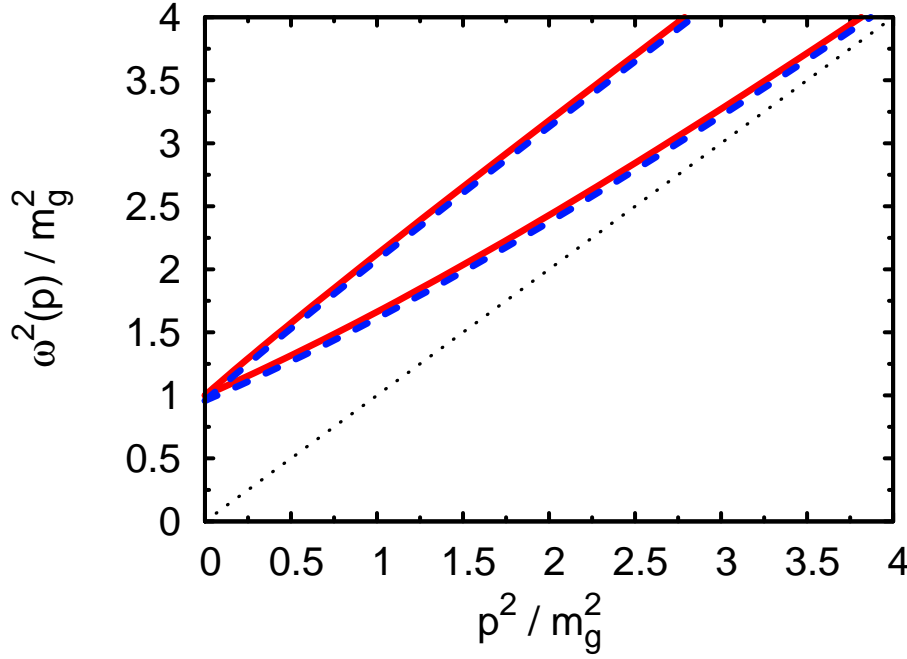


Figure 3.14: The gluon dispersion relations for $N_F = 2 + 1$ quark flavors. The upper (lower) branch corresponds to the transverse (longitudinal) gluon modes. The solid (dashed) lines represent massless (massive) quarks in the loop. In the massive case, the quark masses are $m_{u,d} = 0.4$ and $m_s = T$.

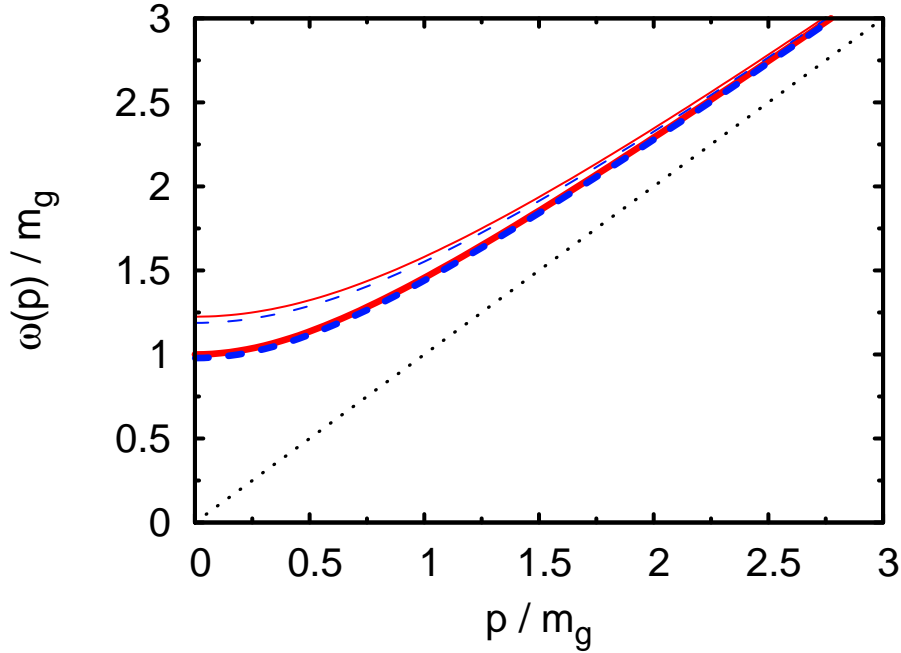


Figure 3.15: Comparison of the full transverse and asymptotic gluon dispersion relations for $N_F = 2 + 1$ massive (massless) quarks, represented by red solid (blue, dashed) lines. The thicker line represents the full dispersion relation, whereas the thinner line represents the asymptotic dispersion relation (3.82) employing the asymptotic gluon mass (3.80).

The decomposition of $\Sigma(P)$ according to the structures given in eq. (2.57)

yields after analytic continuation [Kal98, Pet92]

$$K(p_0, p) = \frac{g^2 C_R}{2\pi^2 p^2} \int_0^\infty dk \left[\frac{k^2}{\epsilon_{\mathbf{k}}} n_F(\epsilon_{\mathbf{k}}) \left(1 + \frac{h_F}{8kp} \ln(a_F^+ a_F^-) + \frac{d_F}{8kp} \ln \frac{a_F^+}{a_F^-} \right) \right. \\ \left. + k n_B(k) \left(1 + \frac{h_B}{8kp} \ln(a_B^+ a_B^-) + \frac{d_B}{8kp} \ln \frac{a_B^+}{a_B^-} - \frac{p}{4k} \ln(a_B^+ a_B^-) \right) \right], \quad (4.3)$$

$$K_0(p_0, p) = \frac{g^2 C_R}{8\pi^2 p} \int_0^\infty dk k \left[n_F(\epsilon_{\mathbf{k}}) \ln \frac{a_F^+}{a_F^-} \right. \\ \left. + n_B(k) \left(\ln \frac{a_B^+}{a_B^-} - \frac{p_0}{k} \ln(a_B^+ a_B^-) \right) \right], \quad (4.4)$$

$$Z(p_0, p) = \frac{C_R}{4\pi^2 p} \int_0^\infty dk k \left[\frac{n_F(\epsilon_{\mathbf{k}})}{\epsilon_{\mathbf{k}}} \ln(a_F^+ a_F^-) - \frac{n_B(k)}{k} \ln(a_B^+ a_B^-) \right], \quad (4.5)$$

with

$$a_F^\pm = \frac{p^2 - m_q^2 - p_0^2 \pm 2\epsilon_{\mathbf{k}} p_0 - 2pk}{p^2 - m_q^2 - p_0^2 \pm 2\epsilon_{\mathbf{k}} p_0 + 2pk}, \quad (4.6)$$

$$a_B^\pm = \frac{p^2 + m_q^2 - p_0^2 \pm 2kp_0 - 2pk}{p^2 + m_q^2 - p_0^2 \pm 2kp_0 + 2pk}, \quad (4.7)$$

and

$$h_F = p^2 - m_q^2 - p_0^2, \quad (4.8)$$

$$d_F = 2\epsilon_{\mathbf{k}} p_0, \quad (4.9)$$

$$h_B = p^2 + m_q^2 - p_0^2, \quad (4.10)$$

$$d_B = 2kp_0. \quad (4.11)$$

This is the medium part of the full one-loop quark self-energy at finite temperature.

4.2 mHTL for the Quark Self-Energy

We will try to apply the *m*HTL approximation scheme, established for the gauge boson self-energy, to extract the leading T^2 behavior and the m_q/T corrections from the full one-loop self-energy. Conveniently we start this calculation with eq. (4.2), elaborating the Dirac structure to yield

$$\gamma_\mu(m_q - \not{Q})\gamma_\mu = -4m_q - 2\not{Q} = -4m_q - 2(\not{K} - \not{P}) \simeq -4m_q - 2\not{K}. \quad (4.12)$$

Neglecting the soft external momentum $P \sim gT$ with respect to the hard loop momentum $K \sim T$, as in the case of the photon self energy, is not permitted since $P^2 = m_q^2$, i.e. the external 4-momentum never becomes soft if the quark is heavy. Therefore, we have to restrict the quark mass to values $m_q \lesssim gT$.

Later on we try to relax this constraint and check whether this is a good approximation also for heavier quarks. This approach is motivated by the results found in the gauge boson sector, where HTL or *mHTL* is unexpectedly a good approximation for large momenta in the vicinity of the light cone, even though the original HTL assumptions ($p \sim gT \ll T$) are not fulfilled for $g \simeq 1$. After performing the frequency sums according to the rules given in Appendix C and analytic continuation we find

$$\begin{aligned}
\Sigma(p_0, p) = & -g^2 C_R \int \frac{d^3 k}{(2\pi)^3} \left\{ \frac{4m_q + 2\vec{\gamma} \mathbf{k}}{4k \epsilon_{\mathbf{k}-\mathbf{p}}} \right. \\
& \times \left[(1 - n_F(\epsilon_{\mathbf{k}-\mathbf{p}}) + n_B(k)) \left(\frac{1}{p_0 + \epsilon_{\mathbf{k}-\mathbf{p}} + k} - \frac{1}{p_0 - \epsilon_{\mathbf{k}-\mathbf{p}} - k} \right) \right. \\
& \left. - (n_F(\epsilon_{\mathbf{k}-\mathbf{p}}) + n_B(k)) \left(\frac{1}{p_0 + \epsilon_{\mathbf{k}-\mathbf{p}} - k} - \frac{1}{p_0 - \epsilon_{\mathbf{k}-\mathbf{p}} + k} \right) \right] \\
& + \frac{\gamma_0}{2\epsilon_{\mathbf{k}-\mathbf{p}}} \left[(1 - n_F(\epsilon_{\mathbf{k}-\mathbf{p}}) + n_B(k)) \left(\frac{1}{p_0 + \epsilon_{\mathbf{k}-\mathbf{p}} + k} + \frac{1}{p_0 - \epsilon_{\mathbf{k}-\mathbf{p}} - k} \right) \right. \\
& \left. \left. - (n_F(\epsilon_{\mathbf{k}-\mathbf{p}}) + n_B(k)) \left(\frac{1}{p_0 + \epsilon_{\mathbf{k}-\mathbf{p}} - k} + \frac{1}{p_0 - \epsilon_{\mathbf{k}-\mathbf{p}} + k} \right) \right] \right\}. \quad (4.13)
\end{aligned}$$

As for the gauge bosons, we are only interested in the medium modifications, and will therefore focus on the terms proportional to the thermal distribution functions. That means we do not consider the vacuum parts, knowing that no new ultraviolet divergencies arise in the medium.

4.2.1 HTL Quark Self-Energy in the Chiral Limit

It is instructive to study the chiral limit first, in order to find the leading T^2 contribution to the self-energy. For $m_q = 0$ we have $\epsilon_{\mathbf{k}-\mathbf{p}} = |\mathbf{k} - \mathbf{p}|$, and terms $\propto m_q$ vanish, thus it is much easier to adopt power counting rules [LeB96] to find the leading T^2 contributions. Since each thermal distribution effectively cuts the k -integration at the scale T , an estimate for the temperature dependence would be obtained just by substituting each $k \rightarrow T$. In eq. (4.13), i.e. in the structure $\propto \gamma_0$, one finds one term which is proportional to the sum of Fermi and Bose distributions and one term that includes the difference of the two thermal distributions, where each term is associated to certain structures in the energy denominators. The terms including the differences have the structure

$$\int dk k^2 \frac{n}{|\mathbf{k} - \mathbf{p}|} \frac{1}{p_0 + k + |\mathbf{k} - \mathbf{p}|} \simeq \int dk n \propto T, \quad (4.14)$$

where the energies in the denominator containing the hard loop momentum have the same sign. In the HTL approximation we may safely neglect p with respect to k , and n stands for either n_F or n_B . Conversely, the terms including the sums of the distributions read

$$\int dk k^2 \frac{n}{k} \frac{1}{p_0 + k - |\mathbf{k} - \mathbf{p}|} \simeq \int dk k^2 \frac{n}{k} \frac{1}{p_0 + p} \propto \int dk k n \propto T^2, \quad (4.15)$$

where in the denominators we now have opposite signs for the hard loop momenta. Therefore we have to expand $k - |\mathbf{k} - \mathbf{p}| \simeq px$ in the denominator. In this sense, only the terms including the sums of the thermal distributions have to be taken into account. They read for $m_q = 0$

$$\begin{aligned} \Sigma(p_0, p) &= g^2 C_R \int \frac{d^3 k}{(2\pi)^3} (n_F(|\mathbf{k} - \mathbf{p}|) + n_B(k)) \\ &\times \left\{ \frac{\vec{\gamma} \mathbf{k}}{2k |\mathbf{k} - \mathbf{p}|} \left(\frac{1}{p_0 + |\mathbf{k} - \mathbf{p}| - k} - \frac{1}{p_0 - |\mathbf{k} - \mathbf{p}| + k} \right) \right. \\ &\left. - \frac{\gamma_0}{2|\mathbf{k} - \mathbf{p}|} \left(\frac{1}{p_0 + |\mathbf{k} - \mathbf{p}| - k} + \frac{1}{p_0 - |\mathbf{k} - \mathbf{p}| + k} \right) \right\}. \end{aligned} \quad (4.16)$$

In the HTL scheme we approximate $|\mathbf{k} - \mathbf{p}| \simeq k - px$ in the energy-denominators, where $x = \cos \theta$ with the angle θ between the vectors \mathbf{k} and \mathbf{p} , and $n_F(|\mathbf{k} - \mathbf{p}|) \simeq n_F(k)$, yielding

$$\begin{aligned} \hat{\Sigma}(p_0, p) &= \frac{g^2 C_R}{8\pi^2} \int dk k (n_F(k) + n_B(k)) \\ &\times \int_{-1}^1 dx \left\{ \vec{\gamma} \hat{\mathbf{p}} \left(\frac{x}{p_0 - px} - \frac{x}{p_0 + px} \right) - \gamma_0 \left(\frac{1}{p_0 - px} + \frac{1}{p_0 + px} \right) \right\}, \end{aligned}$$

where we have substituted $\vec{\gamma} \hat{\mathbf{k}}$ for $\vec{\gamma} \hat{\mathbf{p}} x$. This relation can easily be verified if one notices that the coordinate system for the loop momentum integration is oriented in a way that its z -direction is parallel to $\hat{\mathbf{p}}$. The Cartesian components of the vector $\hat{\mathbf{k}}_i$ in this system read

$$\hat{\mathbf{k}} = \begin{pmatrix} \cos \varphi \sin \theta \\ \sin \varphi \sin \theta \\ \cos \theta \end{pmatrix} \quad (4.17)$$

and hence the φ -integration over one period of the sin and cos functions leaves only the z -component of this vector nonzero, which is $x = \cos \theta$ and the direction is $\hat{\mathbf{p}}$. After the evaluation of the x -integral (cf. Appendix E) the final result for the quark self-energy reads

$$\hat{\Sigma}(p_0, p) = -\frac{m_f^2}{p} \gamma_0 Q_0\left(\frac{p_0}{p}\right) - \frac{m_f^2}{p^2} (\vec{\gamma} \mathbf{p}) \left(1 - \frac{p_0}{p} Q_0\left(\frac{p_0}{p}\right) \right), \quad (4.18)$$

where

$$m_f^2 = \frac{1}{8} C_R g^2 T^2 \quad (4.19)$$

is the characteristic fermionic thermal mass scale and Q_0 is the Legendre function of the second kind

$$Q_0(x) = \frac{1}{2} \ln \frac{x+1}{x-1}. \quad (4.20)$$

Therefore we have

$$K_0(p_0, p) = -\frac{m_f^2}{2p} \ln \frac{p_0 + p}{p_0 - p}, \quad (4.21)$$

$$K(p_0, p) = \frac{m_f^2}{p^2} \left(1 - \frac{p_0}{2p} \ln \frac{p_0 + p}{p_0 - p} \right) \quad (4.22)$$

as the scalar quark self-energy functions in the chiral limit. The real and imaginary parts of these functions are depicted in figs. 4.1 and 4.2 and compared to the full one-loop quark self-energy (cf. eqs. (4.3 – 4.11) for $m_q = 0$). The real parts of both functions have logarithmic divergencies at the light cone due to the Legendre functions and the HTL self-energies only develop imaginary parts below the light cone. But the most remarkable feature is the agreement of the real parts for both approaches just above the light cone. A detailed discussion of the HTL and one-loop self-energies in the chiral limit can be found in [Pes98a].

4.2.2 Finite Quark Masses

Going back now to nonzero fermion masses, we start with eq. (4.13) and use power counting rules in analogy to the case $m_q = 0$. Under the assumption that the mass is of order $m_q \sim gT$ we find that the terms with the differences of the thermal distributions are $\sim T + \mathcal{O}(m_q/T)$ and therefore do not contribute to the leading T^2 behavior as in the chiral limit. On the other hand, the term proportional to the sum of the distribution functions leads, as in the chiral limit, to the leading T^2 behavior with corrections of order m_q/T . We obtain

$$\begin{aligned} \Sigma(p_0, p) = & -g^2 C_R \int \frac{d^3 k}{(2\pi)^3} \left\{ \frac{4m_q + 2\vec{\gamma} \mathbf{k}}{4k \epsilon_{\mathbf{k}-\mathbf{p}}} \right. \\ & \times \left[(n_F(\epsilon_{\mathbf{k}-\mathbf{p}}) + n_B(k)) \left(\frac{1}{p_0 + \epsilon_{\mathbf{k}-\mathbf{p}} - k} - \frac{1}{p_0 - \epsilon_{\mathbf{k}-\mathbf{p}} + k} \right) \right] \\ & + \frac{\gamma_0}{2\epsilon_{\mathbf{k}-\mathbf{p}}} \left[(n_F(\epsilon_{\mathbf{k}-\mathbf{p}}) + n_B(k)) \right. \\ & \times \left. \left. \left(\frac{1}{p_0 + \epsilon_{\mathbf{k}-\mathbf{p}} - k} + \frac{1}{p_0 - \epsilon_{\mathbf{k}-\mathbf{p}} + k} \right) \right] \right\}. \end{aligned} \quad (4.23)$$

Now we start our *mHTL* machinery using the approximations given in eqs. (3.25) and (3.26), approximating $n_F(\epsilon_{\mathbf{k}-\mathbf{p}}) \simeq n_F(\epsilon_{\mathbf{k}})$, which leads to

$$\begin{aligned} \hat{\Sigma}(p_0, p) = & -g^2 C_R \int \frac{d^3 k}{(2\pi)^3} \left\{ \frac{4m_q + 2\vec{\gamma} \mathbf{k}}{4k \epsilon_{\mathbf{k}}} \right. \\ & \times \left[(n_F(\epsilon_{\mathbf{k}}) + n_B(k)) \right. \\ & \times \left(\frac{1}{p_0 + \epsilon_{\mathbf{k}} - k - vpx} - \frac{1}{p_0 - \epsilon_{\mathbf{k}} + k + vpx} \right) \Big] \\ & + \frac{\gamma_0}{2\epsilon_{\mathbf{k}-\mathbf{p}}} \left[(n_F(\epsilon_{\mathbf{k}}) + n_B(k)) \right. \\ & \times \left. \left. \left(\frac{1}{p_0 + \epsilon_{\mathbf{k}} - k - vpx} + \frac{1}{p_0 - \epsilon_{\mathbf{k}} + k + vpx} \right) \right] \right\}. \end{aligned} \quad (4.24)$$

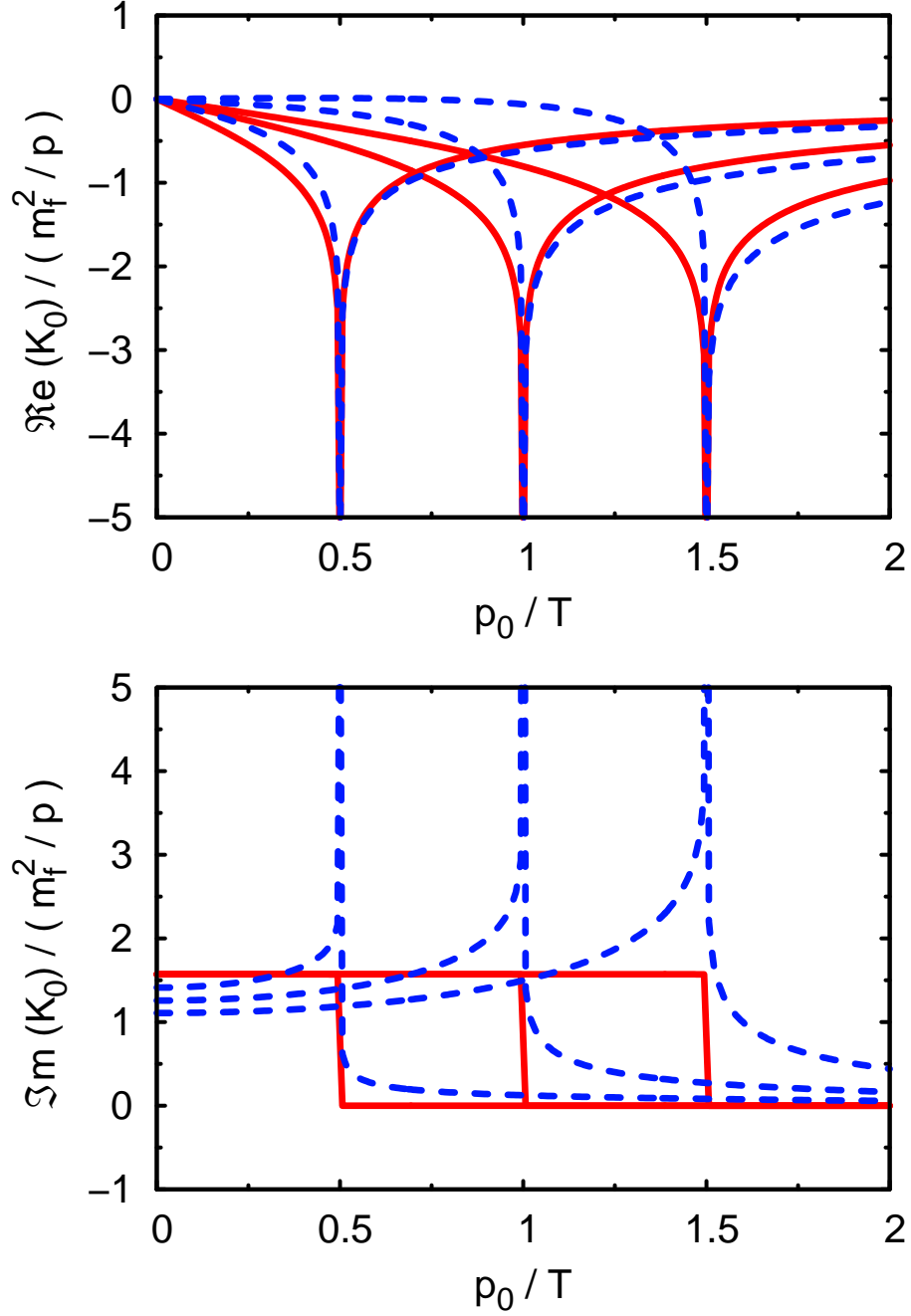


Figure 4.1: The real (top panel) and imaginary parts (bottom panel) of the scaled quark self-energy function $K_0(p_0, p)$ in Feynman gauge for $m_q = 0$. Depicted are the HTL approximation (solid, red) and the full one-loop result (dashed, blue) for momenta $p/T = 0.5, 1.0, 1.5$ (from left to right). The real part has a logarithmic divergency at the light cone. In the HTL approximation scheme, the imaginary part is only nonzero below the light cone.

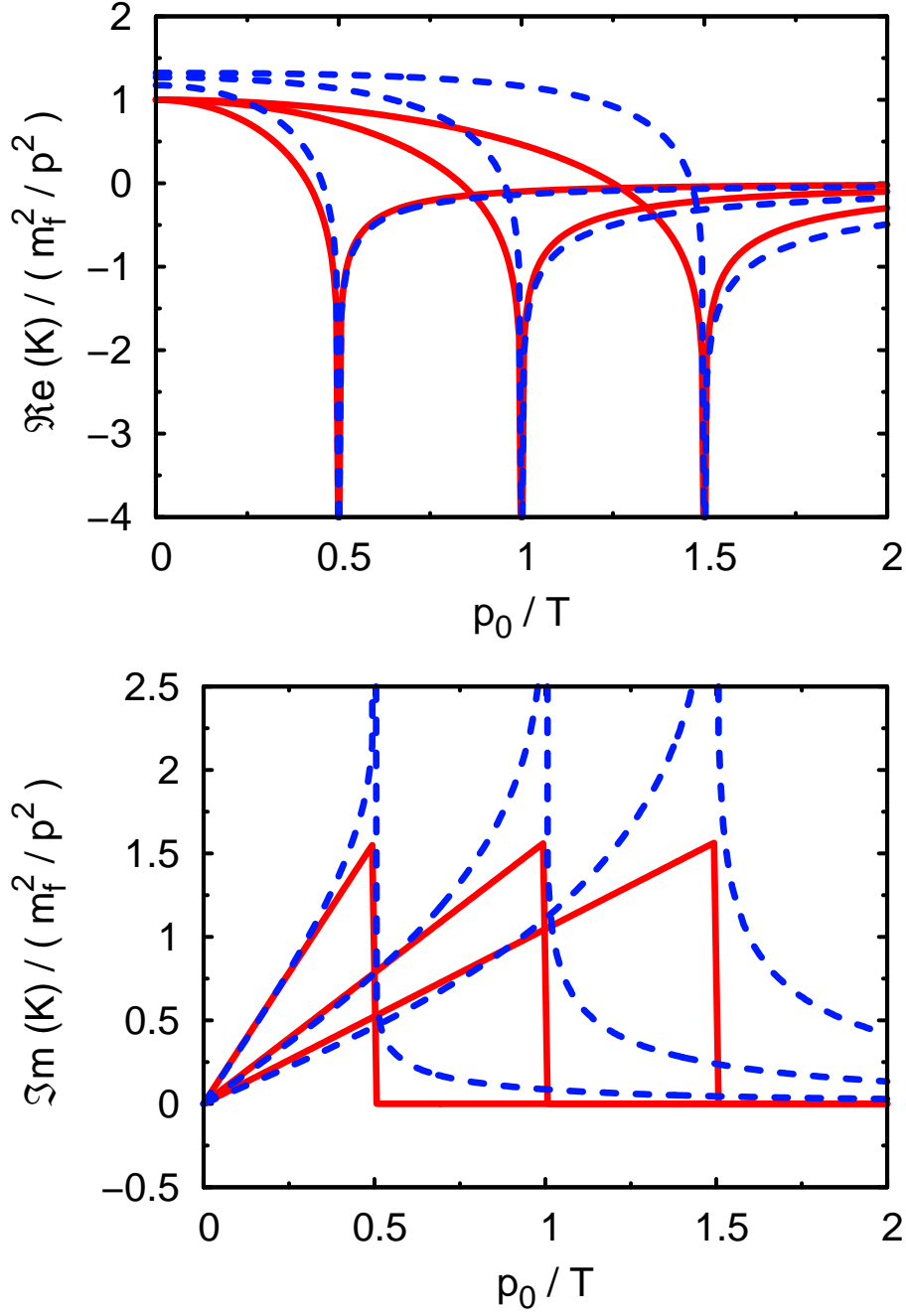


Figure 4.2: Comparison of the real (upper panel) and imaginary parts (lower panel) of the scaled quark self-energy function $K(p_0, p)$. Values of momenta p and the linecode are the same as in fig. 4.1.

After performing the angular integrations, we end up with the three scalar functions

$$\begin{aligned}\hat{K}_0(p_0, p) &= -\frac{g^2 C_R}{8\pi^2 p} \int_0^\infty dk \frac{k^2}{v\epsilon_{\mathbf{k}}} (n_B(k) + n_F(\epsilon_{\mathbf{k}})) \\ &\quad \times \left(\ln \frac{p_0 + \epsilon_{\mathbf{k}} - k + vp}{p_0 + \epsilon_{\mathbf{k}} - k - vp} + \ln \frac{p_0 - \epsilon_{\mathbf{k}} + k + vp}{p_0 - \epsilon_{\mathbf{k}} + k - vp} \right),\end{aligned}\quad (4.25)$$

$$\begin{aligned}\hat{Z}(p_0, p) &= \frac{g^2 C_R}{4\pi^2 p} \int_0^\infty dk \frac{k}{v\epsilon_{\mathbf{k}}} (n_B(k) + n_F(\epsilon_{\mathbf{k}})) \\ &\quad \times \left(\ln \frac{p_0 + \epsilon_{\mathbf{k}} - k + vp}{p_0 + \epsilon_{\mathbf{k}} - k - vp} - \ln \frac{p_0 - \epsilon_{\mathbf{k}} + k + vp}{p_0 - \epsilon_{\mathbf{k}} + k - vp} \right),\end{aligned}\quad (4.26)$$

$$\begin{aligned}\hat{K}(p_0, p) &= \frac{g^2 C_R}{2\pi^2 p^2} \int_0^\infty dk \frac{k^2}{v\epsilon_{\mathbf{k}}} (n_B(k) + n_F(\epsilon_{\mathbf{k}})) \\ &\quad \times \left[1 - \frac{p_0}{2vp} \left(\ln \frac{p_0 + \epsilon_{\mathbf{k}} - k + vp}{p_0 + \epsilon_{\mathbf{k}} - k - vp} + \ln \frac{p_0 - \epsilon_{\mathbf{k}} + k + vp}{p_0 - \epsilon_{\mathbf{k}} + k - vp} \right) \right. \\ &\quad \left. - \frac{\epsilon_{\mathbf{k}} - k}{2vp} \left(\ln \frac{p_0 + \epsilon_{\mathbf{k}} - k + vp}{p_0 + \epsilon_{\mathbf{k}} - k - vp} - \ln \frac{p_0 - \epsilon_{\mathbf{k}} + k + vp}{p_0 - \epsilon_{\mathbf{k}} + k - vp} \right) \right].\end{aligned}\quad (4.27)$$

But this result is unfortunately not unique. For example, we could shift the integration variable from \mathbf{k} to $\mathbf{k} + \mathbf{p}$ in eq. (4.23), producing a new term $\propto \vec{\gamma} \mathbf{p}$ which, however, can be neglected with respect to $\vec{\gamma} \mathbf{k}$ under the HTL assumption. In doing so, the self-energy now reads

$$\begin{aligned}\Sigma(p_0, p) &= -g^2 C_R \int \frac{d^3 k}{(2\pi)^3} \left\{ \frac{4m_q + 2\vec{\gamma} \mathbf{k}}{4|\mathbf{k} + \mathbf{p}| \epsilon_{\mathbf{k}}} \left[(n_F(\epsilon_{\mathbf{k}}) + n_B(|\mathbf{k} + \mathbf{p}|)) \right. \right. \\ &\quad \times \left(\frac{1}{p_0 + \epsilon_{\mathbf{k}} - |\mathbf{k} + \mathbf{p}|} - \frac{1}{p_0 - \epsilon_{\mathbf{k}} + |\mathbf{k} + \mathbf{p}|} \right) \Big] \\ &\quad + \frac{\gamma_0}{2\epsilon_{\mathbf{k}}} \left[(n_F(\epsilon_{\mathbf{k}}) + n_B(|\mathbf{k} + \mathbf{p}|)) \right. \\ &\quad \times \left(\frac{1}{p_0 + \epsilon_{\mathbf{k}} - |\mathbf{k} + \mathbf{p}|} + \frac{1}{p_0 - \epsilon_{\mathbf{k}} + |\mathbf{k} + \mathbf{p}|} \right) \Big] \Big\}\end{aligned}\quad (4.28)$$

which leads in the *mHTL* approximation scheme to the result

$$\begin{aligned}\tilde{K}_0(p_0, p) &= -\frac{g^2 C_R}{8\pi^2 p} \int_0^\infty dk \frac{k^2}{\epsilon_{\mathbf{k}}} (n_B(k) + n_F(\epsilon_{\mathbf{k}})) \\ &\quad \times \left(\ln \frac{p_0 + \epsilon_{\mathbf{k}} - k + p}{p_0 + \epsilon_{\mathbf{k}} - k - p} + \ln \frac{p_0 - \epsilon_{\mathbf{k}} + k + p}{p_0 - \epsilon_{\mathbf{k}} + k - p} \right),\end{aligned}\quad (4.29)$$

$$\begin{aligned}\tilde{Z}(p_0, p) &= \frac{g^2 C_R}{4\pi^2 p} \int_0^\infty dk \frac{k}{\epsilon_{\mathbf{k}}} (n_B(k) + n_F(\epsilon_{\mathbf{k}})) \\ &\quad \times \left(\ln \frac{p_0 + \epsilon_{\mathbf{k}} - k + p}{p_0 + \epsilon_{\mathbf{k}} - k - p} - \ln \frac{p_0 - \epsilon_{\mathbf{k}} + k + p}{p_0 - \epsilon_{\mathbf{k}} + k - p} \right),\end{aligned}\quad (4.30)$$

$$\begin{aligned}\tilde{K}(p_0, p) &= \frac{g^2 C_R}{2\pi^2 p^2} \int_0^\infty dk \frac{k^2}{\epsilon_{\mathbf{k}}} (n_B(k) + n_F(\epsilon_{\mathbf{k}})) \\ &\quad \times \left[1 - \frac{p_0}{2p} \left(\ln \frac{p_0 + \epsilon_{\mathbf{k}} - k + p}{p_0 + \epsilon_{\mathbf{k}} - k - p} + \ln \frac{p_0 - \epsilon_{\mathbf{k}} + k + p}{p_0 - \epsilon_{\mathbf{k}} + k - p} \right) \right. \\ &\quad \left. - \frac{\epsilon_{\mathbf{k}} - k}{2p} \left(\ln \frac{p_0 + \epsilon_{\mathbf{k}} - k + p}{p_0 + \epsilon_{\mathbf{k}} - k - p} - \ln \frac{p_0 - \epsilon_{\mathbf{k}} + k + p}{p_0 - \epsilon_{\mathbf{k}} + k - p} \right) \right],\end{aligned}\quad (4.31)$$

where all factors $\propto v$ disappeared. Another possibility would be to shift the momentum only in the terms containing $n_F(\epsilon_{\mathbf{q}})$ and keeping all the terms $\propto n_B(k)$ unchanged. This "symmetric" choice leads to yet another form of the self-energy, where the terms $\propto n_B$ are the same as in the functions \hat{K} , \hat{K}_0 and \hat{Z} in eqs. (4.25 – 4.28), and the terms $\propto n_F$ are identical to the n_F terms in the functions \tilde{K} , \tilde{K}_0 and \tilde{Z} in eqs. (4.29 – 4.32). This clearly demonstrates that, in the application of the *mHTL* rules to the quark self-energy, ambiguities arise. The origin of this unfortunate behavior is related to the different masses that are associated to the quark and gluon propagators in the loop.

However, all these different versions lead to the same limiting value for $m_q \rightarrow 0$ which agrees with the HTL quark self-energy in the chiral limit, as given in eq. (4.18). The deviations that arise between different possibilities in performing the *mHTL* approximation are solely due to the factor

$$v = \frac{k}{\epsilon_{\mathbf{k}}} \simeq 1 - \frac{m_q^2}{2k^2}, \quad (4.32)$$

which is small, if the value of the fermion mass is restricted to $m_q \lesssim gT$. Because k is the hard loop momentum $k \sim T$, the disagreement is of order g^2 . The self-energy functions are plotted in figs. 4.3 and 4.4, using the full one-loop result and two of the ambiguous *mHTL* approximations, which are marked by hats or tildes. In the upper panels, where the functions are depicted for the smaller masses $m_q = 0.4T$, one may find some agreement between the full one-loop self energies and the *mHTL* approximations, but it is definitely worse than in the chiral limit (cf. figs. 4.1 and 4.2). The *mHTL* develop some double-peak structures in the vicinity of the light cone, which are different for the various *mHTL* versions and absent in the one-loop calculations. From the plots in

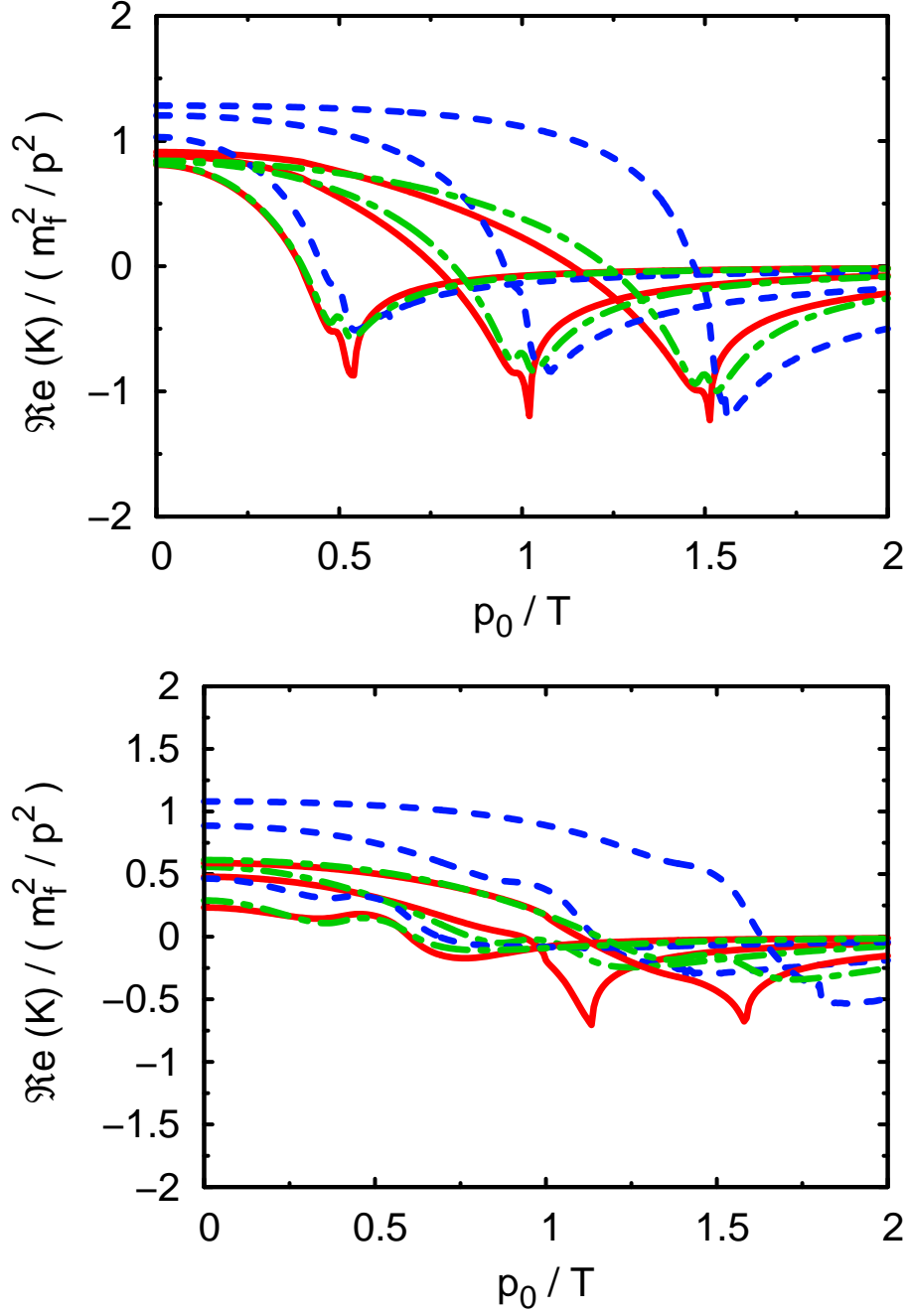


Figure 4.3: Depicted are the real parts of the scaled quark self-energy functions $K(p_0, p)$ as a function of p_0/T for the fermion masses $m_q = 0.4T$ (upper panel) and $m_q = T$ (lower panel), in the one-loop and the mHTL approximations. \hat{K} is represented by the red solid lines, \tilde{K} by the green dash-dotted lines and the 1-loop result K is represented by the blue dashed lines. $p/T = 0.5, 1.0, 1.5$ (from left to right).

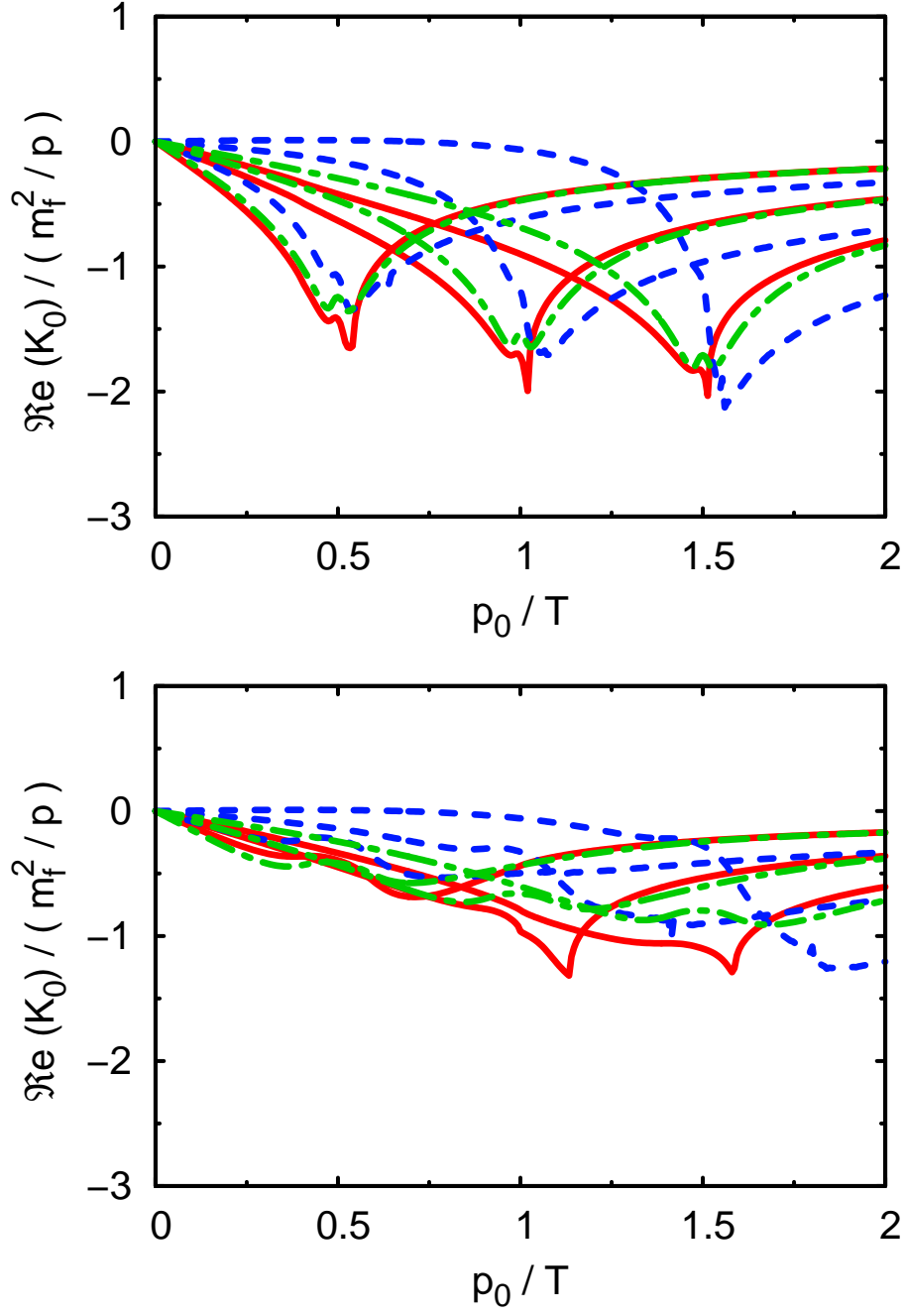


Figure 4.4: As fig. 4.3 but for the real parts of the scaled quark self-energy functions $K_0(p_0, p)$.

the lower panels for the larger masses $m_q = T$ it is evident that, for larger masses, the one-loop result differs substantially from the m HTL approximated self-energy and also the m HTL self-energies, although they coincide quite well for very small or very large p_0 , they are unlike in the vicinity of the light cone, which seems to be the important region for the dispersion relations. Additionally, none of the various possibilities can be preferred to another one by means of agreement with the full one-loop self-energy. Thus, we have to conclude that the m HTL approximation is not suitable for the calculation of quark self-energies. Therefore, we go back to the full one loop result to derive the dispersion relations.

4.3 Quark Dispersion Relations

4.3.1 Chiral Limit

First we study the quark dispersion relations for vanishing quark masses. Then the theory is chirally invariant, which means that chirality is a conserved quantum number and energy eigenstates are also chirality eigenstates. Utilizing the projectors

$$\Lambda^\pm = \frac{1}{2}(1 \pm \vec{\gamma} \hat{\mathbf{p}}), \quad (4.33)$$

which were defined in (2.60), the full quark propagator can be decomposed regarding the eigenvalue of helicity over chirality, which reads

$$\mathcal{S}(\omega, p) = \frac{i\Lambda^+\gamma_0}{\omega - p + \Sigma_+} + \frac{i\Lambda^-\gamma_0}{\omega + p + \Sigma_-} \quad (4.34)$$

with the definition of Σ_\pm given in eq. (2.67). When we assume weak damping, we may neglect the imaginary part of Σ_\pm with respect to the real part. The zeros of the denominators in (4.34) yield the position of the quasi-particle poles, as depicted in fig. 4.5 for $\omega - p + \Sigma_+$. There are three mathematical solutions of this equation shown in the upper panel. The rightmost zero is the regular quark, $p_0 = \omega_+(p)$, the leftmost solution has energy $p_0 = -\omega_-(p)$ and is called anti-plasmino. The third solution is below the light cone and represents a tachyonic solution. However, the imaginary part of $\omega - p + \Sigma_+$ is large below the light cone, as can be seen in the lower panel of fig. 4.5. Therefore, the weak coupling assumption does not hold, and the solution cannot be interpreted as quasi-particle, since the large imaginary part results in a large width in the corresponding spectral density.

The corresponding solutions of $\omega + p + \Sigma_-$ are:

$$p_0 = \omega_-(p), \quad p_0 = -\omega_+(p), \quad (4.35)$$

where $\omega_\pm(p)$ is chosen to be positive. The solution $p_0 = \omega_+(p)$ is the normal quark that is modified by the medium, gaining an effective thermal mass and obeying positive helicity over chirality ratio $\chi = +1$. The other positive energy solution $p_0 = \omega_-(p)$ is called the plasmino and is a pure medium effect. It was first discovered by Klimov [Kli81] and was interpreted as an anti-quark-hole

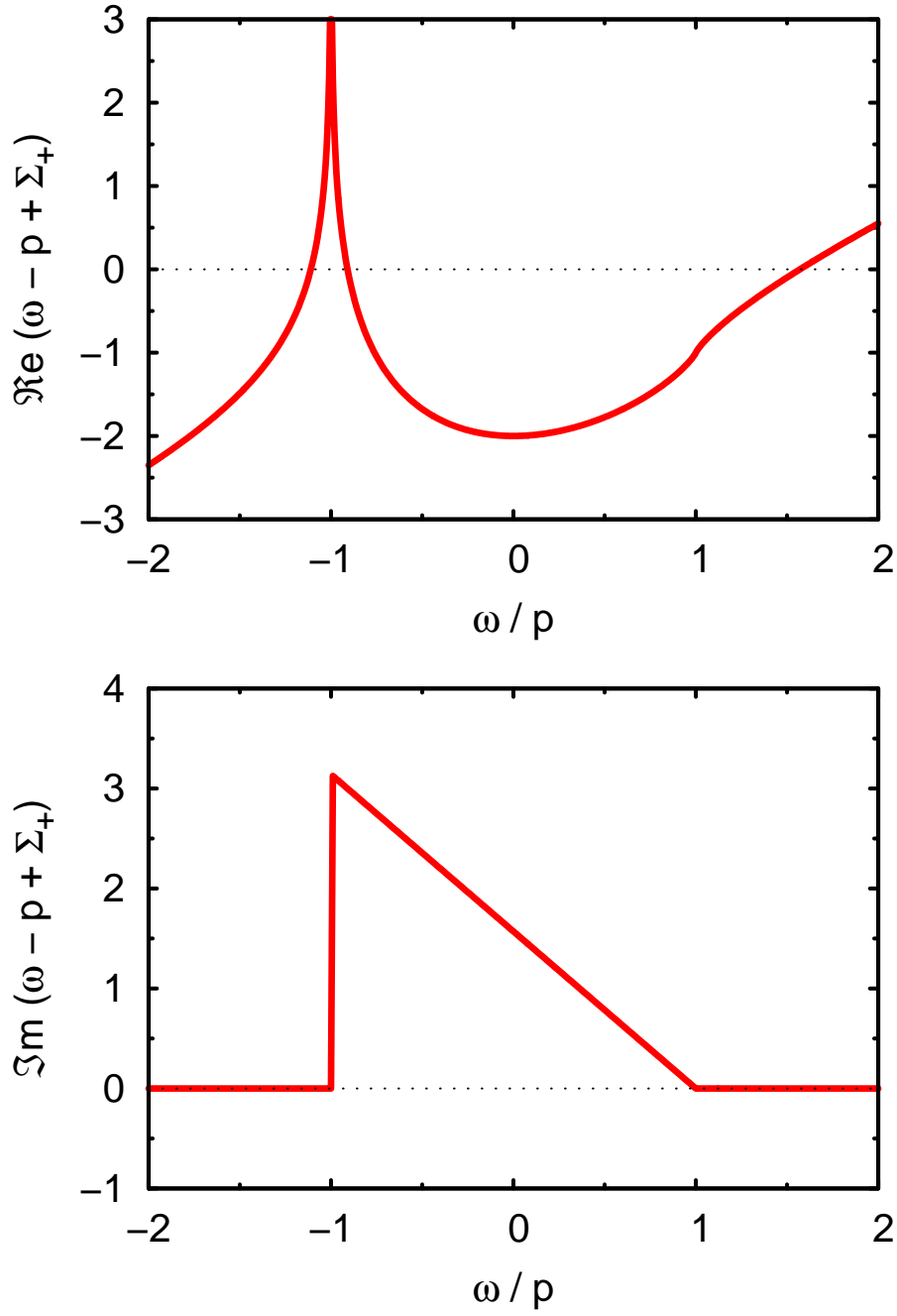


Figure 4.5: Real (upper panel) and imaginary parts (lower panel) of the inverse quark propagator as a function of ω/p in the HTL approximation for $p/T = 1$.

by Weldon [Wel82]. The plasmino has negative helicity over chirality ratio $\chi = -1$ just as the anti-quark, since it is a solution of $\omega + p + \Sigma_-$.

The dispersion relations are exhibited in fig. 4.6, for different values of the coupling constant g . One notes, that in the HTL approximation, the branches do not depend on g in the given scaling. On the other hand, the one-loop dispersion relations depend on g and the validity of the HTL approximation is better for smaller values of g .

For small and large momenta, one can derive simple expressions for the dispersion relations. In the HTL approximation, for $p \ll m_f$, the two branches with positive energy are given by [LeB96]

$$\omega_{\pm} \simeq m_f \pm \frac{1}{3}p. \quad (4.36)$$

At $p = 0$, the two branches coincide at $\omega_{\pm}(0) = m_f$. The quantity $m_f = \frac{1}{8}C_R g^2 T^2$ may be interpreted as an effective long-wavelength mass, generated by interaction with the medium. One notes that the plasmino branch has a negative slope at zero momentum. For large momenta, $p \gg m_f$, one finds

$$\omega_+^2(p) \simeq p^2 + 2m_f^2, \quad (4.37)$$

$$\omega_-(p) \simeq p + 2p \exp\left(-\frac{m_f^2 + 2p^2}{m_f^2}\right). \quad (4.38)$$

The normal quark branch exhibits a finite medium, the asymptotic mass, which is twice the long-wavelength thermal mass, for large momenta, in contrast to the collective plasmino which approaches the light cone exponentially fast for $p \gg m_f$.

A remarkable feature of the plasmino branch is a minimum at finite momentum. The existence of the minimum follows from the fact that the branch has a negative derivative at $p = 0$ and must approach the light cone for large momenta. The emergence of the plasmino and its minimum is a generic feature of chiral quarks propagating in a hot medium; it is not only found in perturbative calculations, see [Sch99, Pes00b]. The emergence of the minimum implies that the group velocity of the plasmino

$$v_{gr} = \frac{d\omega_-(p)}{dp},$$

which then may imply van Hove singularities and gaps in observable quantities, such as in di-lepton production rates (see discussion in [Tho01, Pes00b, Mus03]).

The spectral densities for quarks are defined by

$$\varrho_{\pm}(p_0, p) = -2\Im \mathbf{m}(p_0 \mp p + \Sigma_{\pm}(p_0, p))^{-1} \quad (4.39)$$

and contain contributions from quasi-particles for $p_0^2 > p^2$ and also Landau damping contributions stemming from the imaginary part of the self-energy below the light-cone for $p_0^2 < p^2$ [LeB96]. The quasi-particle contributions have the form $\delta(p_0 \pm \omega_{\pm}(p))$ for the four branches, and are weighted by the

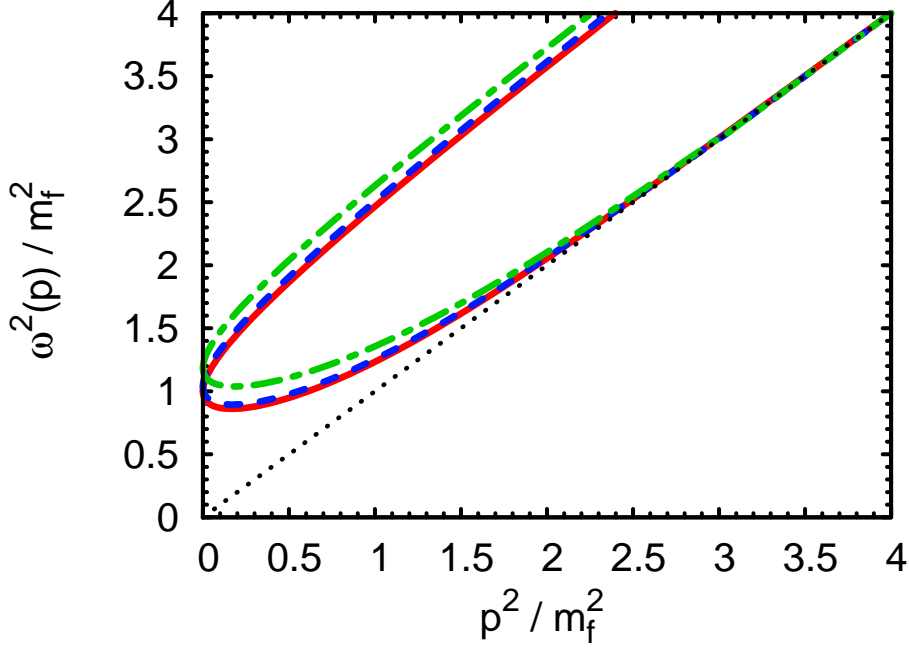


Figure 4.6: The quark dispersion relations for $m_q = 0$ in the HTL approximation (solid, red) and in the one-loop approximation for different values of the coupling constant (the blue dashed line corresponds to $g = 1$, the green dash-dotted line represents $g = 3$).

corresponding residues $Z_{\pm}(p)$. The residues of the spectral density may be interpreted as particle creation possibilities. Thus, the spectral density is given by

$$\varrho_{\pm}(p_0, p) = 2\pi \left[Z_{\pm}(p) \delta(p_0 - \omega_{\pm}(p)) + Z_{\mp}(p) \delta(p_0 + \omega_{\mp}(p)) \right] + \varrho_{\pm}^{LD} \quad (4.40)$$

with the Landau damping contribution ϱ_{\pm}^{LD} . These residues of the spectral density at the quasi-particle poles have simple expressions in the HTL approximation:

$$Z_{\pm}(p) = \frac{\omega_{\pm}^2(p) - p^2}{2m_f^2}, \quad (4.41)$$

giving in the limit of $p \ll m_f$

$$Z_{\pm}(p) \simeq \frac{1}{2} \pm \frac{p}{3m_f}. \quad (4.42)$$

Thus, for soft momenta, both excitations have approximately the same spectral strength and are therefore equally important. For large momenta $p \gg m_f$, one obtains a different behavior for the two branches:

$$Z_{+}(p) \simeq 1 + \frac{m_f^2}{2p^2} \left(1 - \ln \frac{2p^2}{m_f^2} \right), \quad (4.43)$$

$$Z_{-}(p) \simeq \frac{2p^2}{m_f^2} \exp \left(-\frac{m_f^2 + 2p^2}{m_f^2} \right). \quad (4.44)$$

Thus the spectral strength of the plasmino branch vanishes exponentially for large (hard) momenta. The sum rule for the spectral densities $\varrho_{\pm}(p_0, p)$ (cf. eq. (2.28)) can be written as

$$\int_0^{\infty} \frac{dp}{2\pi} \varrho_{\pm}(p_0, p) = Z_+(p) + Z_-(p) + \int_{-p}^{+p} \frac{dp_0}{2\pi} \varrho_{\pm}^{LD}(p_0, p) = 1. \quad (4.45)$$

From (4.42) one notes that for soft momenta the sum rule is almost saturated by the quasi-particles, where both types of quasi-particles give almost the same contribution to the sum rule. For hard momenta, by examining eqs. (4.43) and (4.44), the sum rule is also nearly fulfilled by the quasi-particles, but the collective mode is exponentially suppressed and the regular quark almost saturates the sum rule. Thus, at large momenta, the zero-temperature quark excitations are recovered with an additional dynamically generated mass of $2m_f^2$. The chiral invariance of the theory at $T = 0$ is not broken by this thermal masses, since both the propagator $\mathcal{S}(P)$ in eq. (4.34) and the self-energy $\Sigma(P)$ anti-commute with γ_5 .

4.3.2 Finite Quark Masses

To find the dispersion relations of the elementary plasma excitations, we have to find zeros of the denominator of the full quark propagator, given in eq. (2.59). The finite quark masses m_q , however, explicitly break chiral symmetry. As a consequence, chirality is not a conserved quantum number anymore so that the energy eigenstates do not have a definite chirality. Although it is possible to decompose the bare quark propagator \mathcal{S}_0 into positive and negative energy solutions utilizing the positive(negative) energy eigenstate projectors $\Lambda_{\mathbf{p}}^{\pm}$, this does hold out for the dressed propagator using the same projectors as in the chiral limit. However, one may use the projectors Ξ^{\pm} , defined in eq. (2.80) to decompose, at least formally, the dressed quark propagator into the same structures as for vanishing quark masses. Since the projectors include already the medium corrections, the physical interpretation of the eigenstates might be difficult. However, as [Pis89b] pointed out, the solutions of the dispersion relations smoothly connect with the $\chi = \pm 1$ modes of the chiral limit as $m_q \rightarrow 0$. Assuming again a weak damping of the propagating modes, we neglect the imaginary parts of the self-energy, which leads to the equations

$$0 = \omega - p + \Re \Sigma_+(\omega, p), \quad (4.46)$$

$$0 = \omega + p + \Re \Sigma_-(\omega, p) \quad (4.47)$$

with the definitions of Σ_{\pm} given in eq. (2.83).

In the weak coupling limit, where $g \ll 1$, and the light massive regime [Pis89b], where $m_q \lesssim gT$, the former equation can be simplified, by keeping only terms in the lowest order in gT . Then the functions $K_0(\omega, p)$ and $K(\omega, p)$ can be approximated by their chiral limit, taking $m_q \rightarrow 0$, and only the leading T^2

contributions have to be kept, resulting in the HTL approximated functions \hat{K}_0 and \hat{K} given in (4.22) and (4.21). The function $Z(p_0, p)$ is negligible, since it gives no contribution to the leading order. Hence, we may write for Σ_\pm in the light massive fermions regime

$$\Sigma_\pm^{lm}(\omega, p) = \hat{K}_0(\omega, p) \Big|_{m_q=0} \mp p \pm \sqrt{p^2 \left(1 + \hat{K}(\omega, p) \Big|_{m_q=0}\right)^2 + m_q^2} \quad (4.48)$$

which allows some analytic calculations.

The solutions of eq. (4.46) have to be found numerically and are depicted in fig. 4.7 for different bare quark masses, keeping the coupling constant fixed at $g = 3$. For $p = 0$ one finds a splitting of the two branches for nonzero quark masses, which is a consequence of explicit chiral symmetry breaking by the bare quark masses. The magnitude of this splitting is of order m_q/T and almost symmetric to the common value for the long wavelength limit of the two branches for $m_q = 0$. For small masses, when (4.48) may be employed, Pisarski [Pis89b] gave an analytic formula for the splitting of the branches at $p = 0$, which can be found from

$$0 = \omega \mp p + \Re \Sigma_\pm^{lm}(\omega, p) \quad (4.49)$$

and reads

$$\omega_\pm(p=0) = \frac{1}{2} \left(\sqrt{m_q^2 + 4m_f^2} \pm m_q \right). \quad (4.50)$$

In this limit, the splitting is strictly m_q , and an expansion in powers of m/m_f yields

$$\omega_+(0) \simeq m_f + \frac{m_q}{2}, \quad (4.51)$$

$$\omega_-(0) \simeq m_f - \frac{m_q}{2}. \quad (4.52)$$

For larger values of m_q , especially for $m_q \geq m_f$, the collective branch completely disappears from the spectrum for all p . Then it is obvious that the plasmino cannot exist, since its frequency at $p = 0$ is always below m_f , but the bare mass shell at $p = 0$ – the rest mass m_q – is larger. For values of the mass parameter between these two limits, the plasmino decouples at a finite value of p , which happens if the plasmino branch hits the bare mass shell. These phenomena can be observed in fig. 4.7. There, the plasmino has completely disappeared for $m_q = T$ and it decouples at finite p for $m_q = 0.4T$. For light quarks, the decoupling takes place at sizeable values of p and the limiting value for large momenta reads

$$\omega_-(p) \simeq p + 2p \exp \left(-\frac{m_f^2 + 2p^2}{m_f^2} \right) \exp \left(-\frac{m_q^2 p^2}{m_f^4} \right), \quad (4.53)$$

with the same exponential factor as in the massless case for large p in eq. (4.38), times an additional exponential suppression factor, where the bare mass enters and fortifies the exponential approach of the plasmino branch towards the light cone.

In the same limit, analytic formulae for the quark and plasmino excitation residues can be given. Following [Pet92] one obtains for the residues

$$Z_{\pm}(p) = \frac{\omega^2 - p^2}{2m_f^2} \left(1 - \frac{m_f^2}{2\omega p} \ln \frac{\omega + p}{\omega - p} \right) \left(1 - \frac{m_f^2}{2\omega p} \ln \frac{\omega + p}{\omega - p} + \frac{m_q^2}{2m_f^2} \right)^{-1}. \quad (4.54)$$

By putting the asymptotic form of the plasmino dispersion relation into this equation, one obtains the residue of the plasmino pole for large momenta in the vicinity of the light cone:

$$Z_-(\omega \simeq p) \simeq \frac{2p^2}{m_f^2} \left(1 + \frac{m_q^2 p^2}{m_f^4} \right) \exp \left(-\frac{m_f^2 + 2p^2}{m_f^2} \right) \exp \left(-\frac{m_q^2 p^2}{m_f^4} \right). \quad (4.55)$$

Here the plasmino is even more suppressed for large momenta than in the massless case due to the factor $\exp(-m_q^2 p^2 / m_f^4)$. However, the complete decoupling found using the full dispersion equation (4.46) is absent when performing calculations in the light massive fermion approximation (4.48). The relevant feature that makes the collective mode decouple is the screening of the logarithmic singularity of the self-energy at the light cone for $m_q = 0$, by the finite bare quark masses. In the light fermion approximation, this singularity is present, thus the plasmino does not disappear completely from the spectrum. The screening of this singularity in the inverse quark propagator $\omega - p + \Re \Sigma_+(\omega, p)$ is depicted in fig. 4.8. In the vicinity of the light cone at $\omega = -p = -1.5m_f$, the singularity is screened with increasing quark mass m_q , if the full one-loop self energy is employed to define $\Sigma_+(\omega, p)$. As can be seen in fig. 4.7, the plasmino has already decoupled for $m_q = 0.4T$ at this value of p . When the corresponding functions are utilized in the chiral limit, as in the definition of $\Sigma_+^{lm}(\omega, p)$ in (4.48), the singularity is present for arbitrary values of m_q and one always finds a plasmino branch for any value of p .

4.3.3 Asymptotic Quark Dispersion Relation

For large momenta in the vicinity of the bare mass shell, an analytic expression for the upper branch of the dispersion relation can be found. We begin the calculation with eq. (4.46). When the momentum p is large, the self-energy functions K and Z are small, since $K \sim p^{-2}$ and $Z \sim p^{-1}$. Then we can expand the square root into a Taylor series yielding

$$\omega(p) = -K_0(\omega, p) + p(1 + K(\omega, p)) \left[1 + \frac{m_q^2(1 + Z(\omega, p))^2}{2p^2(1 + K(\omega, p))^2} \right] \quad (4.56)$$

$$= -K_0(\omega, p) + p(1 + K(\omega, p)) + \frac{m_q^2(1 + Z(\omega, p))^2}{2p(1 + K(\omega, p))}, \quad (4.57)$$

and after squaring we obtain

$$\begin{aligned} \omega^2(p) &= \left\{ -K_0(\omega, p) + p(1 + K(\omega, p)) \right\}^2 \\ &+ \left[-\frac{K_0(\omega, p)}{p} + (1 + K(\omega, p)) \right] \frac{m_q^2(1 + Z(\omega, p))^2}{(1 + K(\omega, p))} \\ &+ \mathcal{O} \left(\frac{m_q^4}{p^2} \right), \end{aligned} \quad (4.58)$$

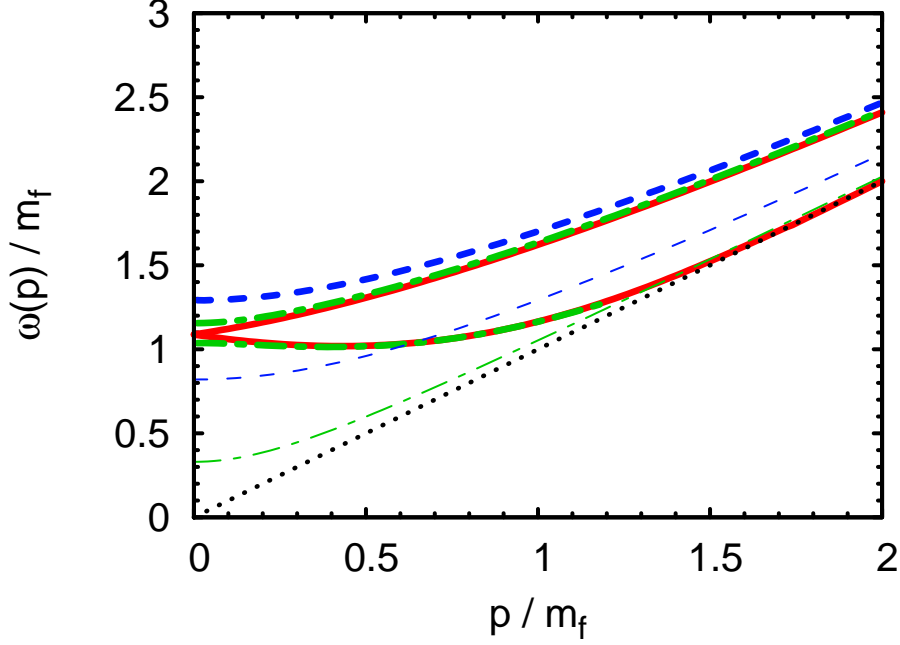


Figure 4.7: The scaled quark dispersion relations for different bare quark masses, keeping the coupling constant fixed at $g = 3$. The used mass parameters are $m_q = 0$ (red, solid), $m_q = 0.4T$ (green, dash-dotted) and $m_q = T$ (blue, dashed). The thin lines represent the corresponding bare mass shell expressions at $\omega(p) = \sqrt{p^2 + m_q^2}$.

where the last term $\propto m_q^4/p^2$ is negligible if p is large. In the second line, we can safely neglect the first term in the square bracket with respect to the second one for large momenta, resulting in

$$\begin{aligned} \omega^2(p) &= p^2 + m_q^2 \left(1 + Z(\omega, p)\right)^2 + 2p \left(p K(\omega, p) + K_0(\omega, p)\right) \\ &\quad + \left[K_0^2(\omega, p) + p K(\omega, p)(p K(\omega, p) - 2)\right], \end{aligned} \quad (4.59)$$

where all the terms in the square bracket go to zero for $p \rightarrow \infty$, due to the overall factor of p^{-1} in $K_0(\omega, p)$ and p^{-2} in $K(\omega, p)$, respectively, cf. eqs. (4.3 – 4.5). The same argument holds for the self-energy function $Z(\omega, p)$, which behaves as p^{-1} for $p \rightarrow \infty$. We obtain

$$\omega^2(p) = p^2 + m_q^2 + 2 \left(p^2 K(\omega, p) + p K_0(\omega, p)\right). \quad (4.60)$$

Employing in the last term the bare mass shell relation $\omega^2 = p^2 + m_q^2$, which can be understood as the first iteration of a self consistent solution of this equation, and afterwards taking the limit $p \rightarrow \infty$, we obtain the asymptotic quark dispersion relation

$$\omega^2(p) = p^2 + m_q^2 + 2M_+^2 \quad (4.61)$$

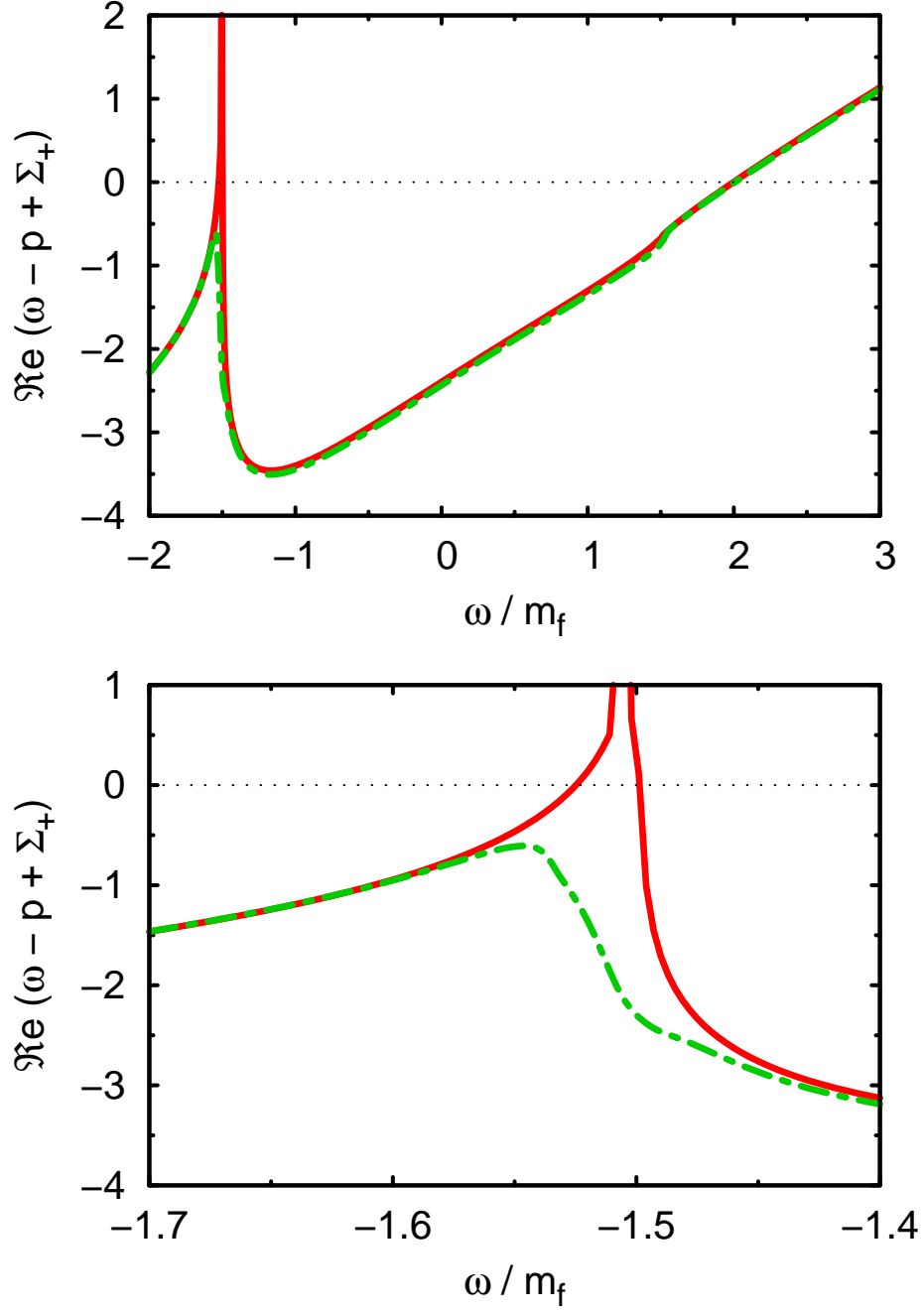


Figure 4.8: Real part of the inverse quark propagator as a function of ω for $p/m_f = 1.5$ and $g = 3$, for $m_q = 0$ (red, solid) and $m_q = 0.4T$ (green, dash-dotted). In the lower panel we show an magnification of the relevant region.

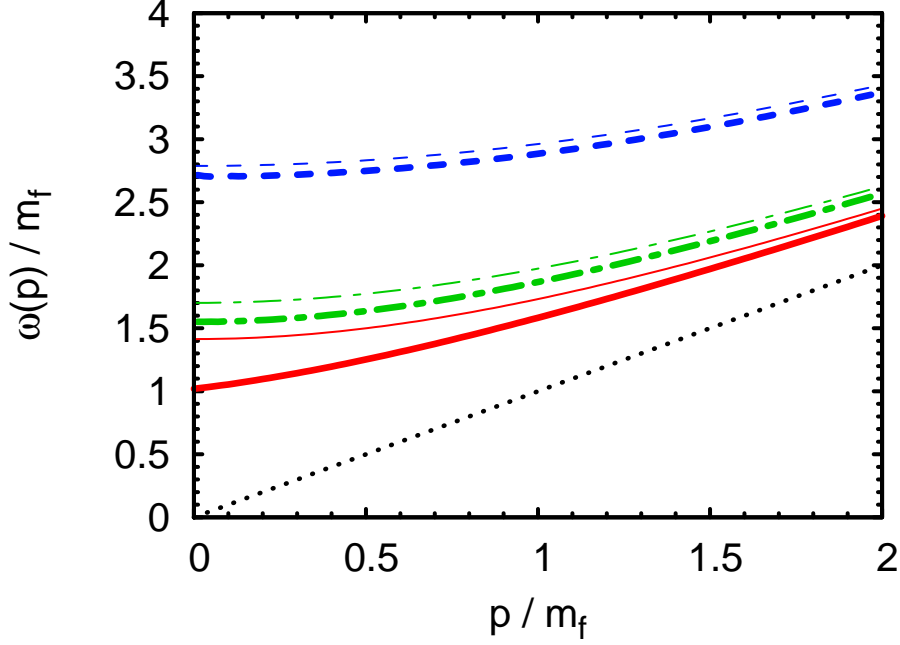


Figure 4.9: Full quark dispersion relations from eq. (4.46) and their asymptotic limits according to eq. (4.61) for $g = 1$ and different values of m_q/T . The same line code for both dispersion relations is applied (thicker lines represent the full dispersion relation and the thinner one corresponds to the asymptotic dispersion relation). The mass parameters are $m_q = 0$ (red, solid), $m_q = 0.4T$ (green, dash-dotted) and $m_q = T$ (blue, dashed).

with the asymptotic thermal quark mass

$$M_+^2 = \frac{g^2 C_R}{2\pi^2} \int_0^\infty dk \left(\frac{k^2}{\epsilon_{\mathbf{k}}} n_F(\epsilon_{\mathbf{k}}) + k n_B(k) \right). \quad (4.62)$$

This limit has to be performed very carefully, since both $p^2 K(\omega, p)$ and $p K_0(\omega, p)$ diverge but the divergencies exactly cancel each other. If one tries to iterate the equation once more by putting the solution (4.61) again into eq. (4.60), one finds exactly the same solution (4.61). Unlike the full quark dispersion relation, which depends on the gauge fixing, this asymptotic dispersion relation is independent of the choice of gauge. This is checked in Appendix D by an explicit calculation of the same asymptotic dispersion relation in the Coulomb gauge. This might be seen as a strong hint to general gauge invariance of the asymptotic dispersion relation (4.61) with the asymptotic thermal quark mass (4.62). In fig. 4.9, the asymptotic dispersion relations are compared to the full dispersion relations, derived from (4.46). The asymptotic dispersion relations are good approximations to the full dispersion relations for p/m_f large for any bare quark mass.

5 Applications

In this section we consider two main issues, which are tending towards an application of the asymptotic dispersion relations in quasi-particle description of thermodynamic properties of strongly interacting matter. We expand the asymptotic thermal mass expressions for small or large values of m_q/T , respectively. Especially the expansion for $m_q/T \approx 0$ will be important for the chiral extrapolation of the equation of state. Furthermore, we analyze the quality of the approximation of the dispersion relations at thermal momenta $p \sim T$ by the asymptotic dispersion relations.

5.1 Chiral Expansion of the Asymptotic Dispersion Relations

The asymptotic dispersion relations for gluons (g) and quarks (q) that have been derived in the preceding chapters read (cf. (3.82), (4.61))

$$\omega_g^2 = p^2 + m_\infty^2, \quad (5.1)$$

$$\omega_q^2 = p^2 + m_q^2 + 2M_+^2 \quad (5.2)$$

with the asymptotic gluon and quark masses

$$m_\infty^2 = \frac{1}{6}g^2T^2 \left(N_c + \frac{1}{2} \sum_q \mathcal{I}_g(m_q/T) \right), \quad (5.3)$$

$$M_+^2 = m_f^2 \mathcal{I}_q(m_q/T), \quad (5.4)$$

where $m_f^2 = \frac{1}{8}C_R g^2 T^2$ and the dimensionless integrals

$$\mathcal{I}_g = \frac{12}{\pi^2} \int_0^\infty d\tilde{k} \frac{\tilde{k}^2}{\tilde{\epsilon}_{\mathbf{k}}} \tilde{n}_F, \quad (5.5)$$

$$\mathcal{I}_q = \frac{4}{\pi^2} \int_0^\infty d\tilde{k} \left(\frac{\tilde{k}^2}{\tilde{\epsilon}_{\mathbf{k}}} \tilde{n}_F + \tilde{k} \tilde{n}_B \right) \quad (5.6)$$

$$= \frac{2}{3} + \frac{1}{3} \mathcal{I}_g. \quad (5.7)$$

For $m_q \rightarrow 0$, $\mathcal{I}_{g,q} \rightarrow 1$. Here we introduced the abbreviations $\tilde{k} = k/T$, $\tilde{\epsilon}_{\mathbf{k}} = \epsilon_{\mathbf{k}}/T = \sqrt{\tilde{k}^2 + m_q^2/T^2}$, $\tilde{n}_F = (e^{\tilde{\epsilon}_{\mathbf{k}}} + 1)^{-1}$ and $\tilde{n}_B = (e^{\tilde{k}} - 1)^{-1}$. The quark mass dependence of these dispersion relations comes, on the one hand, from the

explicit dependence through the term $\propto m_q^2$ in the quark dispersion relation and, on the other hand, also from the thermal quark and gluon masses, M_+^2 and m_∞^2 , depending on the bare quark masses in an involved way. To obtain analytic expressions for the dependence of the asymptotic masses on the bare quark mass m_q , we will expand these integrals in powers of $m_q/T \ll 1$ (chiral expansion) and $m_q/T \gg 1$ (heavy quark expansion). According to eq. (5.7), the integral \mathcal{I}_q can be reduced to a constant term plus another term being proportional to \mathcal{I}_g . Hence, for the calculation of the chiral expansion of both the gluon and quark thermal masses, the only relevant quantity to be studied is the integral $\mathcal{I}_g \equiv \mathcal{I}$.

First of all, we can use the geometric series to write the Fermi distribution function as

$$\frac{1}{e^{\tilde{\epsilon}_{\mathbf{k}}} + 1} = \frac{e^{-\tilde{\epsilon}_{\mathbf{k}}}}{1 - (-e^{-\tilde{\epsilon}_{\mathbf{k}}})} = e^{-\tilde{\epsilon}_{\mathbf{k}}} \sum_{j=0}^{\infty} (-1)^j e^{-j\tilde{\epsilon}_{\mathbf{k}}} = \sum_{j=1}^{\infty} (-1)^{j+1} e^{-j\tilde{\epsilon}_{\mathbf{k}}}. \quad (5.8)$$

Since the integral is absolutely convergent, we can interchange summation and integration and end up with

$$\mathcal{I} = \frac{12}{\pi^2} \sum_{j=1}^{\infty} (-1)^{j+1} \int_0^{\infty} d\tilde{k} \frac{\tilde{k}^2}{\tilde{\epsilon}_{\mathbf{k}}} e^{-j\tilde{\epsilon}_{\mathbf{k}}}. \quad (5.9)$$

The integral in eq. (5.9) however can be evaluated employing the relation given in eq. (E.7), yielding

$$\mathcal{I} = \frac{12}{\pi^2} \sum_{j=1}^{\infty} (-1)^{j+1} \frac{a}{j} K_1(j \cdot a) \quad (5.10)$$

with $a = m_q/T$. We now express the asymptotic gluon mass as an infinite sum over MacDonald functions or modified Bessel functions of the second kind. If it is possible to truncate this series at a certain order, our task is completed. Unfortunately, for $a \rightarrow 0$, eq. (5.10) shows a very poor convergence (cf. fig. 5.1) and is, therefore, not suitable for a chiral expansion. However, it is convenient for the heavy quark expansion, since for large values of a , the higher order terms in the series (5.10) rapidly go to zero. Using the asymptotic behavior of the MacDonald functions [BSMM93]

$$K_1(z) \simeq \sqrt{\frac{\pi}{2z}} e^{-z} \quad (5.11)$$

we obtain

$$\mathcal{I} \simeq \frac{12}{\pi^2} \sqrt{\frac{\pi}{2}} \sum_{j=1}^{\infty} (-1)^{j+1} \frac{a^{1/2}}{j^{3/2}} e^{-ja}. \quad (5.12)$$

Because of the exponential factor, every term with $j > 1$ in the sum tends to zero much faster than the $j = 1$ term, so that keeping only the first term of the sum should be a good approximation for heavy quarks

$$\mathcal{I} \simeq \frac{12}{\pi^2} \sqrt{\frac{m_q \pi}{2T}} e^{-\frac{m_q}{T}}. \quad (5.13)$$

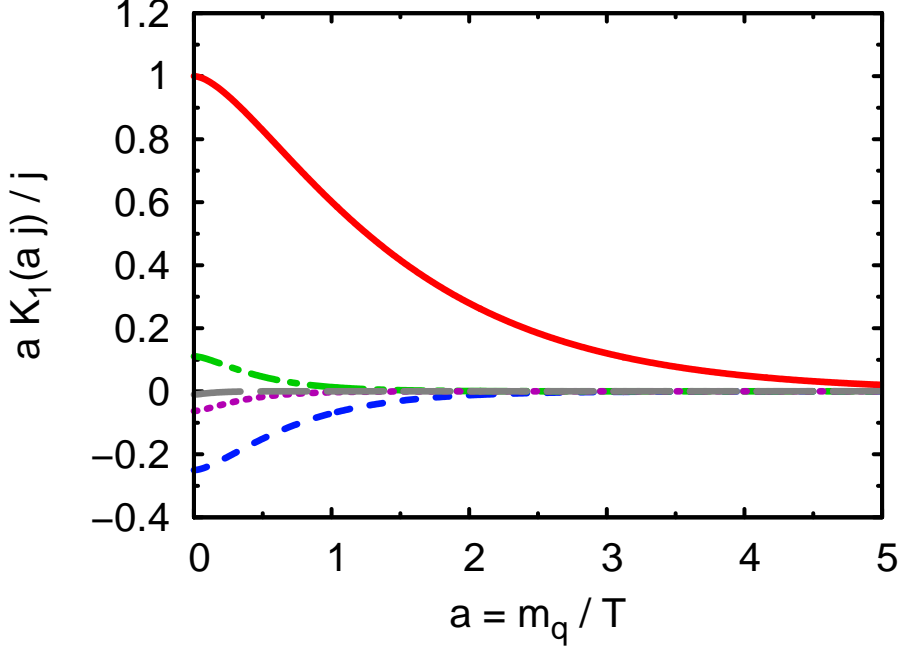


Figure 5.1: Depicted are the first few terms from the sum in eq. (5.10) for $j = 1$ (red, solid), $j = 2$ (blue, dashed), $j = 3$ (green, dash-dotted), $j = 4$ (purple, dotted) and $j = 10$ (grey, long-dashed). For large m_q/T the individual functions converge to zero fast, according to the asymptotic behavior given in (5.11).

Turning back now to the chiral expansion, one notes that, for decreasing quark masses, we have to keep more and more terms of the sum. Thus we should sum up the entire series, which can be done by a Mellin transformation [Bed00]. The Mellin transformation of a function f with $s \in \mathbb{C}$ can be written in the form

$$\mathcal{M}[f; s] = \int_0^\infty \frac{dz}{z} z^s f(z), \quad (5.14)$$

$$f(z) = \frac{1}{2\pi i} \int_{c-i\infty}^{c+i\infty} z^{-s} \mathcal{M}[f; s] ds \quad (5.15)$$

with the inverse transformation in the second line. The Mellin transform \mathcal{M} generally exists only in a strip $\alpha < \Re(s) < \beta$ parallel to the imaginary axis, called the fundamental strip, and the inversion contour must be in this strip: $\alpha < c < \beta$.

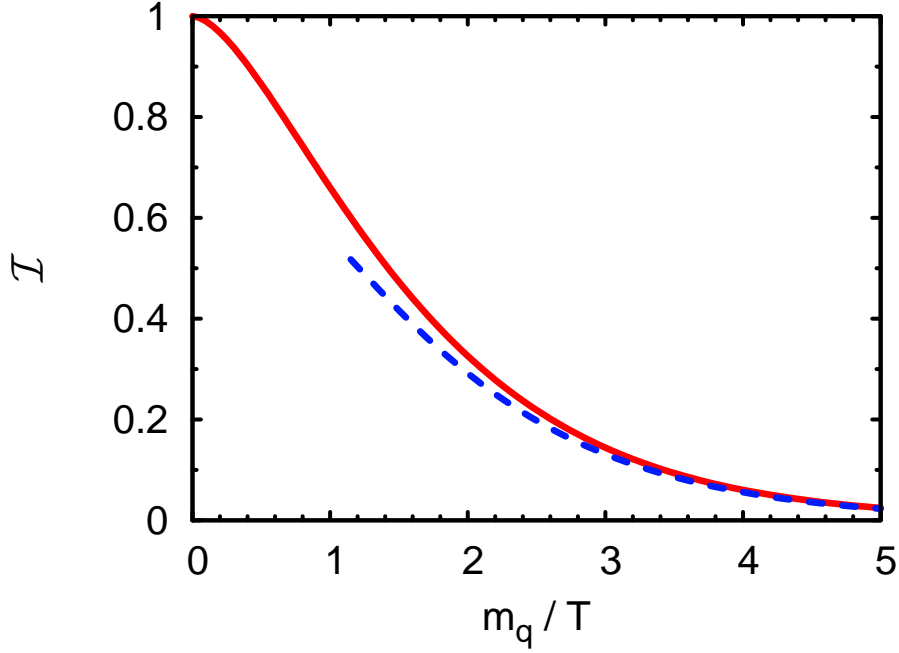


Figure 5.2: The heavy quark expansion of the function \mathcal{I} to the first order as given by (5.13) (blue, dashed). The solid red line represents the full numeric result of the integral in eq. (5.5).

Consider the Mellin transform of the modified Bessel function $K_1(z)$ giving the result

$$\begin{aligned}\mathcal{M}[K_1; s] &= \int_0^\infty z^{s-1} K_1(z) dz \\ &= 2^{s-2} \Gamma\left(\frac{s-1}{2}\right) \Gamma\left(\frac{s+1}{2}\right)\end{aligned}\quad (5.16)$$

which is valid for $\Re(s) > 1$. Thus one needs to choose the contour for the inverse transform, so that $c > 1$. Writing down the inverse transform, one obtains for $z = a \cdot j$

$$K_1(a \cdot j) = \frac{1}{2\pi i} \int_{c-i\infty}^{c+i\infty} j^{-s} a^{-s} \mathcal{M}[K_1; s] ds. \quad (5.17)$$

Using this representation of K_1 in eq. (5.10) yields

$$\mathcal{I} = \frac{1}{2\pi i} \frac{12}{\pi^2} \sum_{j=1}^{\infty} \int_{c-i\infty}^{c+i\infty} (-1)^{j+1} j^{-s-1} a^{1-s} \mathcal{M}[K_1; s] ds. \quad (5.18)$$

Now it is possible to perform the sum because the Mellin transform $\mathcal{M}[K_1; s]$ does not depend on the summation variable j anymore, yielding

$$\sum_{j=1}^{\infty} (-1)^{j+1} j^{-s-1} = \left(1 - \frac{1}{2^s}\right) \zeta(s+1) \quad (5.19)$$

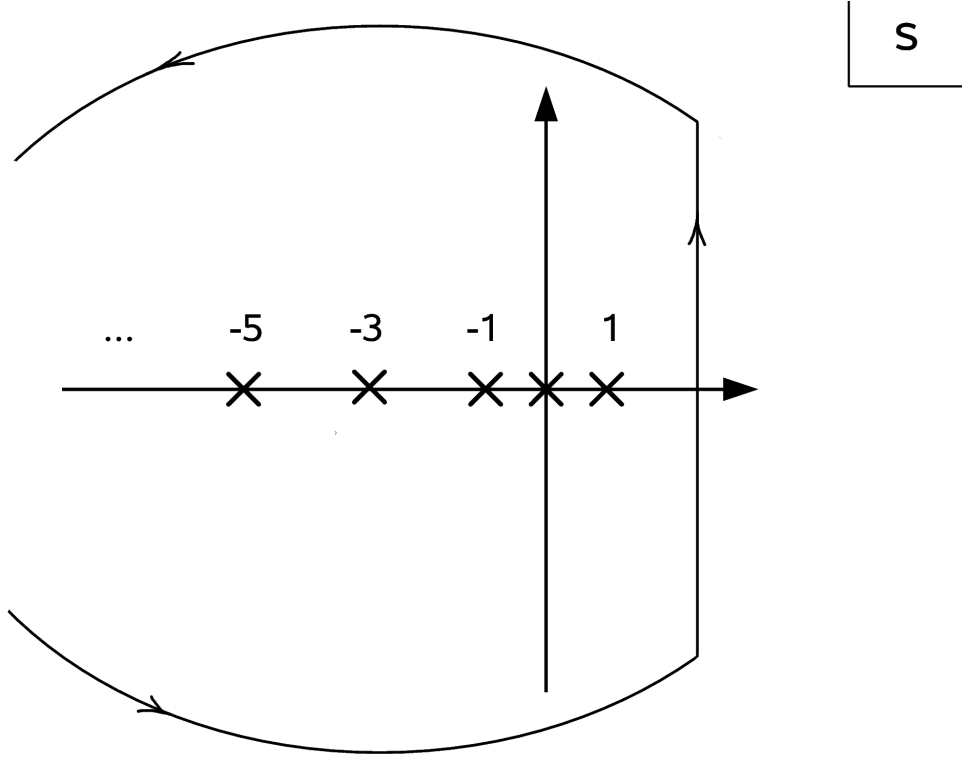


Figure 5.3: The integration contour in eq. (5.20) is closed in a large arc in the left half plane. The crosses mark singularities of the integrand. At $s = 1, -3, \dots$ these are single poles from the gamma functions, at $s = -1$ there is a double pole and at $s = 0$ there is a removable singularity.

with the Riemann zeta function. The above relation is valid for $\Re(s) > 0$, and using this equality with (5.18) we obtain

$$\mathcal{I} = \frac{12}{\pi^2} \frac{1}{2\pi i} \int_{c-i\infty}^{c+i\infty} \frac{a^{1-s}}{2^{2-s}} \left(1 - \frac{1}{2^s}\right) \zeta(s+1) \Gamma\left(\frac{s-1}{2}\right) \Gamma\left(\frac{s+1}{2}\right) ds. \quad (5.20)$$

In order to evaluate this integral we may close the contour in the left half plane as depicted in fig. 5.3, since the integrand vanishes asymptotically on the arc at infinity giving no contribution to the integral. Utilizing the residue theorem, we have now to sum up the residues of the poles of the integrand due to the gamma and Riemann zeta functions. So we end up with

$$\mathcal{I} = \sum_i \text{Res } f(s)|_{s=s_i} \quad (5.21)$$

with

$$f(s) = \frac{6}{\pi^2} \frac{a^{1-s}}{2^{1-s}} \left(1 - \frac{1}{2^s}\right) \zeta(s+1) \Gamma\left(\frac{s-1}{2}\right) \Gamma\left(\frac{s+1}{2}\right). \quad (5.22)$$

The integrand $f(s)$ has singularities at $s = 0$ due to the ζ -function and at $s = 1, -1, -3, \dots$ due to the gamma functions. At $s = 0$ there is a removable

singularity that has zeros residue. All the other emerging singularities are single poles, except the one at $s = -1$ being a double pole. At $s = 1$ we get

$$\text{Res } f(s)|_{s=1} = \frac{6}{\pi^2} a^0 \zeta(2) = 1, \quad (5.23)$$

which is the term proportional to a^0 . The double pole at $s = -1$ yields

$$\text{Res } f(s)|_{s=-1} = -\frac{3}{\pi^2} a^2 \left(\ln \pi + \frac{1}{2} - \gamma_E \right) + \frac{3}{2\pi^2} a^2 \ln a^2 \quad (5.24)$$

with the Euler constant γ_E . From the double pole, the a^2 term emerges and also the nonanalytic term $\propto a^2 \ln a^2$. For $s = -3$ we obtain

$$\text{Res } f(s)|_{s=-3} = -\frac{21}{16\pi^4} \zeta(3) a^4, \quad (5.25)$$

which gives the a^4 term. The other residues for $s = -5, -7, \dots$ give contributions to \mathcal{I} at order a^6, a^8, \dots . Thus we can write

$$\mathcal{I} = 1 + \alpha_2 a^2 + \alpha_L a^2 \ln a^2 + \alpha_4 a^4 + \sum_{j=3} \alpha_{2j} a^{2j}. \quad (5.26)$$

The results are summarized in tab. 5.1. The numeric values of the coefficients decrease very fast showing the importance of the first expansion contributions. We can also give a general formula for all the contributions stemming from the single poles in the negative plane,

$$\alpha_n = (-1)^{\frac{n-2}{2}} \frac{24}{n} \frac{2^{n-1} - 1}{(2\pi)^n} \frac{(n-3)!!}{(n-2)!!} \zeta(n-1), \quad n = 4, 6, 8, \dots \quad (5.27)$$

with the double factorial

$$n!! = \begin{cases} 2 \cdot 4 \cdot \dots \cdot n, & n \text{ even,} \\ 1 \cdot 3 \cdot \dots \cdot n, & n \text{ odd.} \end{cases} \quad (5.28)$$

The chiral expansion has a finite radius of convergence R , which can be calculated by

$$R^2 = \lim_{n \rightarrow \infty} \left| \frac{\alpha_n}{\alpha_{n+2}} \right|, \quad n \geq 4, \quad (5.29)$$

yielding $R = \pi$ utilizing the expansion coefficients in (5.27). The chiral expansion is depicted in fig. 5.4 in various orders, showing the relevance of the term $\propto a^2 \ln a^2$ even for very small values of a , as well as the finite radius of convergence.

We can also write down the chiral expansion for the asymptotic quark masses using the ansatz

$$\mathcal{I}_q = 1 + \beta_2 a^2 + \beta_L a^2 \ln a^2 + \beta_4 a^4 + \dots \quad (5.30)$$

Due to eq. (5.7) we find

$$\beta_j = \frac{1}{3} \alpha_j. \quad (5.31)$$

α_2	$-\frac{3}{\pi^2}(\ln \pi + \frac{1}{2} - \gamma_E)$	≈ -0.32449
α_L	$\frac{3}{2\pi^2}$	≈ 0.15198
α_4	$-\frac{21}{16\pi^4}\zeta(3)$	$\approx -1.619 \cdot 10^{-2}$
α_6	$\frac{93}{128\pi^6}\zeta(5)$	$\approx 7.836 \cdot 10^{-4}$
α_8	$-\frac{1905}{4096\pi^8}\zeta(7)$	$\approx -4.943 \cdot 10^{-5}$

Table 5.1: Summary of the first coefficients of the chiral expansion of the asymptotic gluon mass.

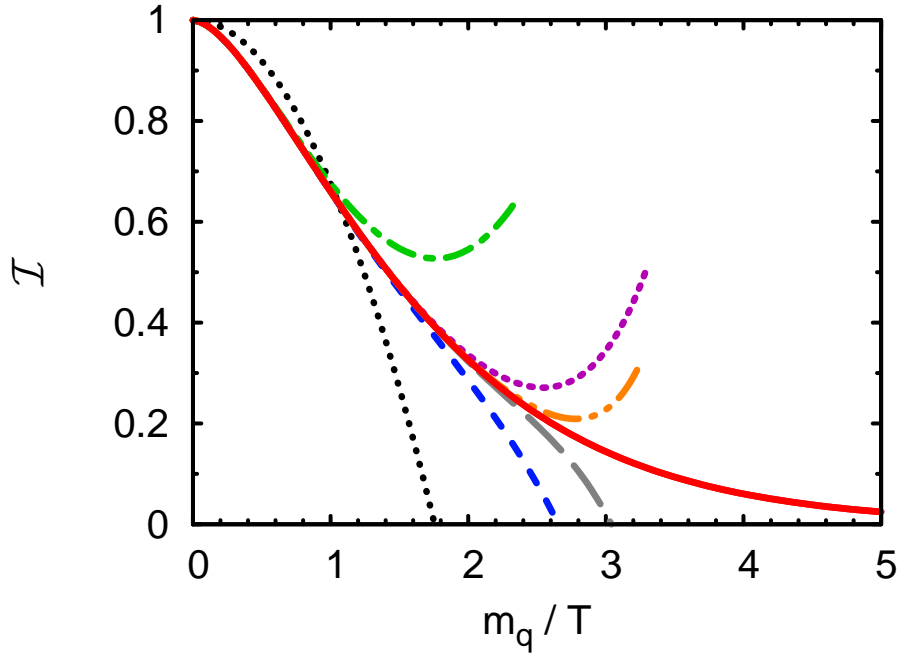


Figure 5.4: The chiral expansion of the function \mathcal{I} to orders a^2 (black, dotted), $a^2 \ln a^2$ (green, dash-dotted), a^4 (blue, dashed), a^6 (purple, dotted), a^8 (grey, long-dashed) and a^{10} (orange, dash-dot-dotted). The solid red line represents the full numeric result of the integral in eq. (5.5).

We now can give the final result of the chiral expansion of the asymptotic gluon and quark masses, which read

$$m_\infty^2 = \frac{1}{6}g^2T^2N_c + \frac{1}{12}g^2T^2 \sum_q \left(1 - \frac{3}{\pi^2}(\ln \pi + \frac{1}{2} - \gamma_E) \frac{m_q^2}{T^2} + \frac{3}{2\pi^2} \frac{m_q^2}{T^2} \ln \frac{m_q^2}{T^2} - \frac{21\zeta(3)}{16\pi^4} \frac{m_q^4}{T^4} + \frac{93\zeta(5)}{128\pi^6} \frac{m_q^6}{T^6} \pm \dots \right) \quad (5.32)$$

$$M_+^2 = \frac{1}{6}g^2T^2 \left(1 - \frac{1}{\pi^2}(\ln \pi + \frac{1}{2} - \gamma_E) \frac{m_q^2}{T^2} + \frac{1}{2\pi^2} \frac{m_q^2}{T^2} \ln \frac{m_q^2}{T^2} - \frac{7\zeta(3)}{16\pi^4} \frac{m_q^4}{T^4} + \frac{31\zeta(5)}{128\pi^6} \frac{m_q^6}{T^6} \pm \dots \right) \quad (5.33)$$

The terms of the structure $a^2 \ln a^2$ resemble chiral logs known from chiral perturbation theory [Ber06]. The idea behind such expansions is that for effective thermodynamic models, which employ asymptotic dispersion relations as relevant degrees of freedom, one has a simple tool to accomplish the chiral extrapolation.

5.2 Asymptotic Dispersion Relations for Thermodynamic Calculations

In thermodynamic descriptions of the quark gluon plasma in terms of massive, non-interacting quasi-particles, the various thermodynamic quantities, such as pressure p , entropy density s or number density n , are calculated by phase space integrals, where the dispersion relations of the corresponding quasi-particles play an important role. For example, the pressure for a system of non-interacting (quasi-)particles of species i with the dispersion relation $\omega_i(p)$ and degeneracy d_i may be written as

$$p_i(T) = \mp \frac{d_i}{2\pi^2} T \int_0^\infty dp p^2 \ln \left(1 \mp \exp \left(\frac{\omega_i(p)}{T} \right) \right), \quad (5.34)$$

where the upper sign (-) stands for bosons and the lower sign (+) is for fermions. Here the dispersion relation enters through the Boltzmann factor. The relevant momentum scale for the integration are hard momenta, $p \sim T$, due to the thermal measure, which is proportional to the distribution function n_F or n_B . At this momentum scale, however, the collective modes, i.e. plasminos and longitudinal gluons, are exponentially suppressed or have even decoupled completely from the spectrum. Therefore, the relevant degrees of freedom are transverse gluons as well as quarks and anti-quarks, respectively. One might try to parameterize the dispersion relation at the thermodynamic momentum scale $p \sim T$ by the asymptotic dispersion relations ($p \rightarrow \infty$). When $g \ll 1$, this is surely a good approximation. But since QCD is strongly

coupled, especially in the vicinity of the transition region, one has to extrapolate the perturbative results to values of $g \simeq 1$. Another fact, which favors the use of the asymptotic dispersion relations before the full dispersion relations, is the gauge invariance of the asymptotic dispersion relations. For $m_q = 0$ one might use the dispersion relations that follow from the gauge invariant HTL self-energies. But if $m \neq 0$ the generalization of HTL to finite masses is not consistently applicable to the quark self-energy. The question now is in how far the asymptotic quark and gluon dispersion relations are good parameterizations of the dispersion relations at thermal momenta of order $p \sim T$. To answer this question, we note that the quark and gluon dispersion relations for arbitrary momenta may be parameterized by

$$\omega_g^2 = p^2 + m_T^2(p), \quad (5.35)$$

$$\omega_q^2 = p^2 + m_q^2 + 2M_T^2(p) \quad (5.36)$$

with the bare quark mass m_q , where we defined momentum dependent thermal masses $m_T^2(p)$ ($M_T^2(p)$) for gluons (quarks) by

$$m_T^2(p) := \omega_g^2(p) - p^2, \quad (5.37)$$

$$M_T^2(p) := \frac{1}{2}(\omega_q^2(p) - p^2 - m_q^2) \quad (5.38)$$

with the exact dispersion relations $\omega_i(p)$, $i \in \{q, g\}$ for quarks and gluons, respectively. For the gluons we use the dispersion relations following from the transverse m HTL self energy, and for the quarks we utilize either the HTL self energy for $m_q = 0$ or the full one-loop self energy for $m_q \neq 0$. In the limit of large momenta, the thermal masses approach the asymptotic masses: $m_T^2(p \rightarrow \infty) = m_\infty^2$ and $M_T^2(p \rightarrow \infty) = M_+^2$, respectively. In the chiral limit we have $m_\infty^2 = \frac{1}{6}g^2T^2(N_c + N_F/2)$ and $M_+^2 = m_f^2 = \frac{1}{8}C_R g^2T^2$, where N_F is the number of active massless quark flavors.

In the upper panel of fig. 5.5 the independent variable is the gluon momentum, scaled by gT , which is the natural scale for in-medium dispersion relations, since the thermal masses are of that order. As the HTL dispersion relations are scale invariant in this picture, we can specify the value of p/T to a typical value that appears in thermodynamic integrals and obtain the dependence on the coupling constant g . In the lower panel of fig. 5.5, the chosen value is $p/T = 4$, for which the integrand of some typical thermodynamic integrals has a maximum. Thus, $p = 4T$ is used as the relevant momentum scale for thermodynamic calculations. The position of the maximum itself depends on the coupling and is shifted to larger values of p/T when g increases, however, this dependence is weak.

For small values of the coupling $g < 1$, as shown in the lower panel of fig. 5.5, the agreement of the asymptotic mass m_∞ and the momentum dependent mass for thermal momenta $m_T(p \sim T)$ is good. Thus, the asymptotic dispersion relation seems to be an appropriate parameterization of the dispersion relation relevant for thermodynamic calculations. For large values of g , the deviations are quite large, namely at the level of 25%, but as mentioned above, the relevant scale p/T increases, and therefore the agreement of the asymptotic

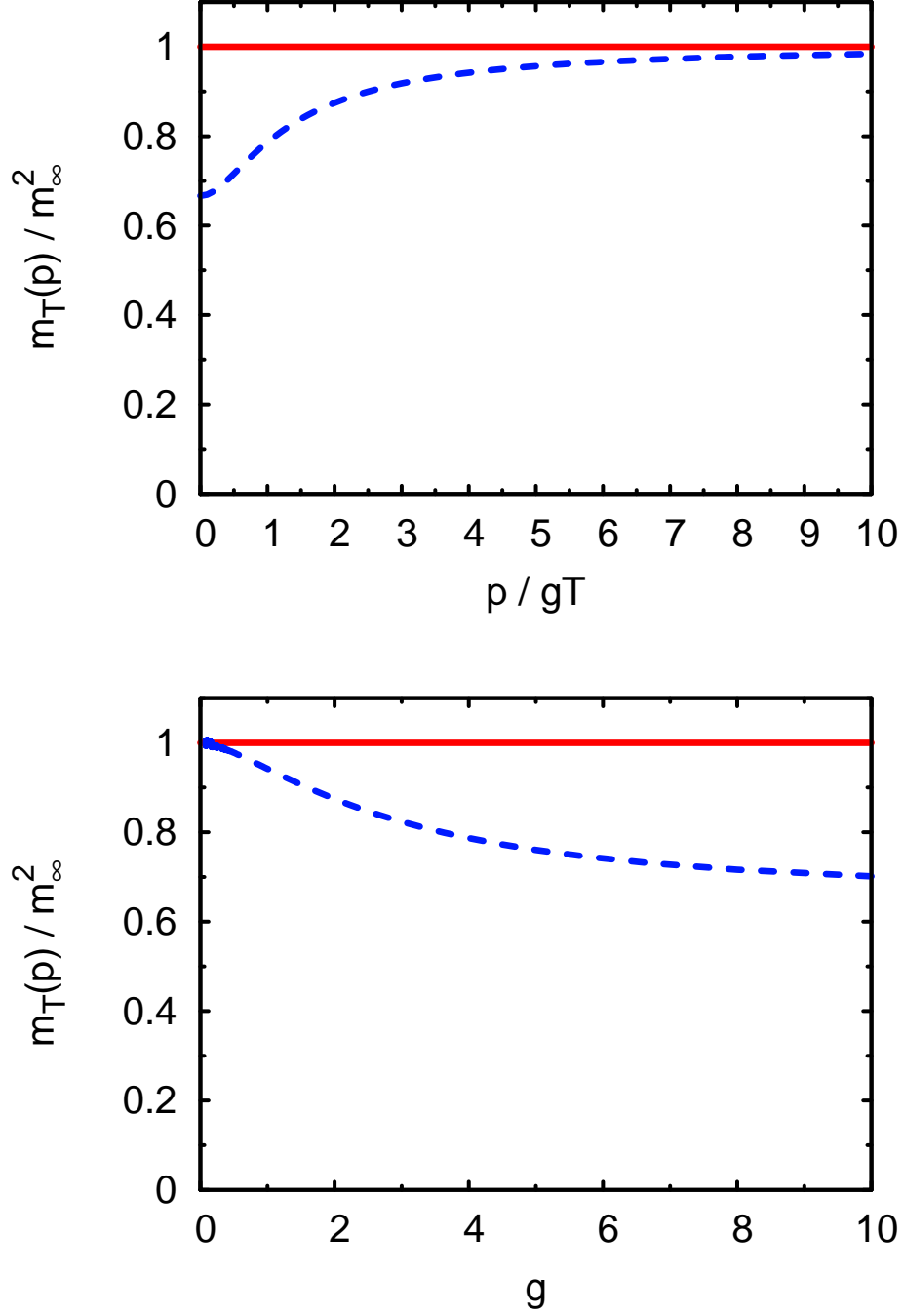


Figure 5.5: *Upper panel: Comparison of the asymptotic gluon mass m_∞^2 (red solid line) and the momentum dependent thermal gluon mass $m_T^2(p)$ (blue dashed line), scaled by m_∞^2 , given by the HTL dispersion relation for $m_q = 0$ as a function of $p/(gT)$. Lower panel: The same as in the upper panel, but as a function of the coupling g . Here the momentum scale is fixed to $p = 4T$, being a typical maximum value of p in typical thermodynamic integrals. Thus, it is assumed to be the relevant momentum scale for thermodynamic calculations.*

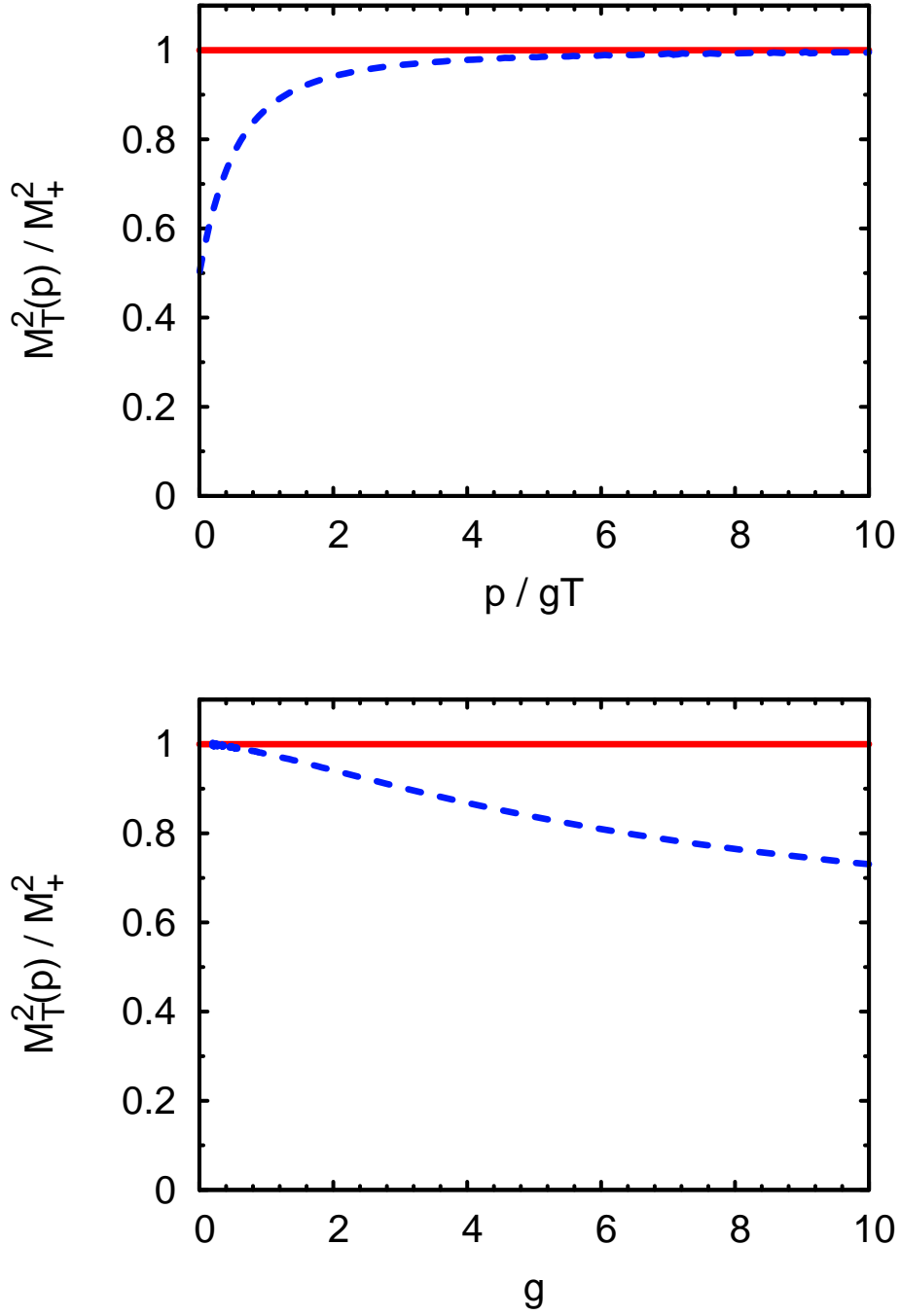


Figure 5.6: Comparison of the asymptotic quark mass M_+^2 (red solid line) and the momentum dependent thermal quark mass $M_T^2(p)$ (blue dashed line), scaled by M_+^2 , given by the HTL dispersion relation for $m_q = 0$, in analogy to fig. 5.5.

mass with m_T should be actually better than shown in the plot. A more detailed analysis would include too many details of the specific thermodynamic model, which is outside of the scope of this work. Hence, we omit an in-depth analysis. For the quark degrees of freedom, we find a similar behavior as in the case of the gluons, see fig. 5.6. The results found in this analysis coincides with eq. (3.59),

$$g^2 \ll \frac{p^2}{T^2} \quad (5.39)$$

which gives a constraint, at fixed coupling g , for which momenta the pole of the dressed propagator is in the vicinity of the light-cone. Turning this around by fixing the momentum, we obtain a constraint for the value of the (running) coupling, for which the asymptotic dispersion relations in the vicinity of the light-cone are good parameterizations for the full dispersion relations.

The next fact to be studied is the inclusion of finite bare quark masses into the preceeding analysis. Inspection of fig. 4.9 suggests that, at least for quarks, for increasing masses m_q and moderate g , the agreement of the full dispersion relation and the asymptotic dispersion relation is not too bad. The corresponding plots are exhibited in fig. 5.7 for quarks (upper panel) and gluons (lower panel). The parameter space now is two dimensional, with the two parameters being the coupling constant g and the dimensionless ratio m_q/T . We keep the parameter g constant at several values and vary the parameter m_q/T , thus generating cuts in the two dimensional parameter space parallel to the m_q/T -axis. These plots are shown in the upper panel of fig. 5.7. Again, for small values of the coupling, the agreement of the asymptotic and the thermal dispersion relation is quite good, which also holds for quite large masses of order of $m_q = 2T$. But as the coupling increases, the agreement is getting worse like in the case of massless quarks.

For gluons in the lower panel of fig. 5.7, we considered only one quark loop, since the non-Abelian gluon loops do not contain any mass dependence. So to say, we solved the equation

$$\omega^2(p) = p^2 + \Pi_T^q(\omega, p), \quad (5.40)$$

which is in fact, despite of the color group factor, the photon dispersion relation. We find that for increasing mass parameters, the thermal mass at typical momenta entering thermodynamic integrals and the asymptotic mass are agreeing very well, even for values of the coupling for which the curves do not coincide for $m_q = 0$. It is remarkable, that all the different curves lie on top of each other if the masses are getting large.

Thus, we conclude that the asymptotic dispersion relations for quarks and gluons are a suitable, gauge-invariant parameterization for the dispersion relations, which are relevant for thermodynamic calculations, if the coupling g is not too large. This fact is not spoiled when taking finite bare quark masses into account, the agreement is even getting better for the gluon dispersion relation. However, one has to be careful, if one uses this parameterization when the coupling is large.

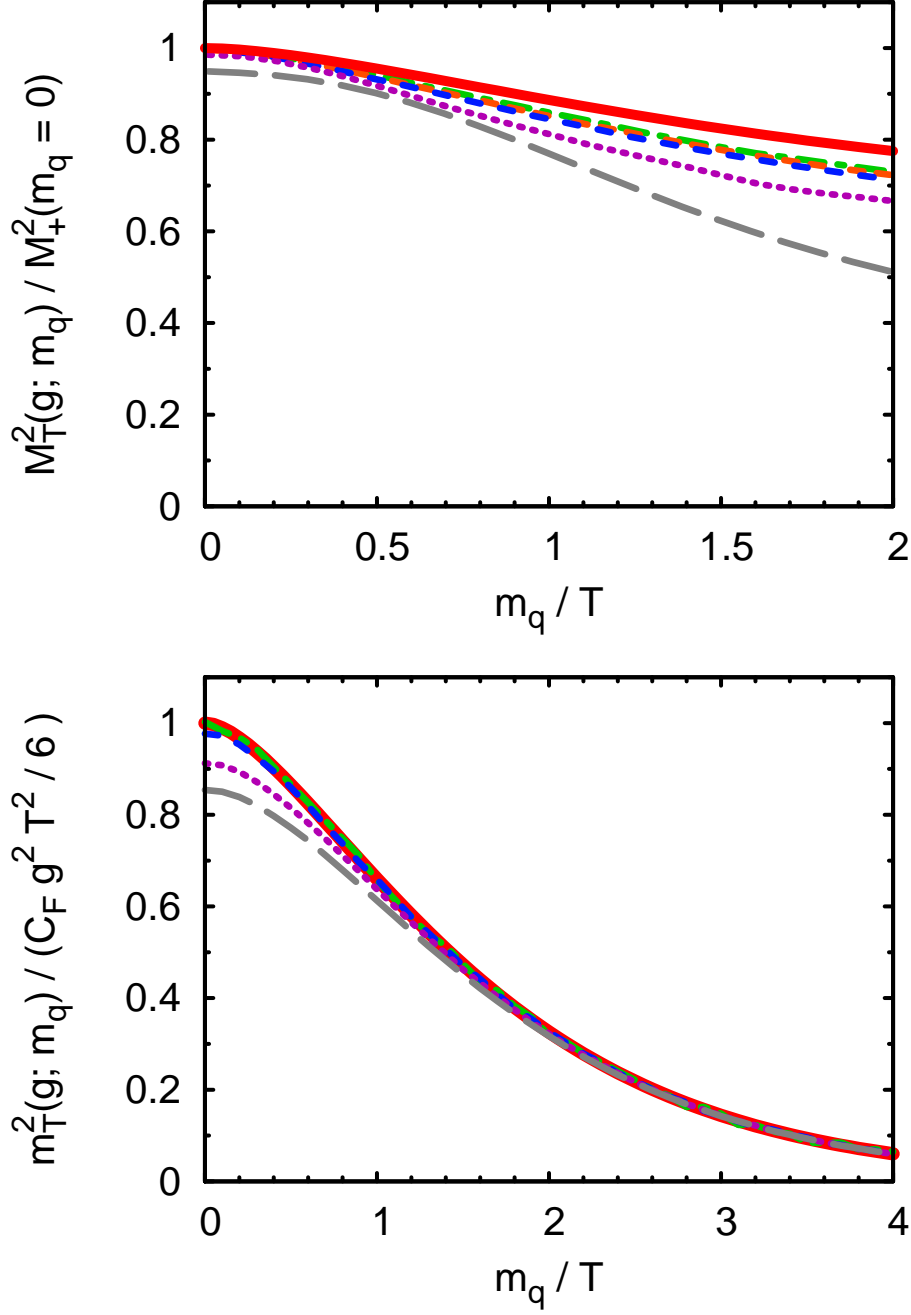


Figure 5.7: Upper panel: The asymptotic thermal quark mass (solid red) and momentum dependent thermal quark masses for various values of the coupling constant g as a function of the bare quark mass m_q scaled by the temperature T . From top to bottom the different curves represent $g = 0.3, 0.4, 0.5, 1.0$ and 3.0 .

Lower panel: Quark loop contribution of one massive flavor to the thermal gluon masses. The asymptotic mass (red solid) is compared with the momentum dependent thermal gluon masses for different values of the coupling, which are $g = 0.3$ (green, dash-dotted), $g = 1$ (blue, short-dashed), $g = 3$ (purple, dotted) and $g = 5$ (grey, long-dashed). We chose the typical thermodynamic momentum $p = 4T$, again.

6 Summary and Outlook

In this work, the quark and gluon self-energies and related dispersion relations, which are important for descriptions of the quark-gluon-plasma at finite temperature in terms of quasi-particles, were studied. The dependence of these quantities on the quark masses m_q has been derived from first principles utilizing methods of statistical quantum chromodynamics. The dispersion relations for quarks and gluons in a hot plasma have been calculated, focusing on hard momenta $p \sim T$ as the relevant momentum scale for thermodynamic bulk properties. The dispersion relations may be parameterized by the asymptotic dispersion relations with asymptotic thermal masses for quarks and gluons. These gauge invariant results were shown to be a good parameterization supposed the coupling is not too large.

Furthermore, a chiral expansion of the asymptotic masses was calculated, yielding a series in m_q/T including chiral logs. This is an easy tool for the chiral extrapolation of a quasi-particle-model equation of state, which is adjusted to lattice QCD results.

In the thermodynamically relevant region, transverse gluons and the ordinary quark modes almost saturate the sum rules of the corresponding spectral densities of gluons and quarks. The collective excitations (longitudinal gluons and plasminos) and also the Landau damping contributions below the light cone give small contributions to the sum rules. Thus, they are expected to give also negligible contributions to the thermodynamic bulk properties such as the pressure. When the quark masses are nonzero, the collective phenomena are additionally suppressed in the momentum region relevant for thermodynamics. It was found that they completely disappear from the excitation spectrum for large quark masses.

Furthermore, the renormalization of ultraviolet divergencies of the vacuum parts of the self-energies was performed in a mass dependent renormalization scheme, so that the renormalized quark masses are fixed constants, rather than running masses as in the Minimal Subtraction schemes. The running coupling in this scheme exhibits an explicit dependence on the quark masses. This allows a convenient parameterization of the effective coupling of quasi-particle models, incorporating mass effects, over a wide range of temperature.

In this way, employing both, m_q -dependent dispersion relations and effective coupling, one achieves the possibility of a reliable chiral extrapolation of the equation of state of strongly interacting matter, adjusted to lattice QCD results.

The new dispersion relations have to be included into the quasi-particle-model, together with a parameterization of the new mass dependent running coupling. As a nice test of the quality of the chiral extrapolation one might use new lattice

data that used much smaller quark masses than previous calculations [Kar07]. Preliminary results obtained in our group, which included only some aspects of the mass dependent dispersion relations, showed an impressive agreement of the equation of state adjusted at the old lattice data with large quark masses extrapolated towards the new lattice equation of state with smaller and thus physically relevant quark masses.

Extrapolation of the equation of state to temperatures in the range of $10T_c - 1000T_c$ provides an equation of state for cosmological purposes. It should be possible to include the heavy charm, bottom and top quarks into the quasi-particle model. These heavy flavors do not contribute to thermodynamic quantities in the temperature region where present day lattice data are available, but they are important at temperatures which are relevant for cosmology.

Appendix A Formulary

A.1 Units, Notations & Conventions

In this work, we employ the unit system often used in high energy physics with

$$c = \hbar = 1.$$

Then spatial distances and times have the same dimension. The relevant length and time scales in high energy physics are

$$1 \text{ fm} / c \hat{=} 3.335 \cdot 10^{-24} \text{ s}.$$

Energies and lengths have inverse physical dimensions. The conversion factor is

$$\hbar c = 197.3 \text{ MeV fm}.$$

Additionally the units can be chosen to have the Boltzmann constant as

$$k_B = 1,$$

so that temperatures are measured in units of energy. The temperature at the MeV scale is therefore in Kelvin:

$$1 \text{ MeV} \hat{=} 1.160 \cdot 10^{10} \text{ K}.$$

Covariant 4-vectors are denoted by Greek upper indices:

$$x : \quad x^\mu = (x_0, \mathbf{x}),$$

where three dimensional vectors like \mathbf{x} are set in bold face lower case letters. The components of three dimensional vectors are denoted by Latin indices:

$$\mathbf{x} \equiv (x_1, x_2, x_3) \equiv x_i$$

The four dimensional distance is given by:

$$ds^2 = g_{\mu\nu} dx^\mu dx^\nu,$$

where we utilize Einstein's sum convention: sum over indices that appear twice from 0 to 3. The Minkowski metric tensor is chosen as

$$g_{\mu\nu} = \begin{pmatrix} 1 & 0 & 0 & 0 \\ 0 & -1 & 0 & 0 \\ 0 & 0 & -1 & 0 \\ 0 & 0 & 0 & -1 \end{pmatrix}$$

with

$$g_{\mu\nu}g^{\nu\lambda} = \delta_\mu^\lambda.$$

Thus the contravariant 4-vector reads:

$$x_\mu = g_{\mu\nu}x^\nu = (x_0, -\mathbf{x}).$$

Scalar products in Minkowski space are written as

$$AB := A_\mu B^\mu$$

to shorten the notation.

4-momenta are denoted by upper case letters and 3-momenta and energies by lower case letters

$$K^\mu = (k_0, \mathbf{k}).$$

The absolute value and the direction of the 3-momentum are denoted by

$$\begin{aligned} k &= |\mathbf{k}|, \\ \hat{\mathbf{k}} &= \frac{\mathbf{k}}{k}. \end{aligned}$$

Scalar products including the Dirac matrices are written using the Feynman-dagger:

$$\not{P} := \gamma_\mu P^\mu.$$

For bosons we note the formulas:

$$\begin{aligned} f(k_0) &= \frac{1}{e^{\beta k_0} - 1}, \\ n_B(k_0) &= \frac{1}{e^{\beta|k_0|} - 1}, \\ f(\omega) &= n_B(\omega), \\ f(-\omega) &= -n_B(\omega) - 1, \end{aligned} \tag{A.1}$$

and for fermions:

$$\begin{aligned} \tilde{f}(k_0) &= \frac{1}{e^{\beta k_0} + 1}, \\ n_F(k_0) &= \frac{1}{e^{\beta|k_0|} + 1}, \\ \tilde{f}(\omega) &= n_F(\omega), \\ \tilde{f}(-\omega) &= -n_F(\omega) + 1. \end{aligned} \tag{A.2}$$

A.2 SU(3)-Color Algebra

Let $\{\mathcal{T}^a, a = 1 \dots 8\}$ be the Hermitian, traceless generators of the Lie group $SU(3)$. They satisfy the Lie algebra (commutation relation)¹

$$[\mathcal{T}^a, \mathcal{T}^b] = if^{abc}\mathcal{T}^c \tag{A.3}$$

¹For color indices we also utilize Einstein's sum convention; one has to sum over $a = 1 \dots 8$.

with the totally antisymmetric structure constants f^{abc} .

In the fundamental representation, the T^a are represented by the 3×3 matrices t^a as

$$t^a = \frac{1}{2}\lambda^a \quad (\text{A.4})$$

with the Gell-Mann matrices λ^a

$$\begin{aligned} \lambda_1 &= \begin{pmatrix} 0 & 1 & 0 \\ 1 & 0 & 0 \\ 0 & 0 & 0 \end{pmatrix}, & \lambda_2 &= \begin{pmatrix} 0 & -i & 0 \\ i & 0 & 0 \\ 0 & 0 & 0 \end{pmatrix}, & \lambda_3 &= \begin{pmatrix} 1 & 0 & 0 \\ 0 & -1 & 0 \\ 0 & 0 & 0 \end{pmatrix}, \\ \lambda_4 &= \begin{pmatrix} 0 & 0 & 1 \\ 0 & 0 & 0 \\ 1 & 0 & 0 \end{pmatrix}, & \lambda_5 &= \begin{pmatrix} 0 & 0 & -i \\ 0 & 0 & 0 \\ i & 0 & 0 \end{pmatrix}, & \lambda_6 &= \begin{pmatrix} 0 & 0 & 0 \\ 0 & 0 & 1 \\ 0 & 1 & 0 \end{pmatrix}, \\ \lambda_7 &= \begin{pmatrix} 0 & 0 & 0 \\ 0 & 0 & -i \\ 0 & i & 0 \end{pmatrix}, & \lambda_8 &= \frac{1}{\sqrt{3}} \begin{pmatrix} 1 & 0 & 0 \\ 0 & 1 & 0 \\ 0 & 0 & -2 \end{pmatrix}. \end{aligned} \quad (\text{A.5})$$

Important relations for the fundamental representation are

$$\text{tr}(t^a t^b) = C_F \delta_{ab}, \quad C_F = \frac{1}{2}, \quad (\text{A.6})$$

$$(t^a t^a)_{ij} = C_R \delta_{ij}, \quad C_R = \frac{N^2 - 1}{2N} = \frac{4}{3}. \quad (\text{A.7})$$

The 8 dimensional adjoint representation is defined by

$$(T^a)_{bc} = -if^{abc}, \quad (\text{A.8})$$

which satisfies the relations

$$\text{tr}(T^a T^b) = N \delta_{ab}, \quad (\text{A.9})$$

$$(T^a T^a)_{bc} = C_A \delta_{bc}, \quad C_A = N = 3. \quad (\text{A.10})$$

A detailed introduction to the application of Lie groups in physics, with special focus on $\mathbf{SU}(N)$ can be found in [Grei5].

A.3 Dirac Matrix Algebra

In Minkowski space, the Dirac γ matrices obey the anti-commutation relation

$$\{\gamma_\mu, \gamma_\nu\} = 2g_{\mu\nu}. \quad (\text{A.11})$$

Contractions of the γ_μ 's are

$$\begin{aligned} \gamma^\mu \gamma_\mu &= 4, \\ \gamma^\mu \gamma^\nu \gamma_\mu &= -2\gamma^\nu, \\ \gamma^\mu \gamma^\nu \gamma^\sigma \gamma_\mu &= 4g^{\nu\sigma}. \end{aligned} \quad (\text{A.12})$$

Traces over γ matrices are

$$\begin{aligned}\mathrm{tr}(\mathbf{1}) &= 4, \\ \mathrm{tr}(\text{any odd number of } \gamma\text{'s}) &= 0, \\ \mathrm{tr}(\gamma^\mu \gamma^\nu) &= 4g^{\mu\nu}, \\ \mathrm{tr}(\gamma^\mu \gamma^\nu \gamma^\sigma \gamma^\tau) &= 4(g^{\mu\nu}g^{\sigma\tau} - g^{\mu\sigma}g^{\nu\tau} + g^{\mu\tau}g^{\nu\sigma}).\end{aligned}\tag{A.13}$$

In addition, one defines the γ_5 matrix by

$$\gamma_5 = i\gamma_0\gamma_1\gamma_2\gamma_3,\tag{A.14}$$

which anti-commutes with γ_μ :

$$\{\gamma_5, \gamma_\mu\} = 0.\tag{A.15}$$

Projections on fermions with left- and right-handed chirality can be defined with the help of γ_5

$$\psi_L = \frac{1}{2}(1 - \gamma_5)\psi,\tag{A.16}$$

$$\psi_R = \frac{1}{2}(1 + \gamma_5)\psi.\tag{A.17}$$

When decomposing the Lagrangian (B.1) into fermions with left- and right-handed chirality, the only term that mixes ψ_L and ψ_R is

$$\mathcal{L}_m = m\bar{\psi}\psi = m(\bar{\psi}_L\psi_R + \bar{\psi}_R\psi_L).\tag{A.18}$$

Thus, when all fermions of the theory are massless, there is no mixing of the left- and right-handed fermions, i.e. right- and left-handed fermions are completely decoupled. This is called chiral symmetry.

Appendix B Feynman Rules

B.1 Feynman Rules in Minkowski Space

The Feynman rules are taken from [PS95] and follow from the QCD Lagrangian

$$\begin{aligned}\mathcal{L} = & \bar{\psi}(i\cancel{\partial} - m)\psi - \frac{1}{4}(\partial_\mu A_\nu^a - \partial_\nu A_\mu^a)^2 + g A_\mu^a \bar{\psi} \gamma^\mu t^a \psi \\ & - g f^{abc}(\partial_\mu A_\nu^a) A_b^\mu A_c^\nu - \frac{1}{4}g^2(f^{eab} A_\mu^a A_\nu^b)(f^{ecd} A_c^\mu A_d^\nu) \\ & - \frac{1}{2\rho}(\partial_\mu A_a^\mu)^2 - \bar{\eta}^a \partial_\mu \partial^\mu \eta^a - g \bar{\eta}^a \partial^\mu f^{abc} A_\mu^b \eta^c.\end{aligned}\quad (\text{B.1})$$

Here ψ denotes the quark fields, A_μ^a stands for the gluon fields and η^a are the ghost fields. The gauge is fixed in a general covariant gauge by the term $\frac{1}{2\rho}(\partial_\mu A_a^\mu)^2$. We further specify propagators and vertices.

Propagators:

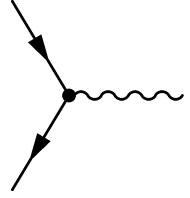
$$k \xrightarrow{\quad \overleftarrow{P} \quad} j \quad = \quad \mathcal{S}_{ij}(P) = \frac{i \delta_{jk}}{\not{P} - m + i\epsilon}, \quad (\text{B.2})$$

$$a, \mu \xrightarrow[\leftarrow P]{\quad \text{wavy} \quad} b, \nu \quad = \quad \mathcal{D}_{\mu\nu}^{ab}(P) = \frac{-i\delta_{ab}}{P^2 + i\epsilon} \left(g_{\mu\nu} + (\rho - 1) \frac{P_\mu P_\nu}{P^2} \right), \quad (\text{B.3})$$

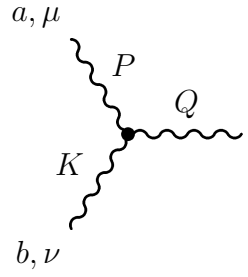
$$a \cdots \cdots \xrightarrow{\quad \overleftarrow{P} \quad} \cdots \cdots b \quad = \quad \mathcal{G}_{ab}(P) = \frac{i\delta_{ab}}{P^2 + i\epsilon}. \quad (\text{B.4})$$

The gluon propagator in eq. (B.3) is given in a general covariant gauge with gauge fixing parameter ρ .

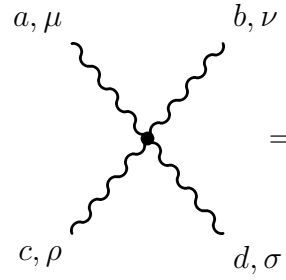
Vertices:



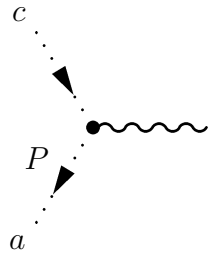
$$a, \mu = ig\gamma^\mu t^a, \quad (\text{B.5})$$



$$= gf^{abc} \left[g^{\mu\nu} (K - P)^\sigma + g^{\nu\sigma} (P - Q)^\mu + g^{\sigma\mu} (Q - K)^\nu \right], \quad (\text{B.6})$$



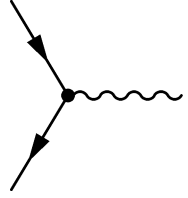
$$= -ig^2 \left[f^{abe} f^{cde} (g^{\mu\rho} g^{\nu\sigma} - g^{\mu\sigma} g^{\nu\rho}) + f^{ace} f^{bde} (g^{\mu\nu} g^{\rho\sigma} - g^{\mu\sigma} g^{\nu\rho}) + f^{ade} f^{bce} (g^{\mu\nu} g^{\rho\sigma} - g^{\mu\rho} g^{\nu\sigma}) \right], \quad (\text{B.7})$$



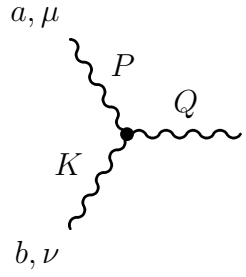
$$= -gf^{abd} P^\mu. \quad (\text{B.8})$$

In (B.6) all momenta are understood to be incoming.

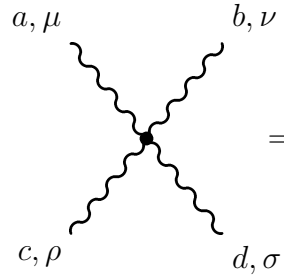
Vertices:



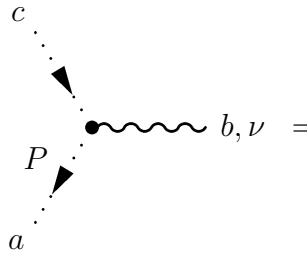
$$a, \mu = g\gamma^\mu t^a, \quad (\text{B.13})$$



$$= igf^{abc} \left[\delta^{\mu\nu}(P - K)^\sigma + \delta^{\nu\sigma}(K - Q)^\mu + \delta^{\sigma\mu}(Q - P)^\nu \right], \quad (\text{B.14})$$



$$= -g^2 \left[f^{abe} f^{cde} (\delta^{\mu\rho} \delta^{\nu\sigma} - \delta^{\mu\sigma} \delta^{\nu\rho}) + f^{ace} f^{bde} (\delta^{\mu\nu} \delta^{\rho\sigma} - \delta^{\mu\sigma} \delta^{\nu\rho}) + f^{ade} f^{bce} (\delta^{\mu\nu} \delta^{\rho\sigma} - \delta^{\mu\rho} \delta^{\nu\sigma}) \right], \quad (\text{B.15})$$



$$= igf^{abd} P^\mu. \quad (\text{B.16})$$

B.3 Analytic Continuation

For the translation of quantities between Euclidean and Minkowski space, we utilize the following rules

<u>Minkowski space</u>	\longleftrightarrow	<u>Euclidean Space</u>
$A_\mu B^\mu$	\longleftrightarrow	$-A_\mu B_\mu$
\not{P}_M	\longleftrightarrow	$-\not{P}_E$
$i\mathcal{S}_M$	\longleftrightarrow	\mathcal{S}_E
γ_0	\longleftrightarrow	$-i\gamma_4$
$\{\gamma_\mu, \gamma_\nu\} = 2g_{\mu\nu}$	\longleftrightarrow	$\{\gamma_\mu, \gamma_\nu\} = -2\delta_{\mu\nu}$
p_0	\longleftrightarrow	$-ip_4 \equiv i\omega_n$
Π_{00}	\longleftrightarrow	$-\Pi_{44}$
Π_μ^μ	\longleftrightarrow	$-\Pi_{\mu\mu}$
$i\mathcal{D}_M$	\longleftrightarrow	\mathcal{D}_E

B.4 Renormalized Lagrangian

The renormalization constants for the parameters g , m and ρ are defined by

$$g = Z_g g_R, \quad \rho = Z_\rho \rho_R, \quad m = Z_m m_R, \quad (\text{B.17})$$

as well as for the gluon (A_μ^a), quark (ψ) and ghost (η^a) field strengths

$$A_\mu^a = Z_3^{1/2} A_{\mu,R}^a, \quad \psi = Z_2^{1/2} \psi_R, \quad \eta^a = \tilde{Z}_3^{1/2} \eta_R^a, \quad (\text{B.18})$$

where renormalized quantities are denoted by a subscript R and are free of divergencies. Plugging these definitions into (B.1), the bare Lagrangian takes the form

$$\mathcal{L} = \mathcal{L}_R + \mathcal{L}_C \quad (\text{B.19})$$

with the renormalized Lagrangian

$$\begin{aligned} \mathcal{L} = & \bar{\psi}_R (i\not{\partial} - m_R) \psi - \frac{1}{4} (\partial_\mu A_{\nu,R}^a - \partial_\nu A_{\mu,R}^a)^2 + g_R A_{\mu,R}^a \bar{\psi}_R \gamma^\mu t^a \psi_R \\ & - g_R f^{abc} (\partial_\mu A_{\nu,R}^a) A_{\mu,R}^{\mu,R} A_{\nu,R}^{\nu,R} - \frac{1}{4} g_R^2 (f^{eab} A_{\mu,R}^a A_{\nu,R}^b) (f^{ecd} A_{\mu,R}^c A_{\nu,R}^d) \\ & - \frac{1}{2\rho_R} (\partial_\mu A_{a,R}^\mu)^2 - \bar{\eta}_R^a \partial_\mu \partial^\mu \eta_R^a - g_R \bar{\eta}_R^a \partial^\mu f^{abc} A_{\mu,R}^b \eta_R^c \end{aligned} \quad (\text{B.20})$$

that has the same structure as the bare Lagrangian \mathcal{L} , but all quantities are the finite renormalized ones, and the counter term Lagrangian

$$\begin{aligned} \mathcal{L}_C = & \bar{\psi}_R (i\delta_2 \not{\partial} - \delta_m) \psi_R - \delta_3 \frac{1}{4} (\partial_\mu A_{\nu,R}^a - \partial_\nu A_{\mu,R}^a)^2 + \delta_1 g_R A_{\mu,R}^a \bar{\psi}_R \gamma^\mu t^a \psi_R \\ & - \delta_1^{3g} g_R f^{abc} (\partial_\mu A_{\nu,R}^a) A_{\mu,R}^{\mu,R} A_{\nu,R}^{\nu,R} - \delta_1^{4g} \frac{1}{4} g_R^2 (f^{eab} A_{\mu,R}^a A_{\nu,R}^b) (f^{ecd} A_{\mu,R}^c A_{\nu,R}^d) \\ & - \tilde{\delta}_3 \bar{\eta}_R^a \partial_\mu \partial^\mu \eta_R^a - g \tilde{\delta}_1 \bar{\eta}_R^a \partial^\mu f^{abc} A_{\mu,R}^b \eta_R^c. \end{aligned} \quad (\text{B.21})$$

with the relations among the counter terms and Z -factors

$$\begin{aligned}
Z_2 &= 1 + \delta_2, & Z_3 &= 1 + \delta_3, \\
\tilde{Z}_3 &= 1 + \tilde{\delta}_3, & \delta_m &= m - m_R = m_R(Z_2 Z_m - 1) \\
Z_1 &= 1 + \delta_1 = Z_g Z_2 Z_3^{1/2}, & \tilde{Z}_1 &= 1 + \tilde{\delta}_1 = Z_g \tilde{Z}_3 Z_3^{1/2}, \\
Z_1^{3g} &= 1 + \delta_1^{3g} = Z_g Z_3^{3/2}, & Z_1^{4g} &= 1 + \delta_1^{4g} = Z_g^2 Z_3^2.
\end{aligned} \tag{B.22}$$

The underlying local gauge invariance of the theory implies that the renormalized gauge coupling g_R is a universal quantity for all four different vertices. This additionally constrains the renormalization factors:

$$\frac{Z_1}{Z_3} = \frac{\tilde{Z}_1}{\tilde{Z}_3} = \frac{Z^{3g}}{Z_3} = \frac{\sqrt{Z^{4g}}}{\sqrt{Z_3}}. \tag{B.23}$$

These are the Slavnov-Taylor identities.

Appendix C Frequency Sums

Performing calculations in the ITF, we have to calculate infinite sums over Matsubara frequencies. In this section, a method for calculating these frequency sums is presented, as also the results for the sums which are needed in this work.

C.1 Path Integral Technique

As an example, let us use the frequency sum over a scalar bosonic propagator

$$S = T \sum_{n=-\infty}^{\infty} \Delta_B(i\omega_n, \omega_k), \quad \Delta_B = \frac{1}{\omega_n^2 + \omega_k^2} \quad (\text{C.1})$$

with the bosonic Matsubara frequencies $\omega_n = 2n\pi T$. The trick here is to use a contour integral in the complex energy plane and taking advantage of the residue theorem. Consider the following complex integral

$$I = \frac{T}{2\pi i} \oint_{\mathcal{C}} h(z)g(z)dz, \quad (\text{C.2})$$

where f and g are meromorphic functions in the whole complex z -plane with well separated poles, and the contour \mathcal{C} surrounding all the poles z_0 , then

$$I = \sum_{z_0} \text{Res} \left[h(z)g(z) \right] \Big|_{z=z_0}. \quad (\text{C.3})$$

Because the poles are separated, we can write

$$I = T \sum_n g(z_n) \text{Res} \ h(z)|_{z=z_n} + T \sum_j f(z_j) \text{Res} \ g(z)|_{z=z_j}. \quad (\text{C.4})$$

Now we choose $g(z) = \Delta_B(z, \omega_k)$ and h as a function that has a unit residue at the values $z = 2in\pi T$ for integer values of n . For example, a function being proportional to f from eq. (A.1) which has the poles at the desired locations but has residues T , so we choose

$$h(z) = T^{-1}f(z) = T^{-1} \frac{1}{e^{z/T} - 1}. \quad (\text{C.5})$$

The value of the contour integral is $I = 0$, hence eq. (C.4) can be written as

$$T \sum_n \Delta_B(i\omega_n, \omega_k) = - \sum_j \frac{1}{e^{z_j/T} - 1} \text{Res} \ \Delta_B(z, \omega_k)|_{z=z_j}. \quad (\text{C.6})$$

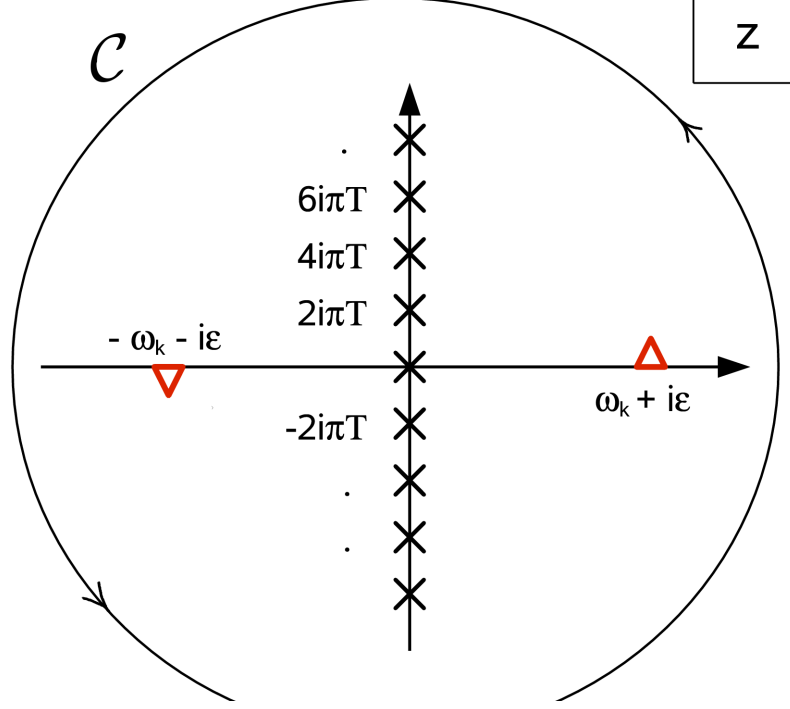


Figure C.1: The pole structure of the integral I in eq. (C.2). The red triangles are the poles of the thermal propagator at $z = \pm(\omega_k + i\epsilon)$, while the black crosses are the poles of the function $h(z) = \beta(e^{\beta z} - 1)^{-1}$ at $z = 2ni\pi T$. The contour \mathcal{C} can be chosen as a large circle around the origin with radius $R \rightarrow \infty$.

The poles of Δ_B are at the values $z = \pm\omega_k$ with residues

$$\text{Res } \Delta_B(z, \omega_k)|_{z=\pm\omega_k} = \mp \frac{1}{2\omega_k}. \quad (\text{C.7})$$

The result reads

$$\begin{aligned} T \sum_n \Delta_B(i\omega_n, \omega_k) &= \frac{1}{2\omega_k} f(\omega_k) - \frac{1}{2\omega_k} f(-\omega_k) \\ &= \frac{1}{2\omega_k} (1 + 2n_B(\omega_k)). \end{aligned} \quad (\text{C.8})$$

When we have to sum over fermionic Matsubara frequencies $\omega_n = (2n+1)\pi T$, we have to choose a function that has poles with unit residues at the values $z = (2n+1)i\pi T$, e.g.

$$h(z) = -T^{-1} \frac{1}{e^{z/T} + 1} \quad (\text{C.9})$$

which is proportional to \tilde{f} from eq. (A.3).

If one has to calculate frequency sums containing more than one Matsubara propagator, like

$$T \sum_n \Delta_B(K) \Delta_B(Q),$$

the procedure is quite similar to the above example. One has to calculate the poles of the propagators and the corresponding residues and then use eq. (C.4) to calculate the frequency sum.

C.2 Listing of Frequency Sums

In the following, we present a selection of frequency sums that are needed in this work:

$$T \sum_n \Delta_B(K) = \frac{1}{2\omega_k} (1 + 2n_B(\omega_k)), \quad (\text{C.10})$$

$$T \sum_n \Delta_F(K) = \frac{1}{2\omega_k} (1 - 2n_F(\omega_k)), \quad (\text{C.11})$$

$$\begin{aligned} T \sum_n \Delta_B(K) \Delta_B(Q) &= -\frac{1}{4\omega_k \omega_q} \left[(1 + n_B(\omega_k) + n_B(\omega_q)) \right. \\ &\quad \times \left(\frac{1}{i\omega - \omega_k - \omega_q} - \frac{1}{i\omega + \omega_k + \omega_q} \right) \\ &\quad + (n_B(\omega_k) - n_B(\omega_q)) \\ &\quad \left. \times \left(\frac{1}{i\omega + \omega_k - \omega_q} - \frac{1}{i\omega - \omega_k + \omega_q} \right) \right], \quad (\text{C.12}) \end{aligned}$$

$$\begin{aligned} T \sum_n \Delta_F(K) \Delta_F(Q) &= -\frac{1}{4\omega_k \omega_q} \left[(1 - n_F(\omega_k) - n_F(\omega_q)) \right. \\ &\quad \times \left(\frac{1}{i\omega - \omega_k - \omega_q} - \frac{1}{i\omega + \omega_k + \omega_q} \right) \\ &\quad - (n_F(\omega_k) - n_F(\omega_q)) \\ &\quad \left. \times \left(\frac{1}{i\omega + \omega_k - \omega_q} - \frac{1}{i\omega - \omega_k + \omega_q} \right) \right], \quad (\text{C.13}) \end{aligned}$$

$$\begin{aligned} T \sum_n \omega_n \Delta_B(K) \Delta_B(Q) &= \frac{i}{4\omega_q} \left[(1 + n_B(\omega_k) + n_B(\omega_q)) \right. \\ &\quad \times \left(\frac{1}{i\omega - \omega_k - \omega_q} + \frac{1}{i\omega + \omega_k + \omega_q} \right) \\ &\quad - (n_B(\omega_k) - n_B(\omega_q)) \\ &\quad \left. \times \left(\frac{1}{i\omega + \omega_k - \omega_q} + \frac{1}{i\omega - \omega_k + \omega_q} \right) \right]. \quad (\text{C.14}) \end{aligned}$$

Here, $\omega_k = \sqrt{\mathbf{k}^2 + m^2}$ for massive particles and $\omega_k = |\mathbf{k}|$ for massless particles. There are many more possible combinations of thermal propagators. However, they can be easily derived from the given ones by the substitution

$$n_B(\omega_k) \rightarrow -n_F(\omega_k) \quad (\text{C.15})$$

if $\Delta_B(K) \rightarrow \Delta_F(K)$ is changed in the frequency sum.

Appendix D Gauge Dependence of the One-Loop Fermion Self-Energy

To check the gauge dependence of the quark self-energy, we compute $\Sigma(P)$ explicitly in the Feynman (Σ^F) and the Coulomb (Σ^C) gauges in the imaginary time formalism. Our goal is the calculation of the difference between Σ^F and Σ^C . We define 3 scalar functions from Σ by

$$\begin{aligned} T_1 &= \text{tr}(\not{u}\Sigma), \\ T_2 &= \text{tr}(\not{P}\Sigma), \\ T_3 &= \text{tr}(\mathbf{1}\Sigma) \end{aligned} \tag{D.1}$$

with the medium 4-velocity u_μ .

In the language of these scalar functions, the gauge dependence is localized in

$$\Delta T_i = T_i^C - T_i^F. \tag{D.2}$$

If the three ΔT_i 's are zero, then one can argue that Σ is gauge independent. We will see that this does not hold in the general case. However, in the asymptotic region, which is relevant for our dispersion relations, all the $\Delta T_i \rightarrow 0$ and, therefore, the dispersion relation is conjectured to be gauge independent, too.

The matrix element for the quark self-energy is given by (4.1). Working in the ITF, first we use the Feynman gauge. Since the gluon propagator is $\propto \delta_{ab}$, the color structure reduces to $t_a t_a = C_R = \frac{N_c^2 - 1}{2N_c} = \frac{4}{3}$ and we obtain

$$\Sigma^F(P) = g^2 C_R T \sum_n \int \frac{d^4 K}{(2\pi)^3} \gamma^\mu (m - \not{Q}) \gamma^\nu \delta_{\mu\nu} \Delta_F(Q) \Delta_B(K), \tag{D.3}$$

where we have to sum over the bosonic Matsubara frequencies $\omega_n = 2n\pi T$. We find

$$\begin{aligned} T_1^F &= \underbrace{g^2 C_R T \sum_n \int \frac{d^3 k}{(2\pi)^3} \Delta_F(Q) \Delta_B(K) \text{tr}(\gamma_4 \gamma_\mu \not{Q} \gamma^\mu)}_{=:\hat{\mathcal{Z}}} \\ &= 8\hat{\mathcal{Z}} q_4, \\ T_2^F &= -\hat{\mathcal{Z}} \text{tr}(\not{P} \gamma_\mu \not{Q} \gamma^\mu) = 8\hat{\mathcal{Z}} Q_\mu P^\mu, \\ T_3^F &= m\hat{\mathcal{Z}} \text{tr}(\gamma_\mu \gamma^\mu) = -16m\hat{\mathcal{Z}}. \end{aligned} \tag{D.4}$$

This characterizes the quark self-energy in the Feynman gauge. Here we have introduced $\hat{\mathcal{Z}}$ as an abbreviation. It has to be understood as an operator, acting on everything that stands on the right side of it. With the gluon propagator in Coulomb gauge one obtains

$$\begin{aligned}\Sigma^C(P) &= g^2 C_R T \sum_n \int \frac{d^3 k}{(2\pi)^3} \gamma^\mu (m - \not{Q}) \gamma^\nu \\ &\quad \times \left(\frac{\delta_{4\mu} \delta_{4\nu}}{k^2} + \frac{(\delta_{ij} - \hat{p}_i \hat{p}_j) \delta_{\mu i} \delta_{\nu j}}{K^2} \right) \Delta_F(Q) \\ &= \hat{\mathcal{Z}} (\gamma^\mu (m - \not{Q}) \gamma^\nu) \left(\frac{\delta_{4\mu} \delta_{4\nu}}{k^2/K^2} + (\delta_{ij} - \hat{p}_i \hat{p}_j) \delta_{\mu i} \delta_{\nu j} \right),\end{aligned}\quad (\text{D.5})$$

and for the T_i^C 's we find after some algebra

$$\begin{aligned}T_1^C &= \text{tr}(\gamma_4 \Sigma^C) \\ &= -\hat{\mathcal{Z}} \text{tr}(\gamma_4 \gamma^\mu \not{Q} \gamma^\nu) \left(\frac{\delta_{4\mu} \delta_{4\nu}}{k^2/K^2} + (\delta_{ij} - \hat{p}_i \hat{p}_j) \delta_{\mu i} \delta_{\nu j} \right) \\ &= 8\hat{\mathcal{Z}} q_4 \left(1 - \frac{1}{2} \frac{K^2}{k^2} \right) = T_1^F - 4\hat{\mathcal{Z}} \frac{q_4 K^2}{k^2},\end{aligned}\quad (\text{D.6})$$

$$\begin{aligned}T_2^C &= -\hat{\mathcal{Z}} \text{tr}(\not{P} \gamma^\mu \not{Q} \gamma^\nu) \left(\frac{\delta_{4\mu} \delta_{4\nu}}{k^2/K^2} + (\delta_{ij} - \hat{p}_i \hat{p}_j) \delta_{\mu i} \delta_{\nu j} \right) \\ &= 8\hat{\mathcal{Z}} \left(Q_\mu P^\mu - \frac{K^2}{2k^2} (2p_4 q_4 - P_\mu Q^\mu) \right)\end{aligned}\quad (\text{D.7})$$

$$= T_2^F - 4\hat{\mathcal{Z}} \frac{K^2}{k^2} (2p_4 q_4 - P_\mu Q^\mu), \quad (\text{D.8})$$

$$\begin{aligned}T_3^C &= \hat{\mathcal{Z}} \text{mtr}(\gamma^\mu \gamma^\nu) \left(\frac{\delta_{4\mu} \delta_{4\nu}}{k^2/K^2} + (\delta_{ij} - \hat{p}_i \hat{p}_j) \delta_{\mu i} \delta_{\nu j} \right) \\ &= -8m\hat{\mathcal{Z}} \left(1 + \frac{K^2}{k^2} \right) = \frac{1}{2} T_3^F - 8m\hat{\mathcal{Z}} \frac{K^2}{k^2}.\end{aligned}\quad (\text{D.9})$$

Now it is straightforward to read off the gauge dependent parts

$$\begin{aligned}\Delta T_1 &= -4g^2 C_R T \sum_n \int \frac{d^3 k}{(2\pi)^3} \Delta_F(Q) \frac{q_4}{k^2}, \\ \Delta T_2 &= -4g^2 C_R T \sum_n \int \frac{d^3 k}{(2\pi)^3} \Delta_F(Q) \frac{2q_4 p_4 - P_\mu Q^\mu}{k^2},\end{aligned}\quad (\text{D.10})$$

$$\Delta T_3 = -8mg^2 C_R T \sum_n \int \frac{d^3 k}{(2\pi)^3} \Delta_F(Q) \frac{1}{k^2} - \frac{1}{2} T_3^F, \quad (\text{D.11})$$

$$\Delta \tilde{T}_3 = \Delta T_3 + \frac{1}{2} T_3^F = -8mg^2 C_R T \sum_n \int \frac{d^3 k}{(2\pi)^3} \Delta_F(Q) \frac{1}{k^2}.$$

Now we perform the frequency sums and find for the gauge-dependence func-

tions

$$\begin{aligned}\Delta T_1 &= 4g^2 C_R \int \frac{d^3 k}{(2\pi)^3} T \sum_n (\omega_n + p_4) \Delta_F(Q) \\ &= -4g^2 C_R \int \frac{d^3 k}{(2\pi)^3} \frac{n_F(\omega_{\mathbf{k}-\mathbf{p}})}{\omega_{\mathbf{k}-\mathbf{p}}} (\omega + p_4) \\ &\equiv 0,\end{aligned}\tag{D.12}$$

$$\tag{D.13}$$

since $\omega = -p_4$. From line one to line two of the above equations, we omitted the vacuum part of the self-energy. The other functions yield

$$\Delta T_2 = 4g^2 C_R \int \frac{d^3 k}{(2\pi)^3} \frac{(\mathbf{k} - \mathbf{p}) \cdot \mathbf{p}}{k^2} \frac{n_F(\omega_{\mathbf{k}-\mathbf{p}})}{\omega_{\mathbf{k}-\mathbf{p}}}, \tag{D.14}$$

$$\Delta \tilde{T}_3 = 8mg^2 C_R \int \frac{d^3 k}{(2\pi)^3} \frac{1}{k^2} \frac{n_F(\omega_{\mathbf{k}-\mathbf{p}})}{\omega_{\mathbf{k}-\mathbf{p}}} \tag{D.15}$$

with $\omega_{\mathbf{k}-\mathbf{p}} = \sqrt{|\mathbf{k} - \mathbf{p}|^2 + m^2}$ and the Fermi distribution function n_F . After shifting the integration variable $\mathbf{k} \rightarrow \mathbf{k} + \mathbf{p}$, we have with $x = \cos \theta$, where θ is the angle between \mathbf{k} and \mathbf{p} :

$$\Delta T_2 = -\frac{g^2 C_R}{\pi^2} \int_0^\infty dk \frac{k^2}{\omega_{\mathbf{k}}} n_F(\omega_{\mathbf{k}}) \int_{-1}^1 dx \frac{\mathbf{k} \cdot \mathbf{p}}{|\mathbf{k} + \mathbf{p}|^2} \tag{D.16}$$

$$= -\frac{g^2 C_R}{\pi^2} \int_0^\infty dk \frac{k^2}{\omega_{\mathbf{k}}} n_F(\omega_{\mathbf{k}}) \left(1 - \frac{k^2 + p^2}{4kp} \ln \frac{k^2 + p^2 + 2kp}{k^2 + p^2 - 2kp} \right),$$

$$\Delta \tilde{T}_3 = m \frac{g^2 C_R}{\pi^2} \int_0^\infty dk \frac{k^2}{\omega_{\mathbf{k}}} n_F(\omega_{\mathbf{k}}) \int_{-1}^1 \frac{dx}{|\mathbf{k} + \mathbf{p}|^2} \tag{D.17}$$

$$= m \frac{g^2 C_R}{2\pi^2 p} \int_0^\infty dk \frac{k}{\omega_{\mathbf{k}}} n_F(\omega_{\mathbf{k}}) \ln \frac{k^2 + p^2 + 2kp}{k^2 + p^2 - 2kp}.$$

Thus, the one-loop quark self-energy depends on the used gauge. Let us further check whether the dispersion relation, especially the asymptotic dispersion relation for $p \rightarrow \infty$, is also gauge dependent. For the calculation of the dispersion relation in the asymptotic region it is more convenient to use another decomposition of Σ :

$$\Sigma(\omega, p) = \gamma_0 K_0 - \vec{\gamma} \mathbf{p} K - m Z. \tag{D.18}$$

These two decompositions can be related by taking the traces over eq. (D.18)

$$\begin{aligned}Z(p_0, p) &= \frac{1}{4m} T_3, \\ K_0(p_0, p) &= \frac{1}{4} T_1, \\ K(p_0, p) &= \frac{1}{4p^2} (p_0 T_1 - T_2)\end{aligned}\tag{D.19}$$

and the definitions

$$\Delta K_0 = K_0^C - K_0^F, \quad \Delta K = K^C - K^F, \quad \Delta Z = Z^C - \frac{1}{2}Z^F \quad (\text{D.20})$$

we find

$$\Delta K_0 = 0, \quad \Delta K = -\frac{\Delta T_2}{4p^2}, \quad \Delta Z = \frac{\Delta \tilde{T}_3}{4m}. \quad (\text{D.21})$$

Writing the asymptotic dispersion relation (4.60) in Feynman and Coulomb gauge yields

$$\omega_F^2(p) = p^2 + m^2 + 2 \left(p^2 K^F(\omega, p) + p K_0^F(\omega, p) \right), \quad (\text{D.22})$$

$$\omega_C^2(p) = p^2 + m^2 + 2 \left(p^2 K^C(\omega, p) + p K_0^C(\omega, p) \right) \quad (\text{D.23})$$

$$= \omega_F^2(p) + 2p^2 \Delta K(\omega, p). \quad (\text{D.24})$$

Thus, the only gauge-dependence function relevant for the asymptotic dispersion relation is $2p^2 \Delta K(\omega, p)$, which reads

$$\begin{aligned} 2p^2 \Delta K(\omega, p) &= -\frac{1}{2} \Delta T_2 \\ &= \frac{g^2 C_R}{2\pi^2} \int_0^\infty dk \frac{k^2}{\omega_{\mathbf{k}}} n_F(\omega_{\mathbf{k}}) \\ &\quad \times \left(1 - \underbrace{\frac{k^2 + p^2}{4kp} \ln \frac{k^2 + p^2 + 2kp}{k^2 + p^2 - 2kp}}_{\rightarrow 1 \text{ for } p \rightarrow \infty} \right) \\ &\rightarrow 0. \end{aligned} \quad (\text{D.25})$$

Thus, we have

$$\omega_C^2(p) = \omega_F^2(p). \quad (\text{D.26})$$

The asymptotic quark dispersion relation is indeed the same for the Feynman and Coulomb gauges. This may be considered as a strong hint to gauge invariance.

Appendix E Elementary Integrals

We recollect a few elementary integrals used in this work:

$$\int_{-1}^1 \frac{dx}{a \pm bx} = \frac{1}{b} \ln \frac{a+b}{a-b}, \quad (\text{E.1})$$

$$\frac{1}{2} \int_{-1}^1 \frac{dx x}{a \pm bx} = \pm \left(\frac{1}{b} - \frac{a}{2b^2} \ln \frac{a+b}{a-b} \right), \quad (\text{E.2})$$

$$\begin{aligned} \int_{-1}^1 \frac{dx x^2}{x^2 + a^2} &= 2 - 2a \arctan \frac{1}{a} \\ &= 2 - ia \ln \frac{ia+1}{ia-1} = -2Q_1(ia), \end{aligned} \quad (\text{E.3})$$

$$\int_{-1}^1 \frac{dx x^2}{x^2 - a^2} = 2 - a \ln \frac{a+1}{a-1} = -2Q_1(a) \quad (\text{E.4})$$

with the Legendre function of the second kind $Q_1(a) = -1 + \frac{a}{2} \ln \frac{a+1}{a-1}$

$$\int_0^\infty \frac{dx x}{e^x + 1} = \frac{1}{12} \pi^2, \quad (\text{E.5})$$

$$\int_0^\infty \frac{dx x}{e^x - 1} = \frac{1}{6} \pi^2, \quad (\text{E.6})$$

$$\int_0^\infty \frac{dx x^{2\nu}}{\sqrt{x^2 + a^2}} e^{-n\sqrt{x^2 + a^2}} = \pi^{-\frac{1}{2}} \Gamma\left(\nu + \frac{1}{2}\right) \left(\frac{2a}{n}\right) K_\nu(n \cdot a), \quad (\text{E.7})$$

where $K_\nu(z)$ is the modified Bessel function of the second kind or MacDonald function with the property

$$\int_0^\infty dt t^{s-1} K_\nu(t) = 2^{s-2} \Gamma\left(\frac{s-\nu}{2}\right) \Gamma\left(\frac{s+\nu}{2}\right), \quad \Re(s) > |\Re(\nu)|. \quad (\text{E.8})$$

Bibliography

- [Alt92] T. Altherr, E. Petitgirard, T. de Rio Gaztelurrutia, *Astropart. Phys.* **1**, 289 (1993).
- [Alt93] T. Altherr, *Int. J. Mod. Phys.* **A8**, 5605 (1993).
- [App75] T. Appelquist, J. Carazzone, *Phys. Rev.* **D11**, 2856 (1975).
- [Bed00] D. J. Bedingham, arXiv: hep-ph/0011012 (2000).
- [Ber06] V. Bernard, U.-G. Meissner, ArXiv: hep-ph/0611231 (2006).
- [Bla02] J.-P. Blaizot, E. Iancu, *Phys. Rept.* **359**, 355 (2002).
- [Blu05a] M. Bluhm, B. Kämpfer, G. Soff, *J. Phys.* **G31**, S1151 (2005).
- [Blu05b] M. Bluhm, B. Kämpfer, G. Soff, *Phys. Lett.* **B620**, 131 (2005).
- [Blu07a] M. Bluhm, B. Kämpfer, R. Schulze, D. Seipt, U. Heinz, arXiv: 0705.0397 [hep-ph] (2007), *to be published in Phys. Rev. C*.
- [Blu07b] M. Bluhm, B. Kämpfer, R. Schulze, D. Seipt, *Eur. Phys. J.* **C49**, 205 (2007).
- [BP90a] E. Braaten, R. D. Pisarski, *Phys. Rev. Lett.* **64**, 1338 (1990).
- [BP90b] E. Braaten, R. D. Pisarski, *Nucl. Phys.* **B339**, 310 (1990).
- [BP92] E. Braaten, R. D. Pisarski, *Phys. Rev.* **D45**, 1827 (1992).
- [BSMM93] Bronstein, Semendjajew, Musiol, Mühlig, *Taschenbuch der Mathematik* (Verlag Harri Deutsch, 1993).
- [Cel79] W. Celmaster, R. J. Gonsalves, *Phys. Rev. Lett.* **42**, 1435 (1979).
- [Col75] J. C. Collins, M. J. Perry, *Phys. Rev. Lett.* **34**, 1353 (1975).
- [DeR76] A. De Rújula, H. Georgi, *Phys. Rev.* **D13**, 1296 (1976).
- [Edw82] B. J. Edwards, T. D. Gottschalk, *Nucl. Phys.* **B196**, 328 (1982).
- [Fle95] F. Flechsig, H. Schulz, *Phys. Lett.* **B349**, 504 (1995).
- [Geo76] H. Georgi, H. D. Politzer, *Phys. Rev.* **D14**, 1829 (1976).
- [Grei5] W. Greiner, B. Müller, *Quantum Mechanics II - Symmetries* (Springer, 1994), 2. rev. ed.

- [Hin05] M. Hindmarsh, O. Philipsen, Phys. Rev. **D71**, 087302 (2005).
- [Huo06] P. Huovinen, P. V. Ruuskanen, Ann. Rev. Nucl. Part. Sci. **56**, 163 (2006).
- [ItZ80] C. Itzykson, J.-B. Zuber, *Quantum Field Theory* (McGraw-Hill Book Company, 1980).
- [Kaj03] K. Kajantie, M. Laine, K. Rummukainen, Y. Schröder, Phys. Rev. **D67**, 105008 (2003).
- [Kaj85] K. Kajantie, J. I. Kapusta, Ann. Phys. **160**, 477 (1985).
- [Kal84] O. K. Kalashnikov, Fortschr. Phys. **32**, 525 (1984).
- [Kal98] O. K. Kalashnikov, JETP Lett. **67**, 1 (1998).
- [Kar01] F. Karsch, E. Laermann, A. Peikert, Nucl. Phys. **B605**, 579 (2001).
- [Kar02] F. Karsch, Lect. Notes Phys. **583**, 209 (2002).
- [Kar07] F. Karsch, ArXiv: hep-ph/0701210 (2007).
- [Kli81] V. V. Klimov, Sov. J. Nucl. Phys. **33**, 934 (1981).
- [Kob91] R. Kobes, G. Kunstatter, A. Rebhan, Nucl. Phys. **B355**, 1 (1991).
- [LeB96] M. Le Bellac, *Thermal Field Theory* (Cambridge University Press, 1996).
- [Moo77] R. G. Moorhouse, M. R. Pennington, G. G. Ross, Nucl. Phys. **B124**, 285 (1977).
- [Mus03] M. G. Mustafa, M. H. Thoma, Pramana **60**, 711 (2003).
- [Muta87] T. Muta, *Foundations of Quantum Chromodynamics* (World Scientific, 1987).
- [Nac78] O. Nachtmann, W. Wetzels, preprint HD-THEP-78-3 .
- [Pes00a] A. Peshier, B. Kämpfer, G. Soff, Phys. Rev. **C61**, 045203 (2000).
- [Pes00b] A. Peshier, M. H. Thoma, Phys. Rev. Lett. **84**, 841 (2000).
- [Pes02] A. Peshier, Nucl. Phys. **A702**, 128 (2002).
- [Pes06] A. Peshier, arXiv: hep-ph/0601119 (2006).
- [Pes94] A. Peshier, B. Kämpfer, O. P. Pavlenko, G. Soff, Phys. Lett. **B337**, 235 (1994).
- [Pes96] A. Peshier, B. Kämpfer, O. P. Pavlenko, G. Soff, Phys. Rev. **D54**, 2399 (1996).

-
- [Pes98a] A. Peshier, K. Schertler, M. H. Thoma, *Ann. Phys.* **266**, 162 (1998).
- [Pes98b] A. Peshier, *Zur Zustandsgleichung heißer stark wechselwirkender Materie - konsistente Beschreibungen stark gekoppelter Quantensysteme*. Ph.D. thesis, TU Dresden (1998).
- [Pet92] E. Petitgirard, *Z. Phys.* **C54**, 673 (1992).
- [Pis89a] R. D. Pisarski, *Physica* **A158**, 146 (1989).
- [Pis89b] R. D. Pisarski, *Nucl. Phys.* **A498**, 423c (1989).
- [Pol78] H. D. Politzer, *Nucl. Phys.* **B146**, 283 (1978).
- [PS95] M. E. Peskin, D. V. Schroeder, *An Introduction to Quantum Field Theory* (Westview Press, 1995).
- [Reb96] A. Rebhan, arXiv: hep-ph/9608410 (1996).
- [Ris04] D. H. Rischke, *Prog. Part. Nucl. Phys.* **52**, 197 (2004).
- [RPP06] W. M. Yao, *et al.*, *J. Phys.* **G33**, 1 (2006).
- [Ryd94] L. H. Ryder, *Quantum Field Theory* (Cambridge University Press, 1994).
- [Sch99] A. Schäfer, M. H. Thoma, arXiv: hep-ph/9903514 (1999).
- [Smi01] A. Smilga, *Lectures on Quantum Chromodynamics* (World Scientific Press, 2001).
- [Tho01] M. H. Thoma, *Nucl. Phys. Proc. Suppl.* **92**, 162 (2001).
- [Wel82] H. A. Weldon, *Phys. Rev.* **D26**, 2789 (1982).

Danksagung

Zu allererst möchte ich Herrn Prof. Dr. Rüdiger Schmidt für die Aufnahme in das Institut für Theoretische Physik der TU Dresden und für den bereitgestellten Arbeitsplatz danken. Herrn Prof. Dr. Burkhard Kämpfer danke ich für die Vergabe und die Betreuung des interessanten und vielseitigen Diplomarbeitsthemas sowie für die Möglichkeit, die Diplomarbeit am Institut für Strahlenphysik am Forschungszentrum Dresden-Rossendorf anzufertigen. Der Arbeitsgruppe danke ich für die angenehme Arbeitsatmosphäre und die vielen anregenden Diskussionen. Marcus Bluhm danke ich für die vielen Anregungen und kritischen Fragen, welche stets zur Verbesserung der Arbeit beigetragen haben. Robert Schulze möchte ich für seine Hilfe bei der Erstellung der Bibliographie danken.

Besonderer Dank gilt jedoch meinen Eltern und Familie für ihre Unterstützung während meines gesamten Studiums.

Eigenständigkeitserklärung

Hiermit versichere ich, dass ich die vorliegende Diplomarbeit ohne Benutzung unzulässiger Hilfsmittel selbständig verfasst habe. Die Stellen meiner Arbeit, die dem Wortlaut oder dem Sinn nach anderen Werken entnommen sind, habe ich in jedem Fall unter Angabe der Quelle als Entlehnung kenntlich gemacht. Dasselbe gilt sinngemäß auch für Abbildungen. Diese Arbeit hat in dieser oder einer ähnlichen Form noch nicht im Rahmen einer anderen Prüfung vorgelegen.

Dresden, den 29.05.2007